NIST **United States Department of Commerce**
National Institute of Standards and Technology

NISTIR 3955

SPHERICAL NEAR-FIELD SCANNING: EXPERIMENTAL AND THEORETICAL STUDIES

Ronald C. Wittmann
Carl F. Stubenrauch

NISTIR 3955

SPHERICAL NEAR-FIELD SCANNING: EXPERIMENTAL AND THEORETICAL STUDIES

Ronald C. Wittmann
Carl F. Stubenrauch

Electromagnetic Fields Division
Center for Electronics and Electrical Engineering
National Engineering Laboratory
National Institute of Standards and Technology
Boulder, Colorado 80303-3328

July 1990

Sponsored by
Rome Air Development Center RADC/EECT
Hanscom AFB, Massachusetts 01731

U.S. DEPARTMENT OF COMMERCE, Robert A. Mosbacher, Secretary
NATIONAL INSTITUTE OF STANDARDS AND TECHNOLOGY, John W. Lyons, Director

CONTENTS

Page

EXECUTIVE SUMMARY 1

CHAPTER 1. EXPERIMENTAL RESULTS 5
- 1.1 Introduction 5
- 1.2 Experimental Details 5
- 1.3 Experimental Results 6
- 1.4 Directivity 10
- 1.5 Conclusions 11

CHAPTER 2. PROBE PATTERN TRANSFORMATIONS 25

CHAPTER 3. THE PROBE AS AN IDEAL DIPOLE 27
- 3.1 Introduction 27
- 3.2 Spherical-Wave Expansions of the Transverse Fields 27
- 3.3 The Electric Dipole Probe 28
- 3.4 The Magnetic Dipole Probe 28
- 3.5 Numerical Results 29
- 3.6 Conclusions 30

CHAPTER 4. TESTING THE PROBE CORRECTION SOFTWARE BY SIMULATION 33
- 4.1 Introduction 33
- 4.2 The Far-Field Pattern of Elemental Electric and Magnetic Dipoles . 34
- 4.3 The Receiving Pattern 36
- 4.4 The Probe Response 37
- 4.5 Summary of the Algorithm 37
- 4.6 Numerical Results 38
- 4.7 Conclusions 39

CHAPTER 5. SPHERICAL-WAVE EXPANSIONS FOR TRANSLATED DIPOLES 43
- 5.1 Theory 43
- 5.2 Computer Program 46

Page

CHAPTER 6. PRODUCTS OF SPHERICAL HARMONICS 53
6.1 Introduction 53
6.2 Expansion of $Y_{\nu\mu}(\hat{\mathbf{r}})\, Y_{nm}(\hat{\mathbf{r}})$ 53
6.3 Expansion of $\mathbf{X}_{\nu\mu}(\hat{\mathbf{r}}) \cdot \mathbf{X}_{nm}(\hat{\mathbf{r}})$ 58
6.4 Expansion of $i\hat{\mathbf{r}} \times \mathbf{X}_{\nu\mu}(\hat{\mathbf{r}}) \cdot \mathbf{X}_{nm}(\hat{\mathbf{r}})$ 59
6.5 Explicit Formulas for the Coefficients 60
6.6 Expansion of Vector Products 66
6.7 Other Notations for Vector Spherical Harmonics 66
6.8 The Clebsch-Gordan Series and the Wigner 3-j Symbols 67

CHAPTER 7. CALCULATION OF TRANSLATED PROBE COEFFICIENTS IN SPHERICAL NEAR-FIELD SCANNING 71
7.1 Introduction 71
7.2 Transmission Formula 71
7.3 Calculation of the Translated Probe Coefficients 72
7.4 Summary 74

CHAPTER 8. SPHERICAL NEAR-FIELD SCANNING TRANSMISSION EQUATIONS: RECEIVING PROBE, TRANSMITTING TEST ANTENNA; TRANSMITTING PROBE, RECEIVING TEST ANTENNA 75
8.1 Introduction 75
8.2 Initial Definitions 75
8.3 Transmitting and Receiving Operators 77
8.4 Rotation of the Vector Spherical Harmonics 78
8.5 Spherical Scanning: Receiving Probe 78
8.6 Spherical Scanning: Transmitting Probe 80
8.7 Reciprocity and the Transmission Equations 81

CHAPTER 9. RECIPROCITY FROM AN OPERATIONAL VIEWPOINT 83
9.1 Introduction 83
9.2 Representation of the Electromagnetic Fields 83
9.3 The Lorentz Reciprocity Integral 84
9.4 Reciprocity Relations 85

CONTENTS (continued)

Page

CHAPTER 10. THE UNIFORMLY EXCITED CIRCULAR APERTURE: SPHERICAL-WAVE FIELD EXPANSIONS 89
10.1 Introduction 89
10.2 Scalar Spectrum and Far-Field Pattern 89
10.3 Expansion of $I(\hat{\mathbf{k}})$ in Spherical Harmonics 90
10.4 The Scalar Field Expanded in Spherical Waves 92
10.5 A Piston Radiator in a Rigid Baffle 93
10.6 Vector Spectrum and Far-Field Pattern 94
10.7 The Vector Field Expanded in Spherical Waves 95
10.8 Computation of α_n 97
10.9 Numerical Results 97
10.10 Cartesian Components of the Vector Spherical Harmonics 99

CHAPTER 11. SPHERICAL NEAR-FIELD SCANNING: DETERMINING THE INCIDENT FIELD NEAR A ROTATABLE PROBE 101
11.1 Introduction 101
11.2 Acoustic Probe Receiving Operator 101
11.3 Rotation of the Acoustic Probe 102
11.4 The Incident Acoustic Field 103
11.5 The Acoustic Transmission Formula 103
11.6 The "Symmetric" Acoustic Probe 104
11.7 The Electromagnetic Transmission Formula 105
11.8 The "Symmetric" Electromagnetic Probe 106
11.9 Practical Implementation 107
11.10 The Ideal Dipole Probe 108

REFERENCES 113

LIST OF FIGURES

Figure Page

1.1 Design of the circular cross-section probe. Lowest order mode cutoff (TE_{11}) is 2.78 GHz. Next mode cutoff (TE_{01}) is 3.62 GHz. The circular waveguide is thus single-moded at the operating frequency of 3.3 GHz. 13

1.2 Comparison of far-field patterns obtained from probe corrected spherical and planar near-field measurements. Probe for the spherical measurements was circular cross-section $\mu = \pm 1$ waveguide. Measurement radius 1.28 m, main polarization, $\phi = 0^0$ cut. 14

1.3 Comparison of far-field patterns obtained from probe corrected spherical and planar near-field measurements. Probe for the spherical measurements was circular cross-section $\mu = \pm 1$ waveguide. Measurement radius 1.28 m, main polarization, $\phi = 90^0$ cut. 14

1.4 Comparison of far-field patterns obtained from probe corrected spherical and planar near-field measurements. Probe for the spherical measurements was circular cross-section $\mu = \pm 1$ waveguide. Measurement radius 1.28 m, cross polarization, $\phi = 0^0$ cut. 15

1.5 Comparison of far-field patterns obtained from probe corrected spherical and planar near-field measurements. Probe for the spherical measurements was circular cross-section $\mu = \pm 1$ waveguide. Measurement radius 1.28 m, cross polarization, $\phi = 90^0$ cut. 15

1.6 Comparison of far-field patterns calculated with and without probe correction from 1.28 m spherical near-field data. Circular probe, cross polarization, $\phi = 0^0$ cut. 16

1.7 Comparison of far-field patterns calculated with and without probe correction from 1.28 m spherical near-field data. Circular probe, cross polarization, $\phi = 90^0$ cut. 16

LIST OF FIGURES (continued)

Figure Page

1.8 Comparison of far-field patterns calculated with and without probe correction from 3.8 m spherical near-field data. Circular probe, cross polarization, $\phi = 0^0$ cut. 17

1.9 Comparison of far-field patterns calculated with and without probe correction from 3.8 m spherical near-field data. Circular probe, cross polarization, $\phi = 90^0$ cut. 17

1.10 Comparison of far-field patterns calculated with and without probe correction from 1.28 m spherical near-field data. Rectangular probe, cross polarization, $\phi = 0^0$ cut. 18

1.11 Comparison of far-field patterns calculated with and without probe correction from 1.28 m spherical near-field data. Rectangular probe, cross polarization, $\phi = 90^0$ cut. 18

1.12 Comparison of far-field patterns calculated with and without probe correction from 3.79 m spherical near-field data. Rectangular probe, cross polarization, $\phi = 0^0$ cut. 19

1.13 Comparison of far-field patterns calculated with and without probe correction from 3.79 m spherical near-field data. Rectangular probe, cross polarization, $\phi = 90^0$ cut. 19

1.14 Comparison of far-field patterns calculated from near-field data acquired at two radii separated by $\lambda/4$. Probe corrected, circular probe, cross polarization, $\phi = 90^0$ cut. 20

1.15 Comparison of far-field patterns calculated from near-field data acquired at two radii separated by $\lambda/4$. Probe corrected, rectangular probe, cross polarization, $\phi = 90^0$ cut. 20

LIST OF FIGURES (continued)

Figure Page

1.16 Probe corrected far-field patterns comparing results obtained with N_p = 1, 3, and 17. Circular probe, scan radius = 1.28 m, main polarization, ϕ = 0° cut. 21

1.17 Probe corrected far-field patterns comparing results obtained with N_p = 1, 3, and 17. Circular probe, scan radius = 1.28 m, cross polarization, ϕ = 0° cut. 21

1.18 Probe corrected far-field patterns comparing results obtained with N_p = 1, 3, and 17. Circular probe, scan radius = 1.28 m, cross polarization, ϕ = 90° cut. 22

1.19 Probe corrected far-field patterns comparing results obtained with N_p = 1, 2, and 17. Rectangular probe, scan radius = 1.28 m, main polarization, ϕ = 0° cut. 22

1.20 Probe corrected far-field patterns comparing results obtained with N_p = 1, 2, and 17. Rectangular probe, scan radius = 1.28 m, cross polarization, ϕ = 0° cut. 23

1.21 Probe corrected far-field patterns comparing results obtained with N_p = 1, 2, and 17. Rectangular probe, scan radius = 1.28 m, cross polarization, ϕ = 90° cut. 23

3.1 Comparison of far-field patterns calculated from near-field data acquired using a rectangular probe. No probe correction was employed but in one case a magnetic dipole probe is assumed and in the other case, an electric dipole is assumed. Main polarization, ϕ = 0° cut. . 31

3.2 Comparison of far-field patterns calculated from near-field data acquired using a rectangular probe. No probe correction was employed but in one case a magnetic dipole probe is assumed and in the other case, an electric dipole is assumed. Main polarization, ϕ = 90° cut. 31

LIST OF FIGURES (continued)

Figure Page

3.3 Comparison of far-field patterns calculated from near-field data acquired using a rectangular probe. No probe correction was employed but in one case a magnetic dipole probe is assumed and in the other case, an electric dipole is assumed. Cross polarization, $\phi = 0^0$ cut. 32

3.4 Comparison of far-field patterns calculated from near-field data acquired using a rectangular probe. No probe correction was employed but in one case a magnetic dipole probe is assumed and in the other case, an electric dipole is assumed. Cross polarization, $\phi = 90^0$ cut.

4.1 Mode amplitudes for a y directed electric dipole offset 25 cm in the +z direction. Normalization is such that amplitude of $t^E_{1,\pm1}$ is -3 dB for the dipole at the origin. 40

4.2 Geometry of the shifted dipole test. The actual scan radius was 127.95 cm. The dipole was thus offset 25 cm from the fictitious radius of 152.95 cm. 40

4.3 Comparison of far-field patterns calculated from data acquired at 127.95 cm and calculated assuming that (a) radius = 152.95 cm (dotted line), (b) radius = 152.95 cm but with probe correction (solid line), and (c) radius = 127.95 cm (dashed line). Main polarization, $\phi = 0^0$ cut. 41

4.4 Comparison of far-field patterns calculated from data acquired at 127.95 cm and calculated assuming that (a) radius = 152.95 cm (dotted line), (b) radius = 152.95 cm but with probe correction (solid line), and (c) radius = 127.95 cm (dashed line). Main polarization, $\phi = 90^0$ cut. 41

LIST OF FIGURES (continued)

Figure Page

4.5 Comparison of far-field patterns calculated from data acquired at 127.95 cm and calculated assuming that (a) radius = 152.95 cm (dotted line), (b) radius = 152.95 cm but with probe correction (solid line), and (c) radius = 127.95 cm (dashed line). Cross polarization, $\phi = 0^0$ cut. 42

4.6 Comparison of far-field patterns calculated from data acquired at 127.95 cm and calculated assuming that (a) radius = 152.95 cm (dotted line), (b) radius = 152.95 cm but with probe correction (solid line), and (c) radius = 127.95 cm (dashed line). Cross polarization, $\phi = 90^0$ cut. 42

9.1 Geometry for the application of the reciprocity theorem 87

11.1 A scanner for probing incident fields 111

11.2 Roll-over-azimuth positioner 111

LIST OF TABLES

Table Page

1.1 On-axis characteristics of probes 6

1.2 Measured spherical mode coefficients for circular and rectangular waveguides 7

1.3 Comparison of directivities 11

5.1 Expansion coefficients for the far-field pattern of an x directed magnetic dipole on the z axis, kz = 10 (see Eqs (5-21) and (5-22)). .. 49

5.2 Expansion coefficients for the far-field pattern of a y directed magnetic dipole on the z axis, kz = 10 (see Eqs (5-21) and (5-23)). .. 50

5.3 Expansion coefficients for the far-field pattern of an x directed electric dipole on the z axis, kz = 10 (see Eqs (5-21) and (5-24)). .. 51

5.4 Expansion coefficients for the far-field pattern of a y directed electric dipole on the z axis, kz = 10 (see Eqs (5-21) and (5-25)). .. 52

6.1 $Y_{1\mu}(\hat{\mathbf{r}})\ Y_{nm}(\hat{\mathbf{r}}) = \sum_{\alpha} a(\alpha,\mu+m|1\mu nm)\ Y_{\alpha,\mu+m}(\hat{\mathbf{r}})$ 56

6.2 $\mathbf{X}_{1\mu}(\hat{\mathbf{r}}) \cdot \mathbf{X}_{nm}(\hat{\mathbf{r}}) = \sum_{\alpha} b(\alpha,\mu+m|1\mu nm)\ Y_{\alpha,\mu+m}(\hat{\mathbf{r}})$ 59

6.3 $\mathbf{i}\hat{\mathbf{r}} \times \mathbf{X}_{1\mu}(\hat{\mathbf{r}}) \cdot \mathbf{X}_{nm}(\hat{\mathbf{r}}) = \sum_{\alpha} c(\alpha,\mu+m|1\mu nm)\ Y_{\alpha,\mu+m}(\hat{\mathbf{r}})$ 59

10.1 Expansion coefficients, aperture radius ka = 10 (see Eq (10-29)) 98

SPHERICAL NEAR-FIELD SCANNING: EXPERIMENTAL AND THEORETICAL STUDIES

Ronald C. Wittmann
Carl F. Stubenrauch

Electromagnetic Fields Division
National Institute of Standards and Technology
Boulder, CO 80303-3328

This report documents the evaluation of spherical near-field scanning algorithms and computer code developed at the National Institute of Standards and Technology. The experimental work is primarily a comparison of probe-compensated spherical and planar near-field measurement results for a common test antenna. Theoretical work is largely supportive of the experimental effort, but some peripheral topics are developed: For example, (1) application of spherical near-field measurements to the determination of incident fields in compact ranges; and, (2) spherical-wave expansions for the fields of a uniformly excited circular aperture (to facilitate the creation of analytic test data).

Key words: antenna measurements; near-field measurements; probe correction; range evaluation; spherical scanning; spherical waves.

EXECUTIVE SUMMARY

This report is divided into eleven chapters, each of which is largely self-contained.

The primary objective of this work was the experimental verification of the spherical scanning algorithm and programs. The test antennas were a set of square microstrip arrays which could be assembled in several configurations. Data were taken for several scan radii and the computed far fields were found to agree as expected. An extensive set of planar data was also taken. Comparison between far-field patterns calculated from spherical and planar data was excellent. A detailed discussion of procedures and results is given in Chapter 1.

In spherical scanning the probe must be oriented so that it points in the -z direction, which is usually not the orientation in which receiving patterns are measured. Also, if the probe was measured in a transmitting mode and is to be used as a receiver, reciprocity constraints must be applied. Chapter 2 discusses the required transformations in light of probe pattern symmetry.

In the experimental work, a symmetric probe and an open-ended rectangular waveguide were used as probes. By default, the software treats an ideal probe (the no-probe correction case) as an electric dipole. Open-ended waveguide probes, however, are better approximated as magnetic dipoles. Therefore, we decided to see whether results (without probe correction) are improved by viewing the ideal probe as a magnetic dipole (Chapter 3). Theoretically, there can be significant differences in the two points of view when the measurement radius is close to the minimum radius. Little difference was observed in our experimental results, however. The magnetic dipole model did give some improvement in the cross-polarized component in the main beam region.

Because of the experimental difficulty in producing a significant probe correction, we simulated probe correction using an ideal dipole probe offset from the measurement sphere. (We can, in principle, simulate an arbitrary $\mu \pm 1$ probe using an endfire dipole array.) Theory and numerical results are described in Chapter 4. We found that large probe pattern effects could be induced which could then be removed (to machine accuracy) by employing probe correction.

In Chapter 4 the spherical harmonic expansion of the receiving pattern of an offset dipole is obtained by numerical integration. In Chapter 5, as an intermediate check of this numerical integration, the spherical-wave expansions for a translated dipole are found using the translation formulas. Some numerical results are given.

Scalar and vector spherical harmonics play a central role in electromagnetic theory. Products of these functions occur frequently, as in the case of spherical near-field scanning theory, where an important issue is the coupling between a probe and the incident field. Chapter 6 is a compendium of useful results. The approach is initially motivational, but a number of practical computational formulas are developed in later sections.

Chapter 7 uses results of Chapter 6 to develop a particularly straightforward algorithm to calculate the translated probe coefficients of spherical scanning.

The operator formalism developed during this project is used in Chapter 8 to give a description of antenna-antenna interactions. The transmission formulas for spherical near-field scanning are derived, in this context, with the probe transmitting or receiving. Reciprocity is used to relate the transmitting and receiving cases.

Chapter 9 is a short derivation of the reciprocity relations between transmitting and receiving patterns from an operational point of view.

The canonical problem of a uniformly excited aperture is treated in Chapter 10. It is possible to give the coefficients of the spherical-wave expansions in closed form for both the acoustic and the electromagnetic cases. Besides the obvious pedagogic value, it is useful to have an analytic solution for a model that closely approximates a practical transducer. The near field of this model can be computed accurately and efficiently.

Many RCS (Radar Cross Section), EMI/EMC (ElectroMagnetic Interference/Compatibility), and antenna measurements require a known incident field within a test volume. To evaluate systems designed to produce a specific incident field (compact ranges, for example), we must measure the actual illumination for comparison with design specifications. Beyond its diagnostic value, this incident-field data can also be used for error estimation and for calculating first order corrections. In Chapter 11, we develop a spherical near-field scanning algorithm for determining incident fields inside a probe's "minimum sphere." This differs from the well-known spherical near-field scanning formulation which determines fields outside the source's minimum sphere. The scanner size depends on the extent of the region of interest but not on the extent of the (possibly much larger) source. The data may be collected using a standard roll-over-azimuth positioner.

1. EXPERIMENTAL RESULTS

1.1 Introduction

In this chapter we describe various measurements made on a representative test antenna. Data were processed using the recently developed spherical near-field scanning software. Comparisons of far-field patterns were made to patterns determined with planar near-field techniques. Measurements were made using two types of open-ended waveguide probes, one with a circular cross section and one with a rectangular cross section. Measurements with both probes were made at several radii. In addition, the data were processed using a reduced number of modes to describe the probe in its own coordinate system.

1.2 Experimental Details

The test antenna was a microstrip array antenna consisting of four 16 × 16 element subpanels operating at 3.3 GHz. The antenna was approximately 1.5 m square. To give a reference for the patterns which were calculated, the antenna was also measured on the NIST Planar Near-Field Range.

The spherical measurements were made on the NIST Spherical Near-Field Range. This rotator is a roll-over-azimuth positioner (model mount) mounted on rails which permit the measurement radius to be varied. This capability also allows on-axis gain measurements to be performed on small antennas using the extrapolation technique.

All measurements were acquired over the range $-180^0 \le \theta < 180^0$ and $0^0 \le \phi < 360^0$. This technique acquires a redundant set of data, with each point being acquired twice. The data are then averaged to get a single non-redundant data set. Use of this technique minimizes certain types of alignment errors and was employed for all data acquired, both spherical near-field scans and the probe far-field pattern data.

The two probes used were rectangular and circular cross-section open-ended waveguides. These probes were calibrated for gain, polarization, and pattern at NIST before the spherical measurements. The rectangular probe was a standard piece of WR-284 waveguide approximately 50 cm long. The circular probe was designed at NIST to allow a single mode to propagate at the test frequency. This constraint required a complex taper to be fabricated in the rectangular-to-circular transition section. The probe was electroformed at a commercial electroplating facility which specializes in custom microwave component fabrication. The design of the probe is shown in Figure 1.1.

The on-axis gain and polarization of the probes were measured on the spherical range using the NIST three-antenna/extrapolation technique. The characteristics of the probes at 3.3 GHz are listed in Table 1.1. Far-field patterns were also measured at this time.

Table 1.1 On-axis characteristics of probes

Probe	Gain	Axial Ratio	Tilt	Sense
Rectangular	6.70 dB	61.4 dB	89.98°	Right
Circular	7.93 dB	60.6 dB	89.81°	Right

1.3 **Experimental Results**

1.3.1 MEASUREMENTS ON PROBES

The first process in the probe corrected spherical measurement is the determination of the spherical mode expansion of the probe. The expansion is calculated from far-field measurements using the spherical near-field program but without applying the probe correction. Theoretically, the circular probe should have only $m = \pm 1$ modes. This characteristic is required by theory for the probe correction technique employed. Also of interest is how well the probe correction works for a rectangular cross-section probe since this probe is readily available. Table 1.2 gives the amplitude of the probe coefficients which were calculated from measured data for the two probe types. Each set of modes were normalized to the maximum coefficient. The $t_{nm}^{H,E}$ are coefficients in the spherical harmonic expansion

$$\mathbf{t}(\hat{\mathbf{r}}) = \sum_{\nu\mu} \left[t_{\nu\mu}^{H} \mathbf{X}_{\nu\mu}(\hat{\mathbf{r}}) + t_{\nu\mu}^{E}\, i\mathbf{k} \times \mathbf{X}_{\nu\mu}(\hat{\mathbf{r}}) \right] , \tag{1-1}$$

where $\mathbf{t}(\hat{\mathbf{r}})$ is the far-field pattern of the antenna (see Chapter 2). In actual calculation for probe correction, coefficients up to $n = 17$ were used.

Table 1.2 Measured spherical mode coefficients for circular and rectangular waveguides

n	m	circular guide		rectangular guide	
		t^H_{nm} (dB)	t^E_{nm} (dB)	t^H_{nm} (dB)	t^E_{nm} (dB)
1	-1	0.00	-1.10	0.00	-3.59
1	0	-42.21	-43.02	-44.03	-37.69
1	1	-0.02	-1.16	-0.01	-3.67
2	-2	-43.73	-43.92	-41.41	-45.05
2	-1	-10.51	-14.77	-9.00	-20.43
2	0	-44.11	-37.81	-45.24	-39.40
2	1	-10.51	-14.68	-8.90	-20.60
2	2	-48.23	-43.73	-38.42	-49.43
3	-3	-47.93	-49.94	-21.47	-17.10
3	-2	-46.29	-63.20	-51.07	-51.83
3	-1	-23.83	-18.47	-22.50	-18.85
3	0	-55.59	-41.47	-54.07	-38.51
3	1	-23.94	-18.45	-22.62	-18.75
3	2	-45.58	-57.18	-45.42	-52.23
3	3	-47.63	-50.33	-21.40	-17.08
4	-4	-58.09	-71.15	-57.85	-58.68
4	-3	-44.71	-52.57	-31.67	-33.97
4	-2	-50.33	-51.15	-49.74	-57.10
4	-1	-28.23	-27.49	-26.01	-27.46
4	0	-57.18	-52.07	-57.10	-46.42
4	1	-28.48	-27.58	-26.11	-27.58
4	2	-49.57	-60.27	-44.36	-63.12
4	3	-44.92	-51.15	-31.87	-33.92
4	4	-71.15	-65.13	-57.10	-59.59
5	-5	-51.15	-54.90	-44.36	-43.41
5	-4	-57.18	-67.63	-54.07	-66.64
5	-3	-44.11	-71.15	-31.75	-37.10
5	-2	-53.09	-47.93	-55.76	-49.74
5	-1	-39.22	-29.64	-37.93	-28.60
5	0	-77.18	-45.81	-66.64	-51.07
5	1	-38.59	-29.87	-38.34	-28.47
5	2	-50.73	-47.93	-46.86	-48.85
5	3	-44.51	-60.27	-31.64	-37.46
5	4	-57.18	-77.18	-54.60	-57.10
5	5	-52.57	-57.18	-44.87	-42.56

The circular cylindrical probe exhibits the predicted $m = \pm 1$ characteristic which is desired. For the rectangular probe, we observe that the dominant modes present are the electric and magnetic dipole modes, $t^{H,E}_{1,\pm 1}$, and the magnetic quadrupole mode, $t^{H}_{2,\pm 1}$, and that the $m = \pm 3$ and ± 5 modes are more than 20 dB below the highest amplitude mode. This indicates that such a probe also approximates the desired characteristic and does have promise for application to spherical near-field scanning. Results of tests exploring this will be discussed in a later section.

1.3.2 PLANAR NEAR-FIELD MEASUREMENTS

Planar measurements were performed on the microstrip array and probe corrected far-field patterns generated using the rectangular waveguide probe. These patterns are valid to approximately 50°, the limiting angle being determined by geometrical considerations relating the scan area and the antenna aperture. These patterns will not be shown separately but as reference patterns for some of the data presented for spherical measurements.

1.3.3 SPHERICAL NEAR-FIELD MEASUREMENTS WITH A CIRCULAR PROBE

Spherical measurements were originally performed at radii of approximately 1.6 and 3.8 m. Comparing far-field patterns calculated with and without probe correction showed that the probe effect was almost nonexistent. Additional measurements were performed at 1.28 m by using a specially built extension to mount the probe. (This is the smallest practical radius, giving several wavelengths clearance between the array corners and the probe during the scanning process.) These data still reveal little probe effect except in the cross-polarization patterns.

Figures 1.2 through 1.5 show the main and cross-polarized patterns for the azimuth and elevation planes ($\phi = 0^0$ and 90^0) for data acquired at 1.28 m. Also shown for comparison are the corresponding far-field patterns obtained from planar measurements. Agreement of the planar and spherical results is very good except in the plane $\phi = 90^0$ for the cross-polarized field over the region in which the planar results are valid. Even in this region, we note striking agreement over most of the pattern even at levels between -60 and -70 dB. We consider this very good considering the very low field levels.

Figures 1.6 and 1.7 show a comparison of the results at 1.28 m between far-field patterns calculated with and without probe correction. Since the co-polarized patterns were virtually identical they will not be shown here. Similar results for patterns calculated from the 3.8 m data are shown in Figures 1.8 and 1.9. Again we do not show the co-polarized patterns. The $\phi = 90^0$ cut produced from the 3.8 m data does not agree well with the 1.28 m data or the planar data. We think that low near field levels and the greater possibility for multiple reflections is the reason for these discrepancies in this very low-level portion of the pattern.

We observe that the probe correction has a pronounced effect only on the cross-polarized pattern in the region of the pattern where the main beam exists in the co-polarized pattern.

1.3.4 SPHERICAL NEAR-FIELD MEASUREMENTS WITH A RECTANGULAR PROBE

Figures 1.10 and 1.11 show the $\phi = 0^0$ and $\phi = 90^0$ far-field patterns calculated from data taken at 1.27 m with and without probe correction. Since the co-polarized patterns are virtually identical to those shown previously for the circular probe, we do not show them. Again we observe that the $\phi = 0^0$ pattern exhibits little effect of probe correction while the $\phi = 90^0$ pattern shows considerable effect. In Figures 1.12 and 1.13 we see the same cuts obtained from data taken at 3.79 m. Comparison of Figure 1.13 with Figure 1.7 shows qualitative agreement which is better than between Figures 1.7 and 1.11. As will be noted in the following section, reflections seem to have an important effect in the low-level parts of the cross-polarized pattern and discrepancies are probably due to this effect. We cannot discount the possibility that the probe correction does not correctly account for the effect of the rectangular probe at the smaller radius since higher order m modes are present as seen in Table 1.2. At the larger radius the effect of these modes will be considerably diminished.

1.3.5 EFFECT OF REFLECTIONS ON CALCULATED FAR FIELD

As noted in Section 1.3.3, data were originally taken at a radius of approximately 1.6 m. Two sets of data were acquired using radii differing by $\lambda/4$ with both the circular and rectangular probes. The purpose of this test was to determine the effect of multiple reflections. No multiple reflection data were acquired at the 1.28 m radius because of time constraints. Figures 1.14 and 1.15 illustrate the effect of reflections on the computed, probe corrected cross-polarized far-field patterns in the $\phi = 90^0$ plane. Effect on the main component and $\phi = 0^0$ patterns was minimal and patterns are not shown here. It is difficult to ascertain from these results whether the differences are due to multiple reflections between the antenna and probe or due to room reflections. The average level of the sidelobes below -50 dB or so remains approximately constant but the structure is considerably altered in detail.

1.3.6 EFFECT OF USING A REDUCED NUMBER OF MODES TO DESCRIBE THE PROBE

Inspection of Table 1.2 reveals that modes higher than n = 3 are at least 20 dB below the dominant n = 1, m = ±1 modes. Tests were performed in which only three, two, or one mode was used to describe the probe in its own coordinate system. Translated multipole coefficients were then calculated for these cases to perform the probe correction. Results of these calculations for several cases of maximum probe mode N_p are presented in Figures 1.16 through 1.18 for the circular probe and in Figures 1.19 through 1.21 for the rectangular probe.

The effect of reducing the number of modes used to describe the probe is observed to be minimal. The cross-polarized fields are the most affected, and the rectangular probe shows the greatest effect. The major application of this result would be in empirical modelling of the probe. If the first two or three modes could be accurately calculated from the probe geometry, it might be possible to eliminate the need to calibrate the probe for many near-field scanning applications. Since the probe measurement is nearly as complicated and time consuming as the spherical measurement itself, the saving would be substantial.

1.4 **Directivity**

On-axis ($\hat{\mathbf{r}} = \hat{\mathbf{z}}$) directivity was calculated for each probe and measurement radius with and without probe correction:

$$D(\hat{\mathbf{r}}) = 4\pi \frac{|\mathbf{t}(\hat{\mathbf{r}})|^2}{\sum_{\nu\mu}\left[|t^H_{\nu\mu}|^2 + |t^E_{\nu\mu}|^2\right]} . \qquad (1\text{-}2)$$

Results of the calculation are shown in Table 1.3. Gain can also be determined from the measurements if the insertion loss of the antenna-probe combination is determined at some reference position. Insertion loss measurements were performed, but because of mixer problems, they were incorrect and are not reported here.

Table 1.3 Comparison of directivities

Probe	Radius (m)	D (dB) (Probe corrected)	D (dB) (No correction)
Circular	1.28	34.369	34.258
Circular	3.80	34.351	34.340
Rectangular	1.27	34.323	34.177
Rectangular	3.79	34.340	34.333

As might be expected, all directivities calculated with probe correction included are very close. Those calculated for the larger radius are also very close to the values determined with probe correction. Values determined from small radius data without probe correction indicate a deviation due to the small pattern changes caused by the probe effect.

1.5 **Conclusions**

We have reviewed selected experimental results and the following conclusions may be drawn. Comparisons of far-field patterns calculated from planar and spherical near-field measurements are generally very good. Spherical measurements obtained at the smallest radius demonstrate the best agreement with the planar results for data acquired with a circular probe. This is understandable since the relative scattering level from the surroundings is the lowest in this case. Agreement to -50 dB is acceptable. In the case of the rectangular probe, however, the larger scan radius seems to produce the better measurement. This probably is due to multiple reflections, though an effect due to the incomplete probe correction, since the rectangular probe possesses higher order m = odd modes, is also a possibility. For co-polarized fields and cross-polarized fields in the region away from the main beam, agreement to -40 dB seems to be obtainable.

Surprisingly, little effect of the probe directivity on the beamwidth was observed even for the smallest scan radius. This is in contrast to previous measurements at NIST on a different antenna design. The effect on directivity seems to be the greatest with a reduction of about 0.1 to 0.2 dB if no probe correction is performed. The only real practical penalty to probe correction is the need to obtain a probe pattern, and results indicate that, for small probes at least, good results can be obtained with a relatively simple model perhaps with only three magnetic and electric coefficients. Computation of the translated coefficients is very efficient.

Further discussion of the probe effect is found in Chapter 4, where a more complicated probe is simulated by employing a radially offset dipole. Additional experimental work would also be valuable if a more directive probe could be employed which would accentuate the effect of probe directivity. A circularly symmetric horn is available at NIST which has interchangeable apertures of various diameters. Comparison of measurements made with a series of similar but different sized horns could yield valuable results which would shed further light on the conditions which require probe correction.

The programs all currently run on a 25 MHz 80386-based desktop computer with an 80387 math coprocessor. Computation times are of the order of five minutes for analysis of a complete set of near-field data (180 × 180 points) to produce probe-corrected, far-field patterns. In general the experimental work and the results of Chapter 4 validate the spherical near-field package developed at NIST.

Measurements were performed by Darlene Agee, Saturnino Canales, and Douglas Kremer. Helpful discussions with Lorant Muth, especially in finding a particularly vexing coding error, are also gratefully acknowledged.

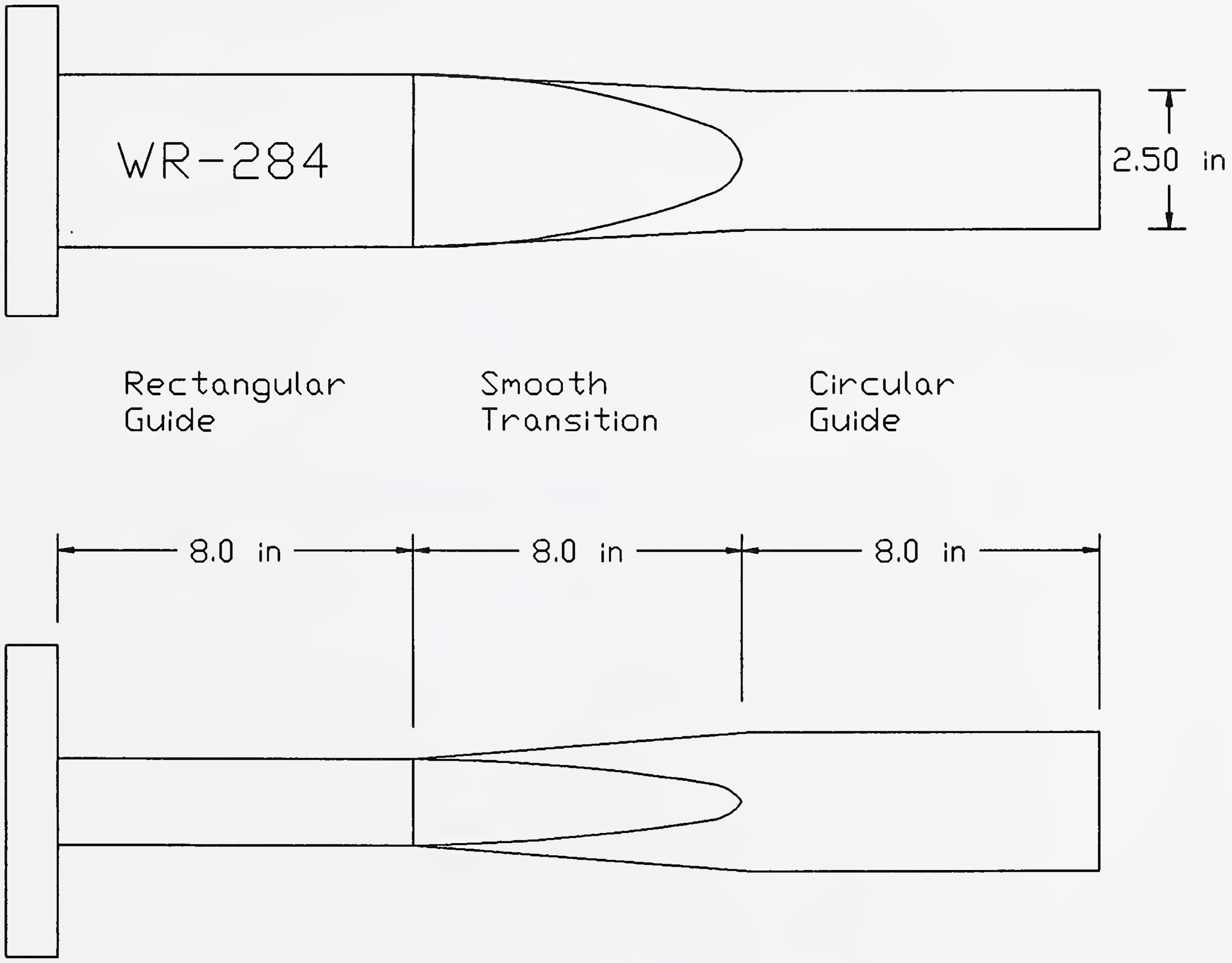
WR-284
2.50 in
Rectangular Guide
Smooth Transition
Circular Guide
8.0 in
8.0 in
8.0 in

Figure 1.1 Design of the circular cross-section probe. Lowest order mode cutoff (TE_{11}) is 2.78 GHz. Next mode cutoff (TE_{01}) is 3.62 GHz. The circular waveguide is thus single-moded at the operating frequency of 3.3 GHz.

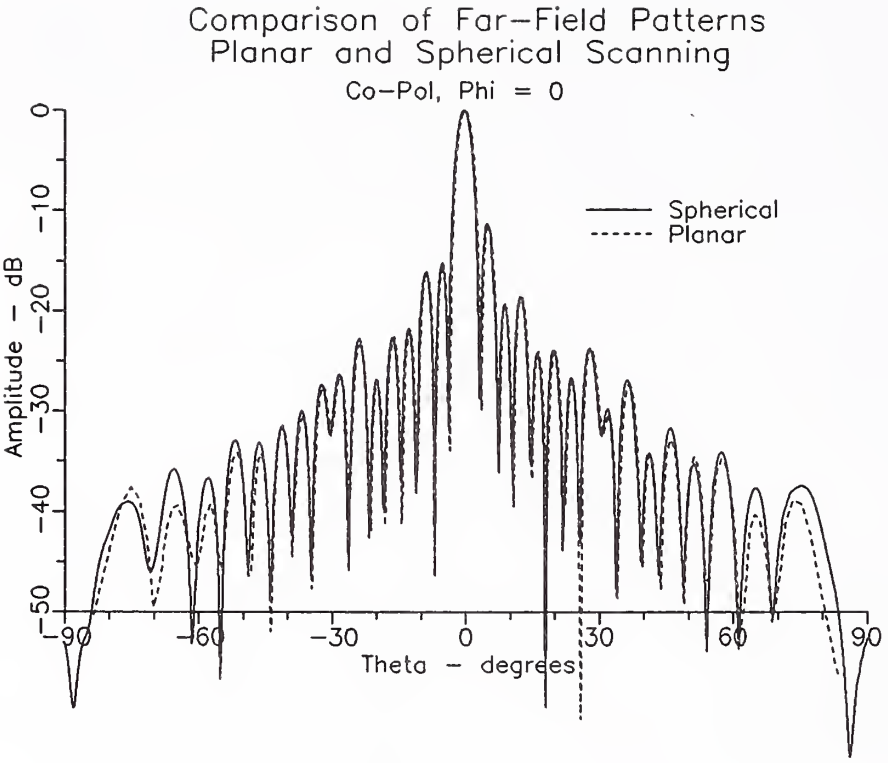

Figure 1.2 Comparison of far-field patterns obtained from probe corrected spherical and planar near-field measurements. Probe for the spherical measurements was circular cross-section $\mu = \pm 1$ waveguide. Measurement radius 1.28 m, main polarization, ϕ = 0° cut.

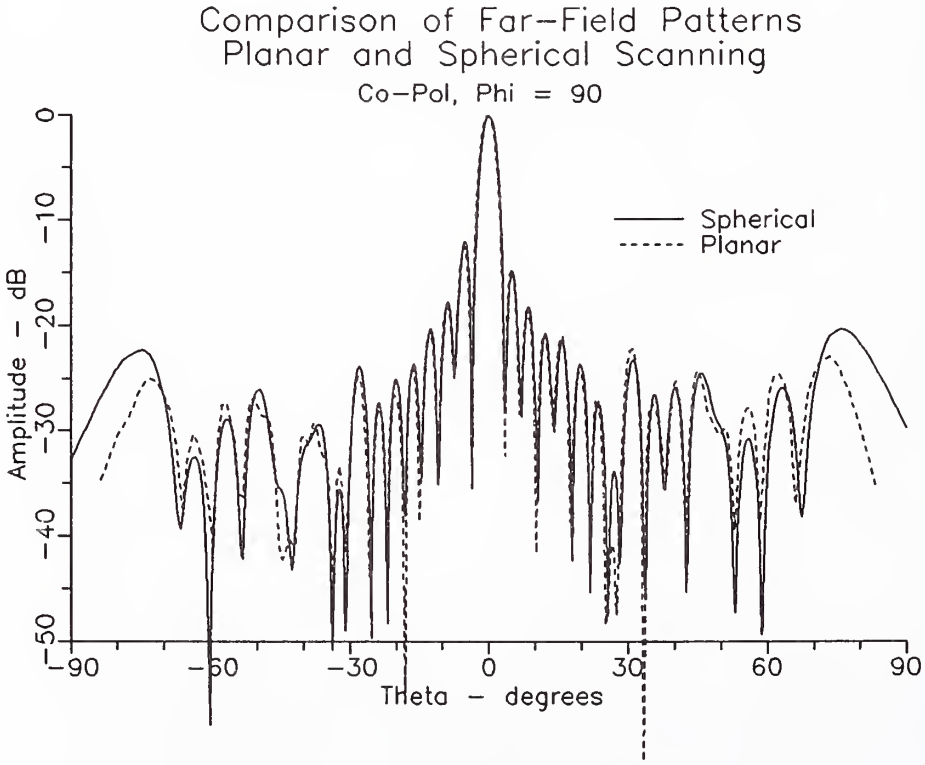

Figure 1.3 Comparison of far-field patterns obtained from probe corrected spherical and planar near-field measurements. Probe for the spherical measurements was circular cross-section $\mu = \pm 1$ waveguide. Measurement radius 1.28 m, main polarization, ϕ = 90° cut.

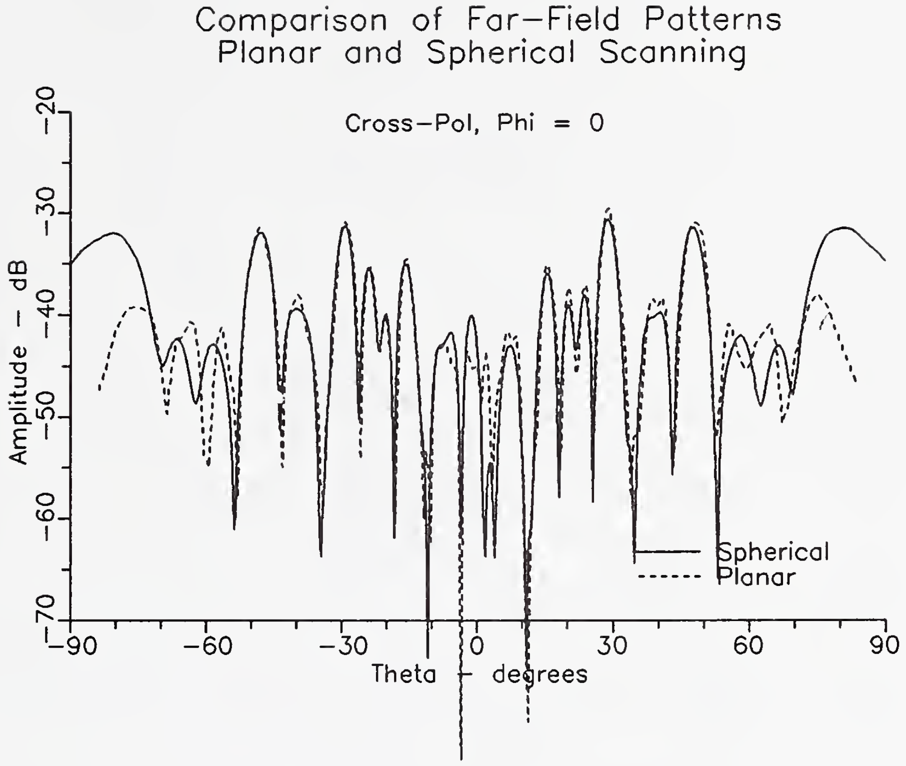

Figure 1.4 Comparison of far-field patterns obtained from probe corrected spherical and planar near-field measurements. Probe for the spherical measurements was circular cross-section $\mu = \pm 1$ waveguide. Measurement radius 1.28 m, cross polarization, $\phi = 0°$ cut.

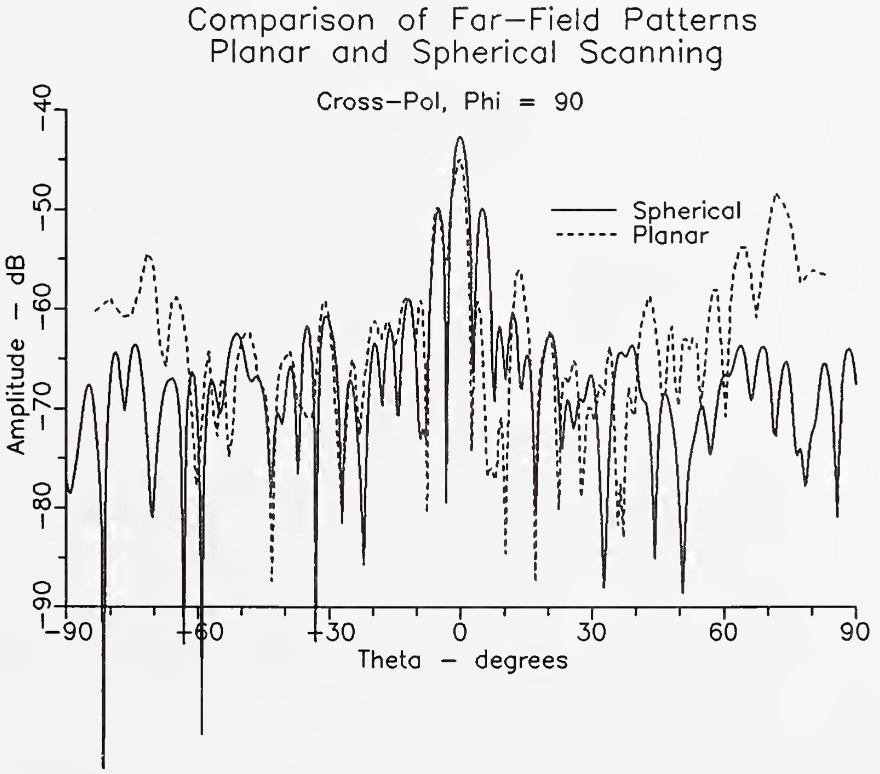

Figure 1.5 Comparison of far-field patterns obtained from probe corrected spherical and planar near-field measurements. Probe for the spherical measurements was circular cross-section $\mu = \pm 1$ waveguide. Measurement radius 1.28 m, cross polarization, $\phi = 90°$ cut.

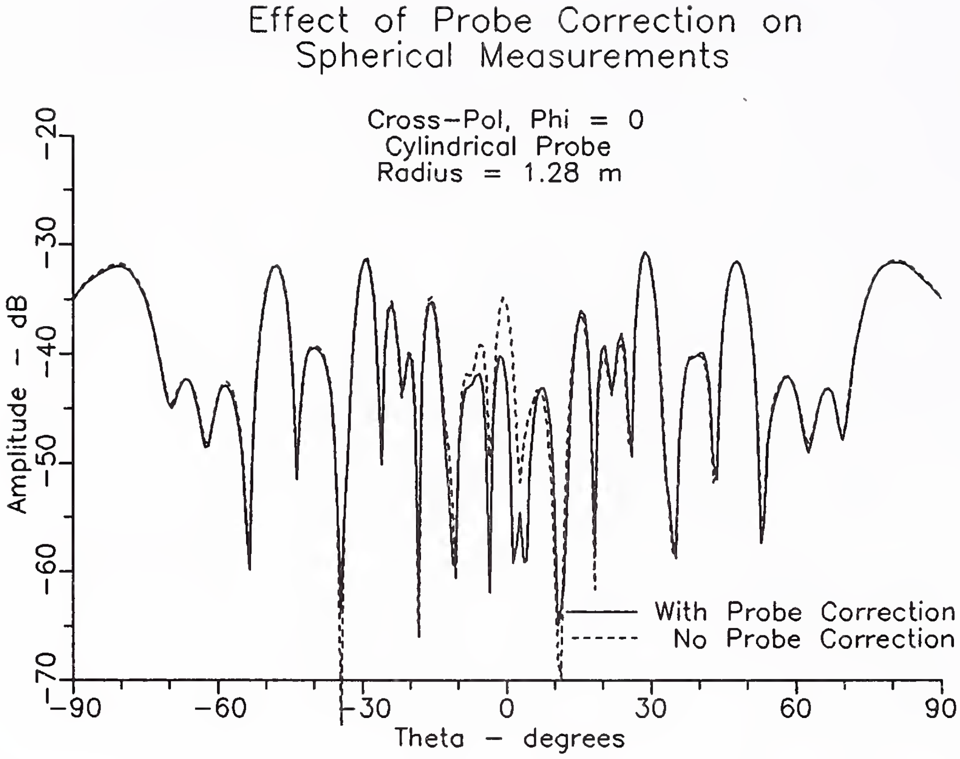

Figure 1.6 Comparison of far-field patterns calculated with and without probe correction from 1.28 m spherical near-field data. Circular probe, cross polarization, ϕ = 0° cut.

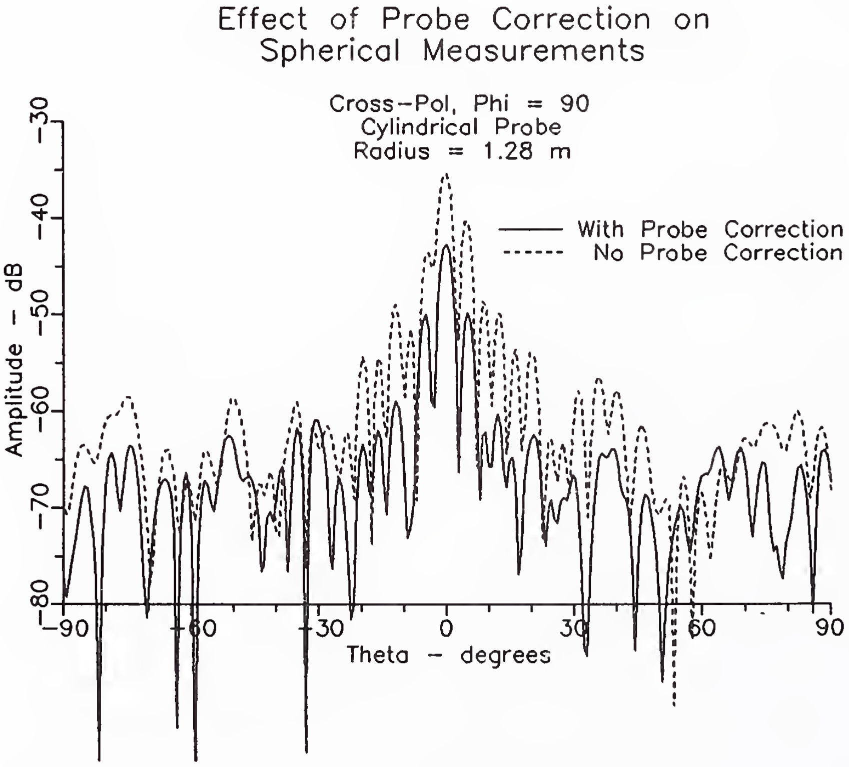

Figure 1.7 Comparison of far-field patterns calculated with and without probe correction from 1.28 m spherical near-field data. Circular probe, cross polarization, ϕ = 90° cut.

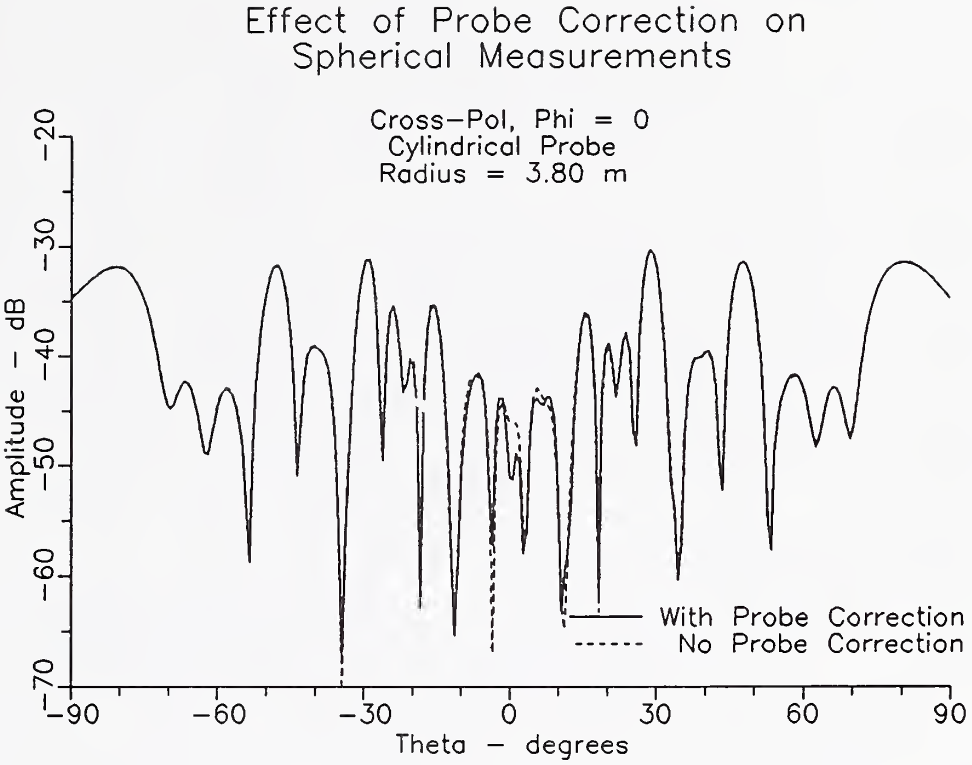

Figure 1.8 Comparison of far-field patterns calculated with and without probe correction from 3.8 m spherical near-field data. Circular probe, cross polarization, ϕ = 0° cut.

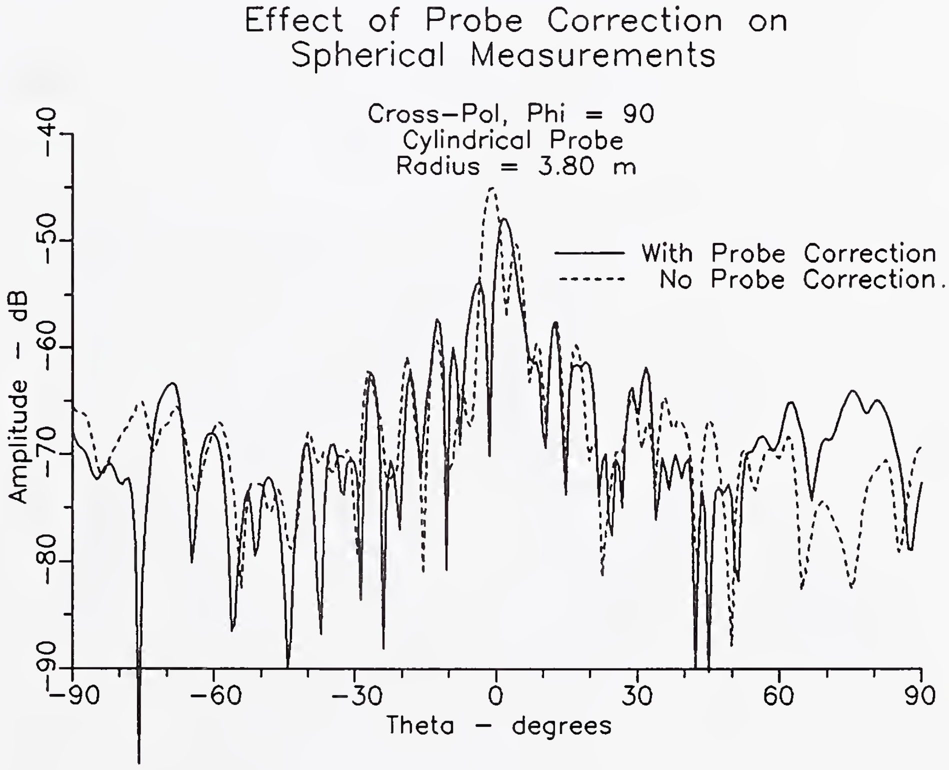

Figure 1.9 Comparison of far-field patterns calculated with and without probe correction from 3.8 m spherical near-field data. Circular probe, cross polarization, ϕ = 90° cut.

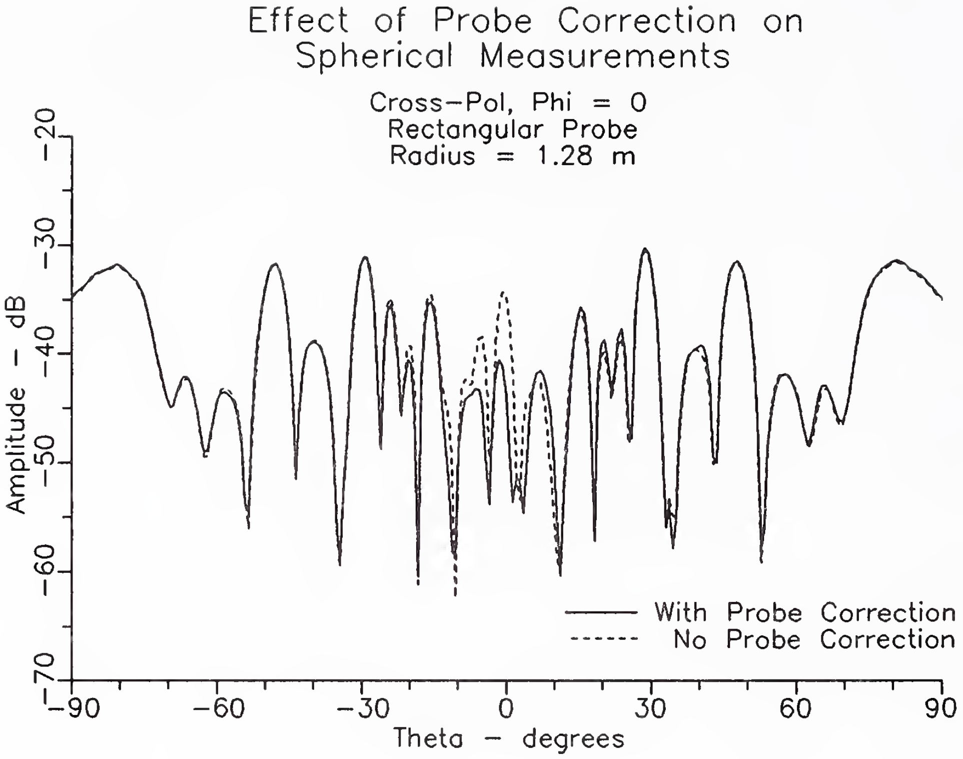

Figure 1.10 Comparison of far-field patterns calculated with and without probe correction from 1.28 m spherical near-field data. Rectangular probe, cross polarization, ϕ = 0° cut.

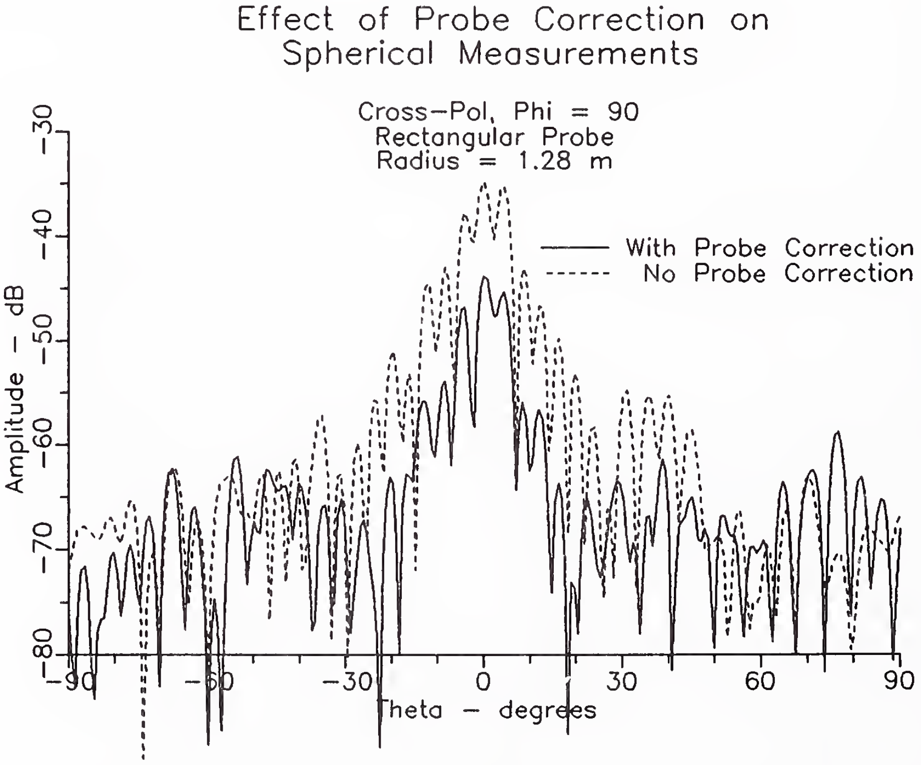

Figure 1.11 Comparison of far-field patterns calculated with and without probe correction from 1.28 m spherical near-field data. Rectangular probe, cross polarization, ϕ = 90° cut.

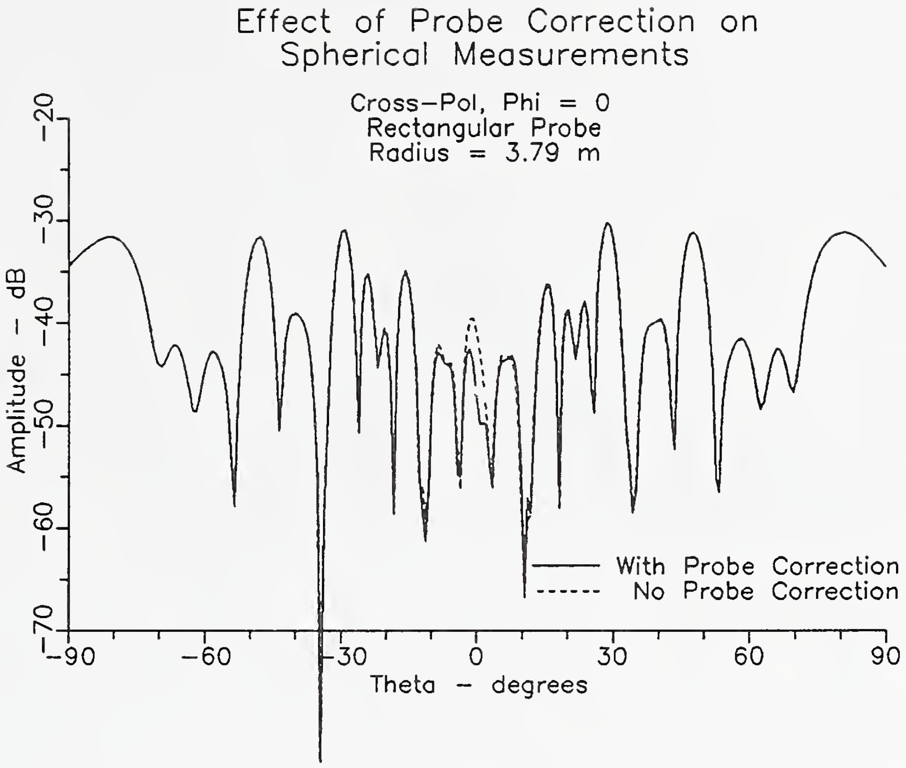

Figure 1.12 Comparison of far-field patterns calculated with and without probe correction from 3.79 m spherical near-field data. Rectangular probe, cross polarization, ϕ = 0° cut.

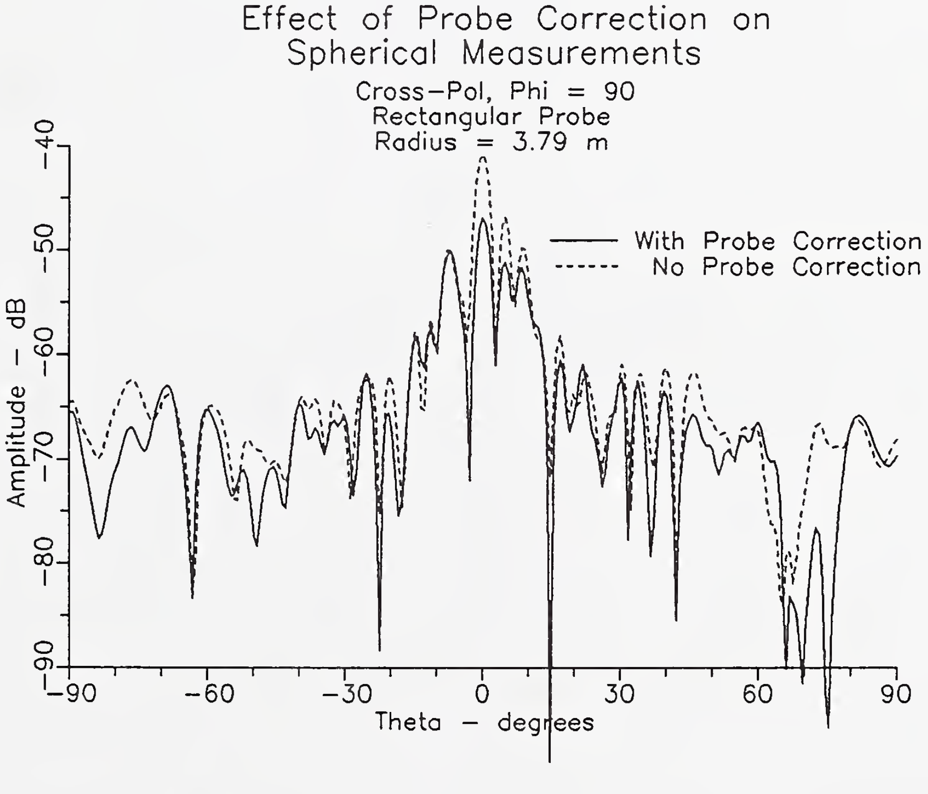

Figure 1.13 Comparison of far-field patterns calculated with and without probe correction from 3.79 m spherical near-field data. Rectangular probe, cross polarization, ϕ = 90° cut.

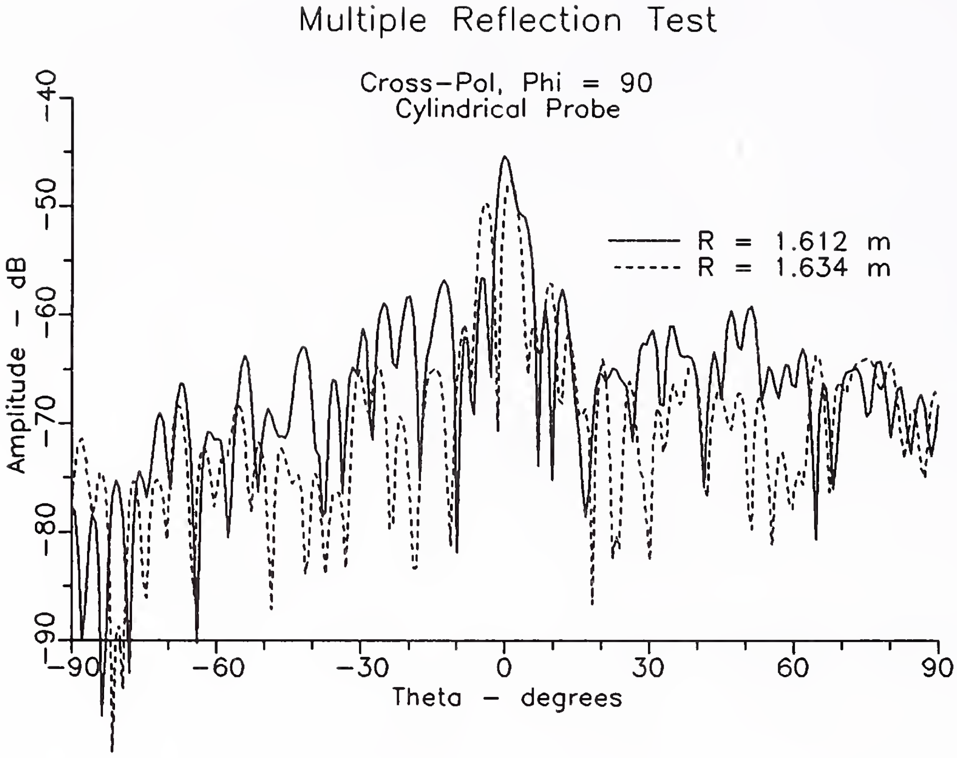

Figure 1.14 Comparison of far-field patterns calculated from near-field data acquired at two radii separated by λ/4. Probe corrected, circular probe, cross polarization, ϕ = 90° cut.

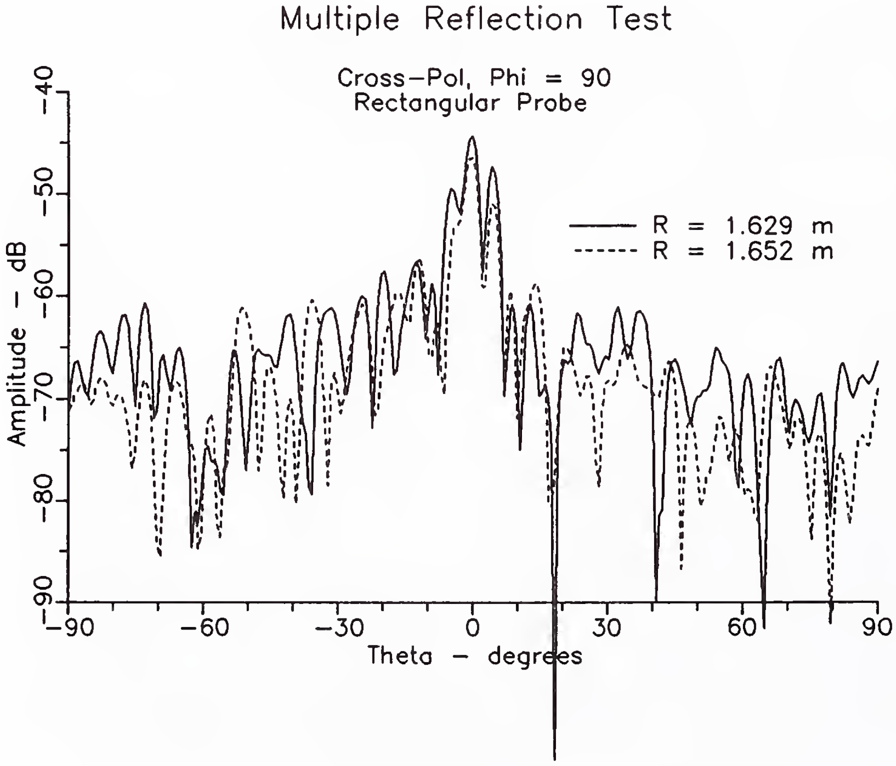

Figure 1.15 Comparison of far-field patterns calculated from near-field data acquired at two radii separated by λ/4. Probe corrected, rectangular probe, cross polarization, ϕ = 90° cut.

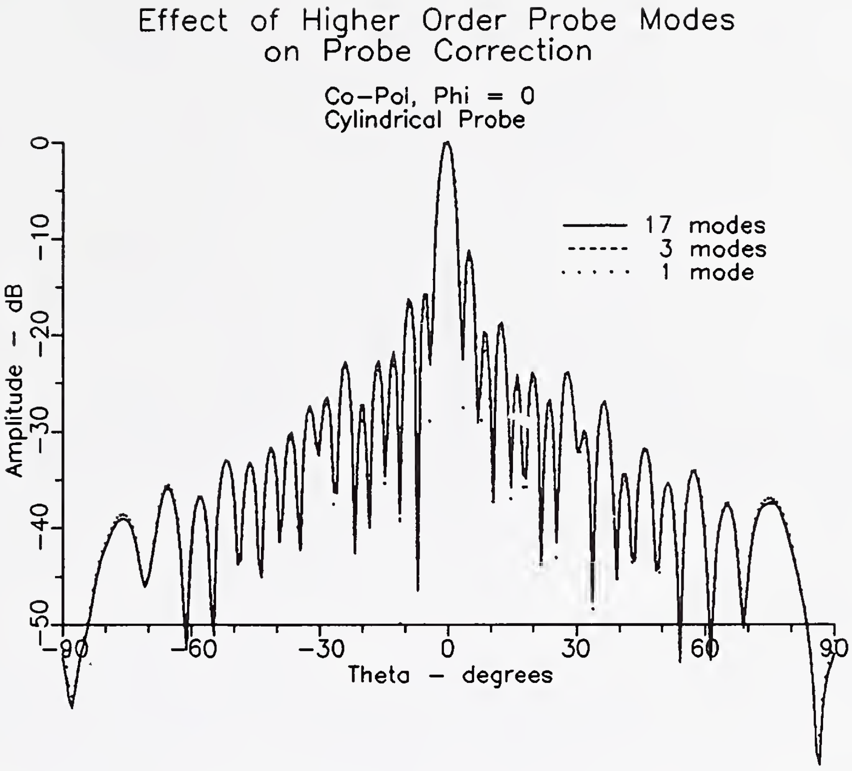

Figure 1.16 Probe corrected far-field patterns comparing results obtained with N_p = 1, 3, and 17. Circular probe, scan radius = 1.28 m, main polarization, ϕ = 0° cut.

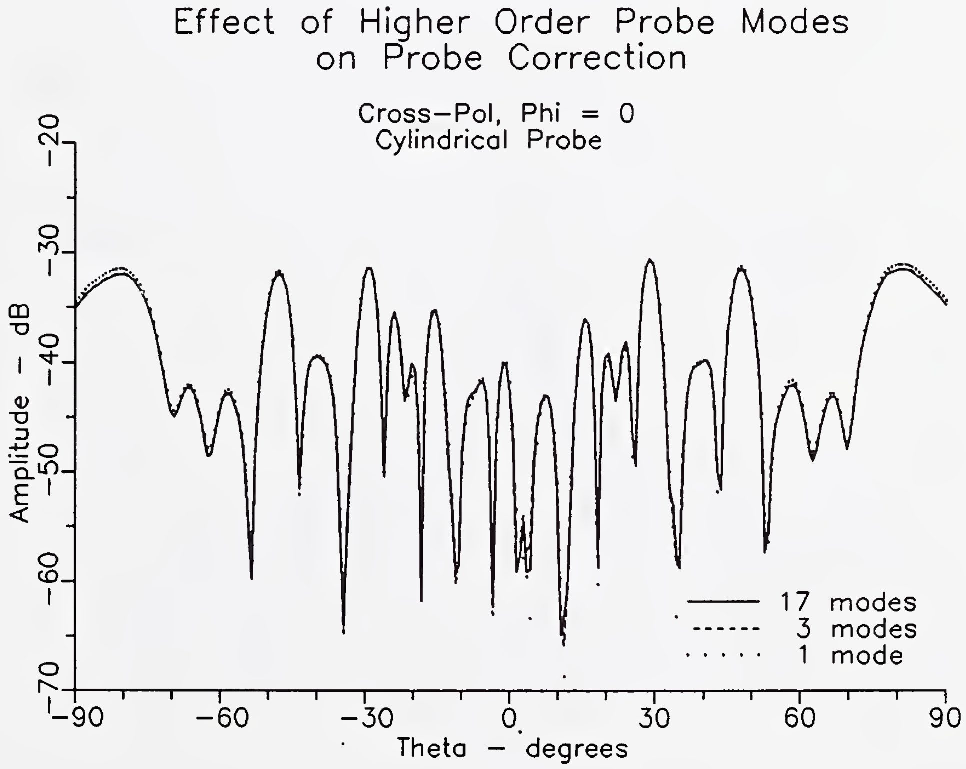

Figure 1.17 Probe corrected far-field patterns comparing results obtained with N_p = 1, 3, and 17. Circular probe, scan radius = 1.28 m, cross polarization, ϕ = 0° cut.

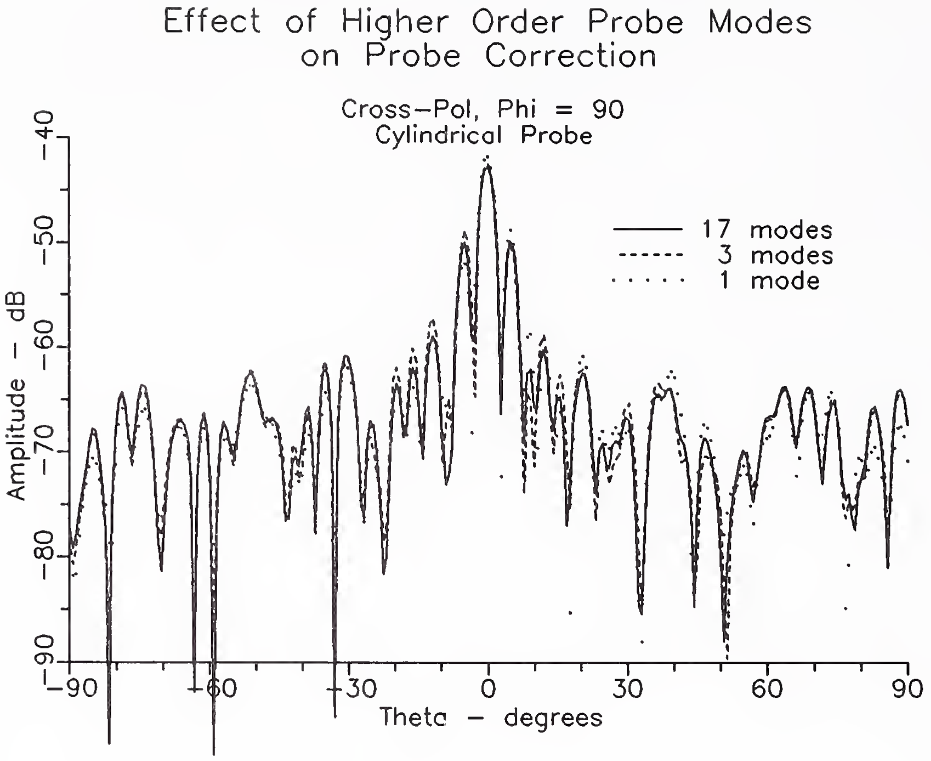

Figure 1.18 Probe corrected far-field patterns comparing results obtained with N_p = 1, 3, and 17. Circular probe, scan radius = 1.28 m, cross polarization, ϕ = 90° cut.

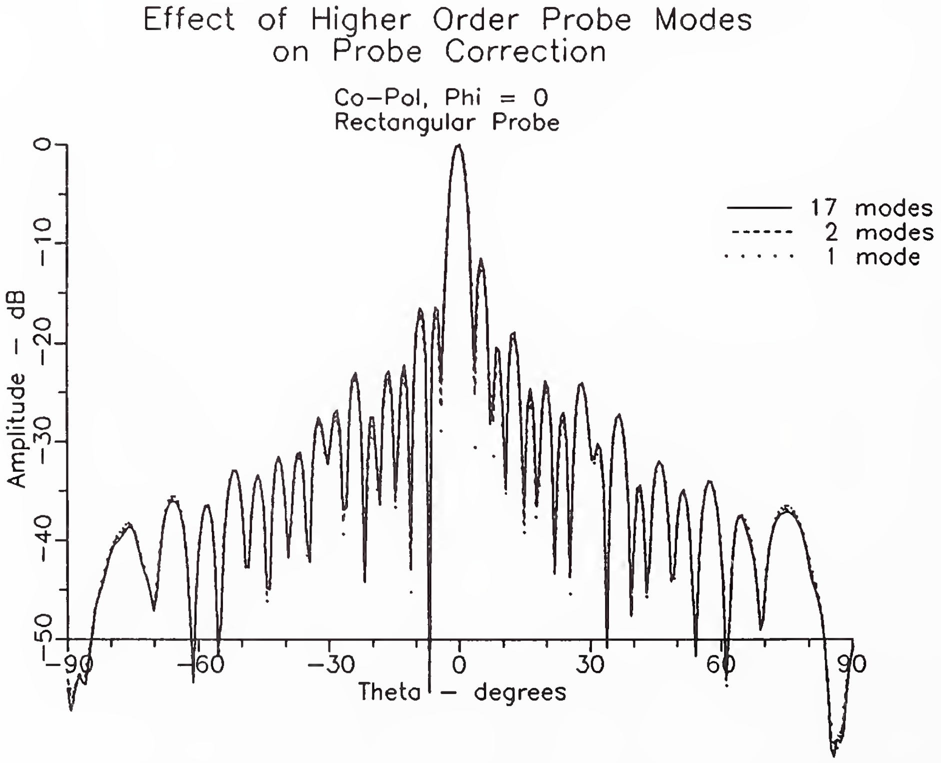

Figure 1.19 Probe corrected far-field patterns comparing results obtained with N_p = 1, 2, and 17. Rectangular probe, scan radius = 1.28 m, main polarization, ϕ = 0° cut.

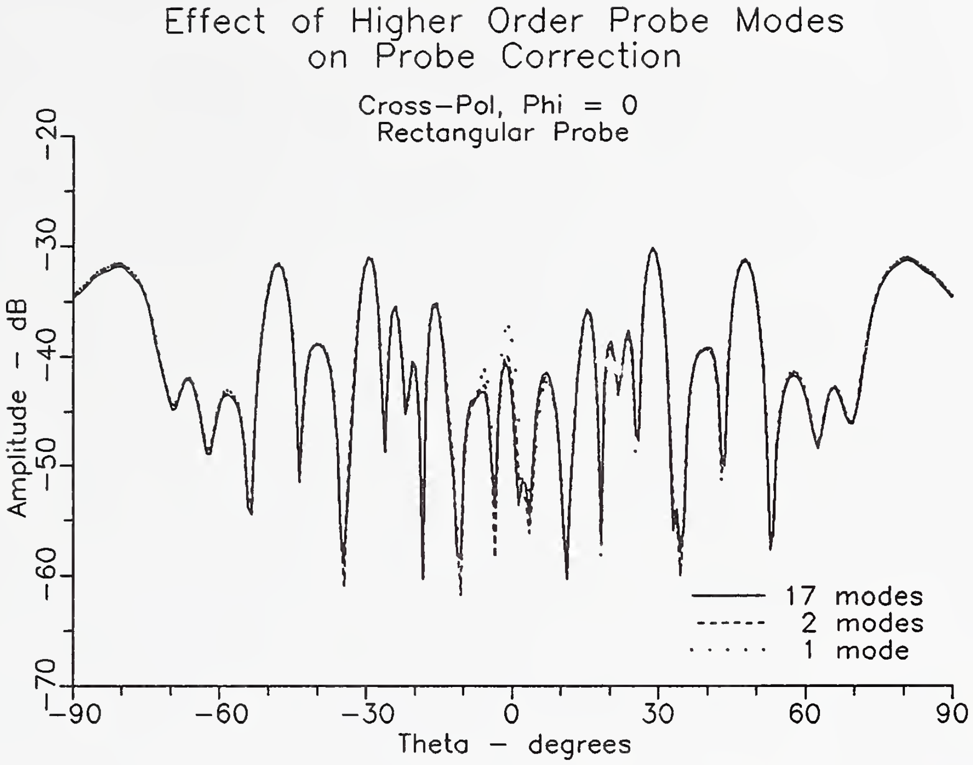

Figure 1.20 Probe corrected far-field patterns comparing results obtained with $N_p = 1, 2,$ and 17. Rectangular probe, scan radius = 1.28 m, cross polarization, $\phi = 0°$ cut.

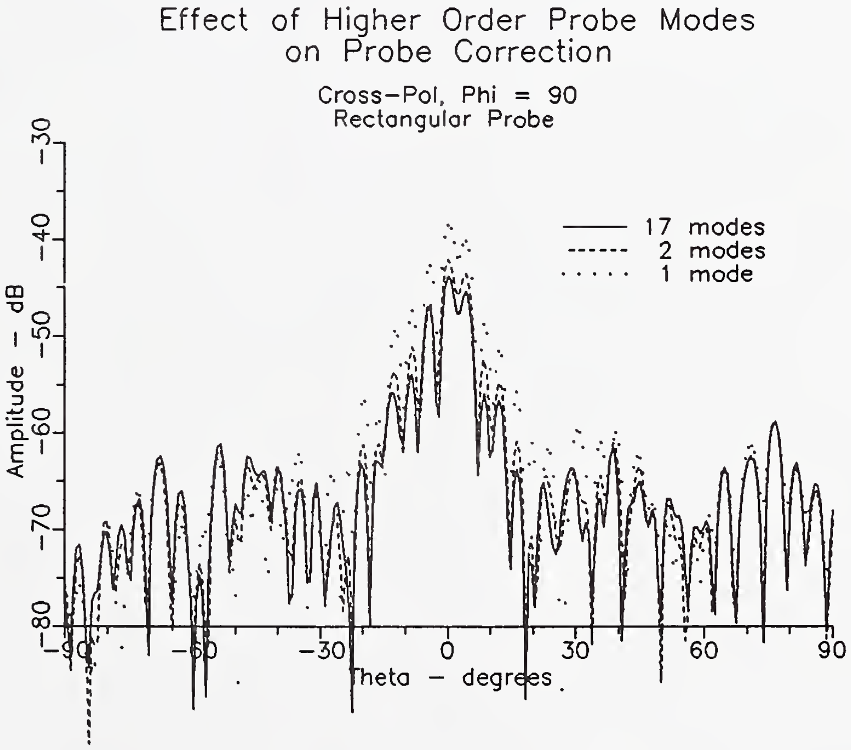

Figure 1.21 Probe corrected far-field patterns comparing results obtained with $N_p = 1, 2,$ and 17. Rectangular probe, scan radius = 1.28 m, cross polarization, $\phi = 90°$ cut.

2. PROBE PATTERN TRANSFORMATIONS

For a reciprocal probe, the receiving pattern $\mathbf{r}(\hat{\mathbf{k}})$ is given in terms of the far-field (transmitting) pattern $\mathbf{t}(\hat{\mathbf{k}})$ by the relationship (see Chapter 9),

$$\mathbf{r}(\hat{\mathbf{k}}) = \underline{\mathbf{S}}_y\ \mathbf{t}(-\hat{\mathbf{k}})/K\ , \qquad K = a_0\, k^2\, \eta_0\, Z_0\ , \tag{2-1}$$

where a_0 is the amplitude of the incident wave in the feed, η_0 is the characteristic admittance of the feed and $Z_0 = \sqrt{\frac{\mu_0}{\epsilon_0}}$ is the characteristic impedance of free space. The operator $\underline{\mathbf{S}}_y$, which produces a rotation of 180° about the y-axis, is included since the receiving pattern is desired with the probe pointed in the negative z-direction.

The far-field pattern is defined by the asymptotic formula

$$\mathbf{E}(\mathbf{r}) \xrightarrow[r \to \infty]{} \mathbf{t}(\hat{\mathbf{r}})\ \frac{\exp(ikr)}{(ikr)} \tag{2-2}$$

and may be expressed as an expansion in spherical harmonics:

$$\mathbf{t}(\hat{\mathbf{k}}) = \sum_{\nu\mu} \left[t^H_{\nu\mu}\ \mathbf{X}_{\nu\mu}(\hat{\mathbf{k}}) + t^E_{\nu\mu}\ i\mathbf{k} \times \mathbf{X}_{\nu\mu}(\hat{\mathbf{k}}) \right] . \tag{2-3}$$

(Spherical harmonics are defined according to Jackson [1, Chapter 16].) Because

$$\underline{\mathbf{S}}_y\ \mathbf{X}_{\nu\mu}(-\hat{\mathbf{k}}) = (-)^{\mu}\ \mathbf{X}_{\nu,-\mu}(\hat{\mathbf{k}})\ , \tag{2-4}$$

$\mathbf{r}$ is given by

$$\mathbf{r}(\hat{\mathbf{k}}) = \frac{1}{K} \sum_{\nu\mu} (-)^{\mu} \left[t^H_{\nu,-\mu}\ \mathbf{X}_{\nu\mu}(\hat{\mathbf{k}}) - t^E_{\nu,-\mu}\ i\hat{\mathbf{k}} \times \mathbf{X}_{\nu\mu}(\hat{\mathbf{k}}) \right] . \tag{2-5}$$

The probes that are commonly used in spherical scanning can be oriented so that the following symmetries apply:

$$t^{H,E}_{\nu\mu} = 0 \text{ if } \mu \text{ is even}$$

$$t^{H}_{\nu\mu} = - t^{H}_{\nu,-\mu} \qquad (2\text{-}6)$$

$$t^{E}_{\nu\mu} = t^{E}_{\nu,-\mu} .$$

Under these conditions the receiving pattern is directly proportional to the far-field pattern:

$$\mathbf{r}(\hat{\mathbf{k}}) = \mathbf{t}(\hat{\mathbf{k}})/K . \qquad (2\text{-}7)$$

3. THE PROBE AS AN IDEAL DIPOLE

3.1 Introduction

In spherical near-field scanning it is common to view a probe as an ideal dipole which measures the electric field at the probe position. When the spin angle χ is 0, the probe is considered (by convention) to measure the ϕ component of the incident electric field. When $\chi = -90^0$, the probe is considered to measure the θ component of the incident electric field. For an arbitrary probe, this assignment has no physical significance as long as probe correction is employed correctly. However, for certain simple probes (usually small) a dipole approximation may be very good. An open-ended rectangular waveguide probe, for example, can give excellent results if it is treated as an electric dipole centered in the aperture and directed parallel to the shorter sides. On the other hand, theory and experiment indicate that the open-ended rectangular waveguide probe is better approximated by a magnetic dipole directed parallel to the longer sides. In these notes we compare the description of a probe as an electric dipole with its description as a perpendicularly oriented magnetic dipole. While as the measurement sphere recedes to infinity the two points of view become equivalent, there can be significant differences in the near field.

3.2 Spherical-Wave Expansions of the Transverse Fields

The transverse electric and magnetic fields may be written

$$\begin{aligned} \mathbf{E}_t(\mathbf{r}) &= \sum_{nm}\left[b^H_{nm}\, f_n(kr)\, \mathbf{X}_{nm}(\hat{\mathbf{r}}) + b^E_{nm}\, g_n(kr)\, i\hat{\mathbf{r}} \times \mathbf{X}_{nm}(\hat{\mathbf{r}})\right] \\ \mathbf{H}_t(\mathbf{r}) &= \frac{1}{iZ_0}\sum_{nm}\left[b^H_{nm}\, g_n(kr)\, i\hat{\mathbf{r}} \times \mathbf{X}_{nm}(\hat{\mathbf{r}}) + b^E_{nm}\, f_n(kr)\, \mathbf{X}_{nm}(\hat{\mathbf{r}})\right] , \end{aligned} \tag{3-1}$$

where

$$f_n(x) = h_n^{(1)}(x) , \qquad g_n(x) = \frac{1}{ix}\frac{d}{dx}\left[x\, f_n(x)\right] .$$

Here, $h_n^{(1)}(x)$ is a spherical Hankel function of the first kind and $\mathbf{X}_{nm}(\hat{\mathbf{r}})$ is vector spherical harmonic. Jackson [1, Chapter 16] may be consulted for the elementary properties of these functions.

3.3 **The Electric Dipole Probe**

Consider an electric dipole located at $r_0\hat{\mathbf{z}}$ and directed in the $\hat{\mathbf{y}}$ direction. (This corresponds to the spin angle $\chi = 0^0$.) The probe is positioned at $r_0\hat{\mathbf{r}} = (r_0,\theta,\phi)$ by first rotating it by an angle θ about the laboratory y axis followed by a rotation by an angle ϕ about the laboratory z axis. When positioned in this way, the dipole will point in the $\hat{\boldsymbol{\phi}}$ direction; hence, the probe output will be $W(r_0,\phi,\theta,\chi=0^0) = E_\phi$. Similarly, we may begin with the probe at $r_0\hat{\mathbf{z}}$ but directed in the $\hat{\mathbf{x}}$ direction. (This corresponds to the spin angle $\chi = -90^0$.) When the probe is positioned at $r_0\hat{\mathbf{r}}$ as described above, it will point in the $\hat{\boldsymbol{\theta}}$ direction; hence, the probe output will be $W(r_0,\phi,\theta,\chi=-90^0) = E_\theta$. Data taken in the two spin orientations can be combined into a vector probe response

$$\mathbf{W}(r_0\hat{\mathbf{r}}) = W(r_0,\phi,\theta,\chi=-90^0)\ \hat{\boldsymbol{\theta}} + W(r_0,\phi,\theta,\chi=0^0)\ \hat{\boldsymbol{\phi}} = \mathbf{E}_t(r_0\hat{\mathbf{r}})$$

$$= \sum_{nm}\left[b_{nm}^H\ f_n(kr_0)\ \mathbf{X}_{nm}(\hat{\mathbf{r}}) + b_{nm}^E\ g_n(kr_0)\ i\hat{\mathbf{r}} \times \mathbf{X}_{nm}(\hat{\mathbf{r}})\right] . \qquad (3\text{-}2)$$

With Eq (2) and the orthonormality of vector spherical harmonics, the modal coefficients can be calculated in terms of the measured data:

$$b_{nm}^H = \frac{1}{f_n(kr_0)} \int \mathbf{W}(r_0\hat{\mathbf{r}}) \cdot \mathbf{X}_{nm}^*(\hat{\mathbf{r}})\ d\hat{\mathbf{r}}$$

$$(3\text{-}3)$$

$$b_{nm}^E = \frac{1}{g_n(kr_0)} \int \mathbf{W}(r_0\hat{\mathbf{r}}) \cdot [i\hat{\mathbf{r}} \times \mathbf{X}_{nm}(\hat{\mathbf{r}})]^*\ d\hat{\mathbf{r}} .$$

3.4 **The Magnetic Dipole Probe**

Now consider a probe at $r_0\hat{\mathbf{z}}$ with $\chi = 0^0$ corresponding to a $-\hat{\mathbf{x}}$ directed magnetic dipole and $\chi = -90^0$ corresponding to a $\hat{\mathbf{y}}$ directed magnetic dipole. Following the conventions of Section 3.3 we may define a vector response

$$\mathbf{W}(r_0\hat{\mathbf{r}}) = H_\phi\hat{\boldsymbol{\theta}} - H_\theta\hat{\boldsymbol{\phi}} = \mathbf{H}_t(r_0\hat{\mathbf{r}}) \times \hat{\mathbf{r}}$$

$$= \frac{1}{Z_0}\sum_{nm}\left[b_{nm}^H\, g_n(kr_0)\, \mathbf{X}_{nm}(\hat{\mathbf{r}}) + b_{nm}^E\, f_n(kr_0)\, i\hat{\mathbf{r}} \times \mathbf{X}_{nm}(\hat{\mathbf{r}})\right] . \qquad (3\text{-}4)$$

Remember that the ϕ component of **W** corresponds to $\chi = 0$ and the θ component corresponds to $\chi = -90^0$.

With Eq (4) and the orthonormality of vector spherical harmonics, the modal coefficients can be calculated in terms of the measured data:

$$b_{nm}^H = \frac{Z_0}{g_n(kr_0)} \int \mathbf{W}(r_0\hat{\mathbf{r}}) \cdot \mathbf{X}_{nm}^*(\hat{\mathbf{r}})\, d\hat{\mathbf{r}}$$

$$(3\text{-}5)$$

$$b_{nm}^E = \frac{Z_0}{f_n(kr_0)} \int \mathbf{W}(r_0\hat{\mathbf{r}}) \cdot [i\hat{\mathbf{r}} \times \mathbf{X}_{nm}(\hat{\mathbf{r}})]^*\, d\hat{\mathbf{r}} .$$

Equations (3) and (5) are quite similar in form but differ importantly in the reversed roles of f and g. In the limit $r_0 \longrightarrow \infty$,

$$f_n(x) \approx g_n(x) \sim i^{-n} \frac{\exp(ikr)}{ikr}$$

so that the fields calculated assuming an electric or magnetic dipole probe are proportional. In the near field, on the other hand, the corresponding coefficients can disagree appreciably, especially near the mode cutoff limit $kr_0 \approx n$.

3.5 **Numerical Results**

The spherical near-field program was modified to reverse the roles of f and g as described above. Near-field data acquired with the rectangular probe were then processed using the modified program. Figures 3.1 through 3.4 show the comparison between far-field patterns processed assuming an electric dipole probe (using the standard program which assumes that the probe measures the electric field at a point) and a magnetic dipole probe. The co-polarization results are very similar. In the cross polarization, the $\phi = 0^0$ cut obtained with the magnetic dipole assumption agrees somewhat more closely to the probe corrected results taken with the cylindrical probe than the corresponding cut processed with the electric dipole approximation. The $\phi = 90^0$ cut does not agree well in either case for cross polarization.

If measurements are performed with no probe correction, one caution must be observed. To minimize errors due to the tilt angle of the probe, the probe should be aligned with the electrical polarization axis parallel to x or y in the laboratory coordinate system. This does require that the probe be calibrated prior to use rather than after use as is often the case.

3.6 **Conclusions**

From the results presented, it is not clear whether the magnetic dipole model gives better results than the electric dipole model for the rectangular waveguide probe. This may be understood by observing that the patterns of the electric dipole, the magnetic dipole, and the rectangular waveguide are very similar over the angle subtended by the antenna under test. This results in very similar patterns for the antenna under test except for regions of very low levels of cross polarization.

For the examples presented, not using a probe correction is certainly feasible as long as the cross-polarized data are not needed below about 30 dB. Also, unless the probe is aligned so that the electrical axis is parallel to the reference coordinate, we are likely to get poor results for cross polarization near the main beam. (This may be a serious limitation for the technique.)

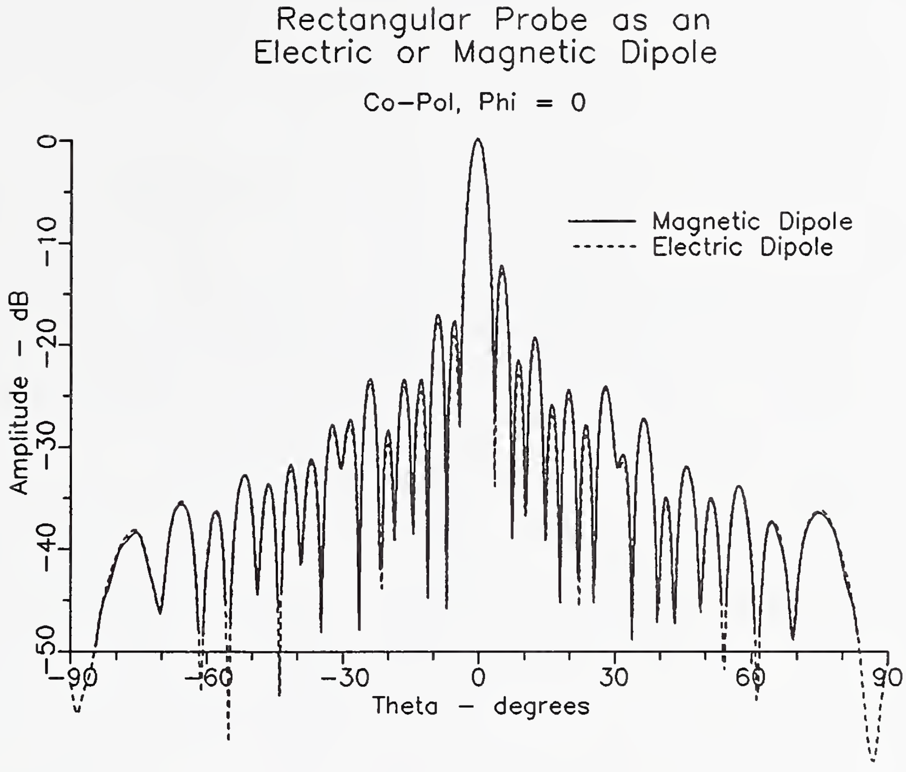

Figure 3.1 Comparison of far-field patterns calculated from near-field data acquired using a rectangular probe. No probe correction was employed but in one case a magnetic dipole probe is assumed and in the other case, an electric dipole is assumed. Main polarization, $\phi = 0°$ cut.

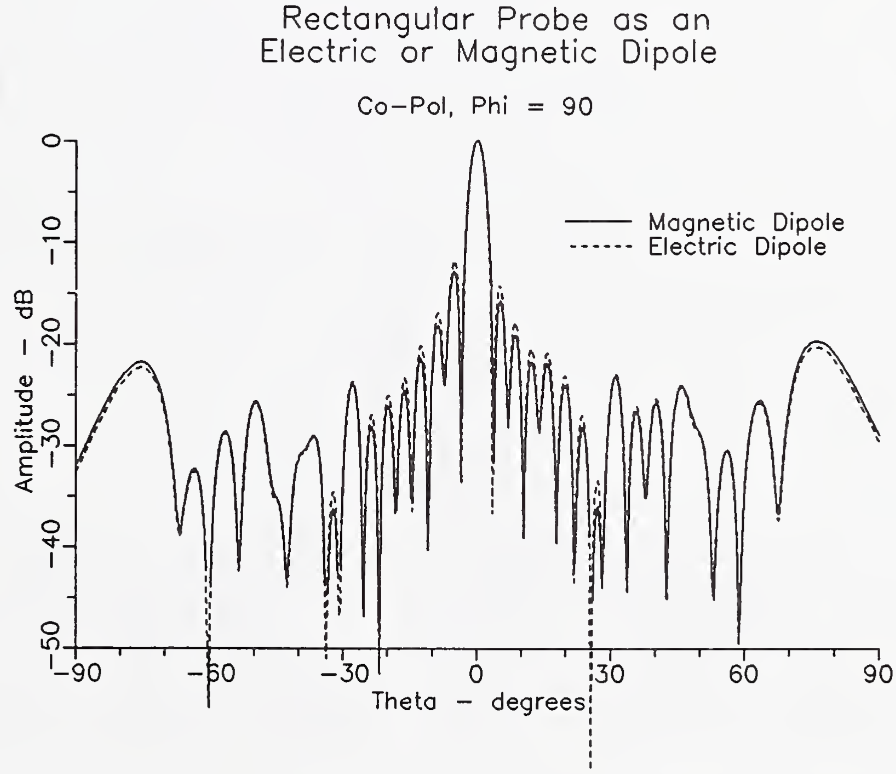

Figure 3.2 Comparison of far-field patterns calculated from near-field data acquired using a rectangular probe. No probe correction was employed but in one case a magnetic dipole probe is assumed and in the other case, an electric dipole is assumed. Main polarization, $\phi = 90°$ cut.

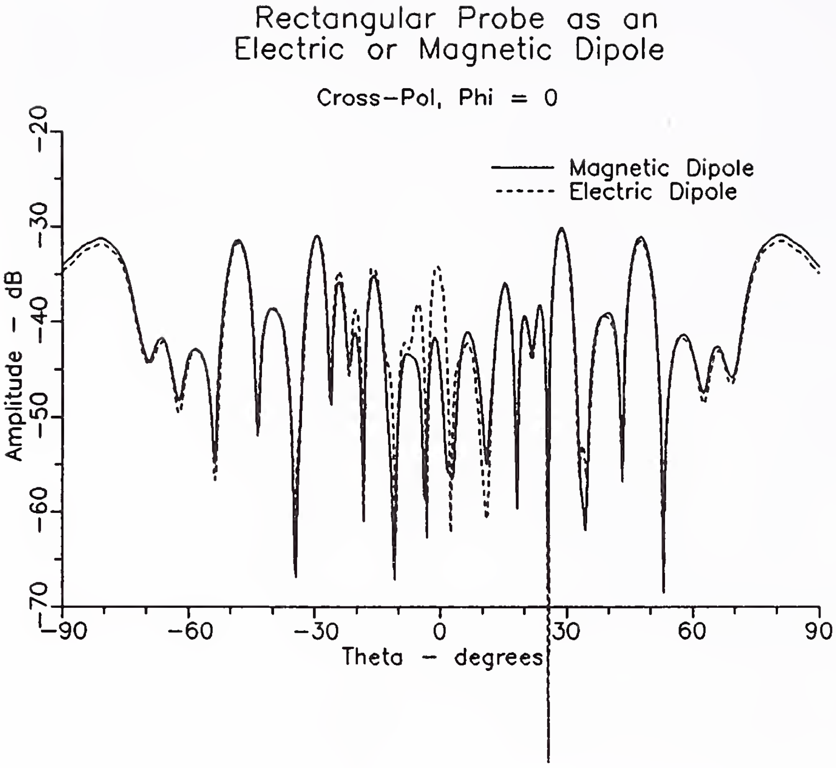

Figure 3.3 Comparison of far-field patterns calculated from near-field data acquired using a rectangular probe. No probe correction was employed but in one case a magnetic dipole probe is assumed and in the other case, an electric dipole is assumed. Cross polarization, ϕ = 0° cut.

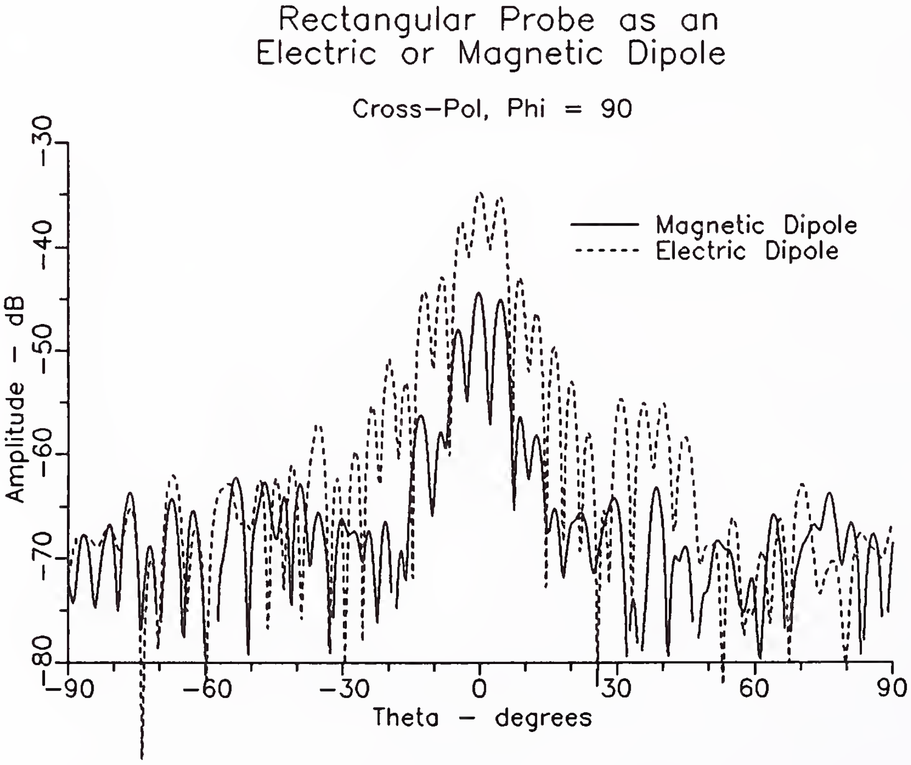

Figure 3.4 Comparison of far-field patterns calculated from near-field data acquired using a rectangular probe. No probe correction was employed but in one case a magnetic dipole probe is assumed and in the other case, an electric dipole is assumed. Cross polarization, ϕ = 90° cut.

4. TESTING THE PROBE CORRECTION SOFTWARE BY SIMULATION

4.1 Introduction

Experimental verification of the probe correction software has been a difficult task since, at least for the small probes employed so far, the probe effect is difficult to separate from normal measurement uncertainties. As a result, it is apparent that a more thorough test by simulation is desirable. An analytical check will allow verification to full machine precision. In addition, since there is no physical restriction on the size of the "minimum sphere," the probe effect can be made relatively more important.

To test the probe correction software analytically we must be able to compute the coupling between the test antenna and probe. This can be done generally by one of the following two methods: (1) The coupling integral can be computed numerically for each measurement orientation [2]; or, (2) the coupling can be computed by applying a differential operator representation for the probe [3]. Both approaches are computationally intensive. The former is approximate since the integration range must be truncated. The latter requires extensive symbolic manipulations. As a first attempt, we propose to adopt a less general approach by restricting our attention to elemental dipole probes which measure components of the electric and magnetic field.

When a dipole probe is located on the measurement sphere, the transmission formula reduces to the ideal probe case; however, if the dipole is offset from the measurement sphere, the result is nontrivial. The far-field pattern of an offset dipole probe can be generated easily and the no-probe correction program can be used to calculate the spherical mode expansion coefficients. In turn these can be used to generate the translated probe coefficients in the standard fashion, assuming reciprocity and rotating about the laboratory y axis so the probe z axis points in the laboratory -z direction. On the other hand, the offset probe still measures the field, though at a location displaced from the actual measurement sphere. Armed with the translated probe coefficients and the "measured" data we can then run the spherical near-field scanning program to verify that the probe compensation is correct.

Since an arbitrary $\mu = \pm 1$ probe can be uniformly approximated by an endfire (radial) array of transverse dipoles [4], our approach is actually quite general. Although not proposed as part of the present effort, transverse displacement of the probe could be considered. This would allow simulation of the effects of higher order azimuthal dependence and evaluation of methods of accounting for these terms in a more general probe correction scheme.

4.2 The Far-Field Pattern of Elemental Electric and Magnetic Dipoles

In the limit $\mathbf{r} \longrightarrow \infty$, the electric fields of elemental dipoles are given by the asymptotic expressions

$$\begin{aligned}
\mathbf{m}_{10}(\mathbf{r}) &\sim \mathbf{p}^{H}(\hat{\mathbf{z}},\hat{\mathbf{r}})\,\frac{\exp(ikr)}{ikr} \\
\mathbf{m}_{1,\pm1}(\mathbf{r}) &\sim \mp\frac{1}{\sqrt{2}}\left[\mathbf{p}^{H}(\hat{\mathbf{x}},\hat{\mathbf{r}}) \pm i\mathbf{p}^{H}(\hat{\mathbf{y}},\hat{\mathbf{r}})\right]\frac{\exp(ikr)}{ikr} \qquad (4\text{-}1) \\
\mathbf{n}_{1\mu} &= i\hat{\mathbf{r}} \times \mathbf{m}_{1\mu}\ ,
\end{aligned}$$

where

$$\mathbf{p}^{H}(\hat{\mathbf{n}},\hat{\mathbf{r}}) = \sqrt{\frac{3}{8\pi}}\,\hat{\mathbf{n}} \times \hat{\mathbf{r}} \qquad (4\text{-}2)$$

is the far-electric-field pattern of a $\hat{\mathbf{n}}$ directed magnetic dipole. The far-electric-field pattern of an $\hat{\mathbf{n}}$ directed electric dipole is given by

$$\mathbf{p}^{E}(\hat{\mathbf{n}},\hat{\mathbf{r}}) = i\hat{\mathbf{r}} \times \mathbf{p}^{H}(\hat{\mathbf{n}},\hat{\mathbf{r}}) = i\sqrt{\frac{3}{8\pi}}\,\hat{\mathbf{n}} \cdot (\mathbf{1} - \hat{\mathbf{r}}\hat{\mathbf{r}})\ . \qquad (4\text{-}3)$$

When $\mu = \pm1$, the elemental fields are circularly, rather than linearly polarized.

A transverse dipole probe can be expressed as a superposition of x and y directed dipoles. For reference we give the spherical harmonic expansions and polar coordinate forms:

$$\begin{aligned}
\mathbf{p}^{H}(\hat{\mathbf{x}},\hat{\mathbf{r}}) &= \frac{i}{\sqrt{2}}\,[\mathbf{X}_{11}(\hat{\mathbf{r}}) - \mathbf{X}_{1,-1}(\hat{\mathbf{r}})] = -\sqrt{\frac{3}{8\pi}}\,[\ \sin\phi\ \hat{\boldsymbol{\theta}} + \cos\theta\ \cos\phi\ \hat{\boldsymbol{\phi}}] \\
& \qquad (4\text{-}4) \\
\mathbf{p}^{H}(\hat{\mathbf{y}},\hat{\mathbf{r}}) &= \frac{1}{\sqrt{2}}\,[\mathbf{X}_{11}(\hat{\mathbf{r}}) + \mathbf{X}_{1,-1}(\hat{\mathbf{r}})] = -\sqrt{\frac{3}{8\pi}}\,[-\cos\phi\ \hat{\boldsymbol{\theta}} + \cos\theta\ \sin\phi\ \hat{\boldsymbol{\phi}}]\ .
\end{aligned}$$

Let

$$\hat{\mathbf{n}} = -\sin\chi_0\ \hat{\mathbf{x}} + \cos\chi_0\ \hat{\mathbf{y}}\ , \tag{4-5}$$

where χ_0 is measured in the positive sense from the y axis (laboratory coordinates). The far-field patterns

$$\begin{aligned} \mathbf{p}^{H}(\chi_0,\hat{\mathbf{r}}) &= -\sin\chi_0\ \mathbf{p}^{H}(\hat{\mathbf{x}},\hat{\mathbf{r}}) + \cos\chi_0\ \mathbf{p}^{H}(\hat{\mathbf{y}},\hat{\mathbf{r}}) \\ \mathbf{p}^{E}(\chi_0,\hat{\mathbf{r}}) &= i\hat{\mathbf{r}} \times \mathbf{p}^{H}(\chi_0,\hat{\mathbf{r}}) \end{aligned} \tag{4-6}$$

represent arbitrarily oriented transverse dipoles. When $\chi_0 = 0^0$, the dipoles are y directed (vertical in the laboratory coordinate system). When $\chi_0 = -90^0$, the dipoles are x directed. Although we have stayed with linear polarization, elliptical polarization could be incorporated by including a relative phase component between the x and y directed dipole components.

The final degree of freedom we allow the probe is a translation in the z direction. This introduces higher order multipoles while still preserving the $\mu = \pm 1$ character. Consider a translation of $\rho\hat{\mathbf{z}}$ where ρ may be positive or negative. The far-field dipole patterns are

$$\begin{aligned} \mathbf{p}^{H}(\rho,\chi_0,\hat{\mathbf{r}}) &= \mathbf{p}^{H}(\chi_0,\hat{\mathbf{r}})\ \exp(-ik\rho\cos\theta) \\ \mathbf{p}^{E}(\rho,\chi_0,\hat{\mathbf{r}}) &= i\hat{\mathbf{r}} \times \mathbf{p}^{H}(\rho,\chi_0,\hat{\mathbf{r}})\ . \end{aligned} \tag{4-7}$$

The far field patterns of Eq (7) may be expanded in spherical harmonics to get

$$\mathbf{p}^{H,E}(\rho,\chi_0,\hat{\mathbf{r}}) = \sum_{n=1}^{\infty} {\sum_{m=-1}^{1}}' \left[B_{nm}^{H,E}(\rho,\chi_0)\ \mathbf{X}_{nm}(\hat{\mathbf{r}}) + C_{nm}^{H,E}(\rho,\chi_0)\ i\hat{\mathbf{r}} \times \mathbf{X}_{nm}(\hat{\mathbf{r}}) \right]\ . \tag{4-8}$$

The prime (′) indicates that m = 0 is not included in the summation. While the coefficients B and C can be computed analytically using translation formulas for the dipole case, this basically repeats the procedure used in calculating the translated probe coefficients. It is preferable and probably easier to generate a sampled far field from Eq (7) and compute the coefficients numerically using the well-tested, no-probe correction program. Of course the sampling criteria and the number of multipoles must be computed as they would be for an antenna with a minimum sphere of radius ρ. The degenerate cases given in Eq (4) can be used to check the procedure. (Nevertheless, to provide a further comparison, we have created a stand-alone program to calculate the coefficients directly from the translation formulas. See Chapter 5.)

4.3 **The Receiving Pattern**

For a reciprocal antenna

$$\mathbf{r}'(\hat{\mathbf{k}}) = \mathbf{t}(-\hat{\mathbf{k}})/K \ , \qquad K = i\sqrt{3\pi/2} \ , \tag{4-9}$$

where $\mathbf{r}'$ and $\mathbf{t}$ are the receiving and far-field (transmitting) patterns of our probe. The choice of K ensures that the probe is "calibrated" to measure field strength.

To orient the probe correctly for spherical scanning, it must be rotated by 180^0 about the laboratory y axis (see Chapter 2)

$$\mathbf{r}(\mathbf{k}) = \underline{\mathbf{S}}_y \ \mathbf{r}'(\mathbf{k}) \ , \tag{4-10}$$

where $\underline{\mathbf{S}}_y$ is the appropriate rotation matrix. Since

$$\underline{\mathbf{S}}_y \ \mathbf{X}_{nm}(-\hat{\mathbf{r}}) = (-)^m \ \mathbf{X}_{n,-m}(\hat{\mathbf{r}}) \ , \tag{4-11}$$

we have from Eq (8)

$$\mathbf{r}^{H,E}(\hat{\mathbf{k}}) = -\frac{1}{K} \sum_{n=1}^{\infty} {\sum_{m=-1}^{1}}' \left[B_{n,-m}^{H,E} \ \mathbf{X}_{nm}(\hat{\mathbf{k}}) - C_{n,-m}^{H,E} \ i\hat{\mathbf{r}} \times \mathbf{X}_{nm}(\hat{\mathbf{k}}) \right] \ . \tag{4-12}$$

Dependence on ρ and χ_0 has been suppressed in Eq (12). As a check, for a y directed electric dipole or an x directed magnetic dipole,

$$\mathbf{r}^{H,E}(\hat{\mathbf{k}}) = \mathbf{p}^{H,E}(\hat{\mathbf{k}})/K \ ,$$

while for an x directed electric dipole or a y directed magnetic dipole,

$$\mathbf{r}^{H,E}(\hat{\mathbf{k}}) = -\mathbf{p}^{H,E}(\hat{\mathbf{k}})/K \ .$$

The coefficients of the vector spherical harmonics in Eq (12) are the input data for the translated probe coefficient program.

4.4 **The Probe Response**

We have created a probe with a minimum sphere of radius $|\rho|$ which we will scan on a measurement sphere of radius $r_0 > |\rho|$. Because of the construction of this probe it is apparent that it actually measures the field strength on a sphere of radius $r_0 - \rho$:

$$W^H(r_0,\phi,\theta,\chi=0^\circ) = \sin\chi_0 \; iZ_0H_\theta(r_0-\rho,\theta,\phi) + \cos\chi_0 \; iZ_0H_\phi(r_0-\rho,\theta,\phi) \tag{4-13}$$

$$W^H(r_0,\phi,\theta,\chi=-90^\circ) = \cos\chi_0 \; iZ_0H_\theta(r_0-\rho,\theta,\phi) - \sin\chi_0 \; iZ_0H_\phi(r_0-\rho,\theta,\phi) \tag{4-14}$$

$$W^E(r_0,\phi,\theta,\chi=0^\circ) = \sin\chi_0 \; E_\theta(r_0-\rho,\theta,\phi) + \cos\chi_0 \; E_\phi(r_0-\rho,\theta,\phi) \tag{4-15}$$

$$W^E(r_0,\phi,\theta,\chi=-90^\circ) = \cos\chi_0 \; E_\theta(r_0-\rho,\theta,\phi) - \sin\chi_0 \; E_\phi(r_0-\rho,\theta,\phi) \; . \tag{4-16}$$

Equations (13) through (16) follow from Eqs (2), (3), (9), and (10). The spin angle χ should not be confused with χ_0, which is an alignment parameter built into the probe definition. Modal expansions for **E** and $iZ_0\mathbf{H}$ can be written as follows:

$$\mathbf{E}(\mathbf{r}) = \sum_{nm} \left[b^H_{nm} \, \mathbf{m}_{nm}(\mathbf{r}) + b^E_{nm} \, \mathbf{n}_{nm}(\mathbf{r}) \right] \tag{4-17}$$

$$iZ_0\mathbf{H}(\mathbf{r}) = \sum_{nm} \left[b^H_{nm} \, \mathbf{n}_{nm}(\mathbf{r}) + b^E_{nm} \, \mathbf{m}_{nm}(\mathbf{r}) \right] \; . \tag{4-18}$$

4.5 **Summary of the Algorithm**

The major steps in the probe simulation test are given here:

(1) Use Eq (7) to create the far field of the desired offset probe, $-r_0 < \rho < r_0$. Abide by the sampling theorem for a minimum sphere of radius ρ.

(2) Use the program (without probe compensation) to find the coefficients of the vector spherical harmonic expansion Eq (8).

(3) Obtain the coefficients of the receiving pattern as given in Eq (12).

(4) Calculate translated probe coefficients for the offset probe using the existing program.

(5) Calculate the "measured" data with Eqs (13)-(16).

(6) Run the program (with probe compensation). The probe correction should become severe when ρ approaches r_0.

4.6 **Numerical Results**

A verification of the probe correction software was undertaken using the test outlined in the previous section. A program was written which calculates the far-field pattern of the offset dipole as given in Eq (7). The far-field pattern for a y directed dipole located 25 cm from the origin along the z axis was calculated and used as input to program SPHERE which calculates the transmitting coefficients of this translated dipole. The coefficients which were calculated are shown in Figure 4.1. The 31 modes calculated are sufficient to completely describe the translated dipole. These coefficients are then used as input to the probe translation program TRPRCF which calculates the coefficients for a probe which is translated back to the true measurement sphere. These coefficients were compared to those calculated analytically in Chapter 5. Agreement between the two techniques was to machine accuracy. Near-field data obtained with the rectangular probe were used to calculate spherical modes with a maximum n = 87. From these modes a new near-field was calculated for the same radius as the original data which was then used as the hypothetical measured data. The probe coefficients which were calculated for the offset dipole were then used for probe correction using a measurement radius of 152.95 cm (the sum of the true measurement radius of 127.95 and the 25 cm offset). The geometry is illustrated in Figure 4.2.

Results of this procedure are given in Figures 4.3 to 4.6. The probe correction applied to the shifted radius data agrees extremely well with the no-probe correction results calculated for 127.95 cm. For comparison, we also show the results when no probe correction is employed but a radius of 152.95 cm is used for the calculation.

4.7 Conclusions

The probe correction correctly accounts for the offset dipole, whereas the incorrect radius with no probe correction gives grossly incorrect results. The uncorrected results illustrate the expected effect of neglecting the correction in severe cases, such as broadening of the main beam and null filling. In contrast to the probe correction observed in Chapter 1 on real data, the effect of probe correction is clearly present and correctly accounts for the radius shift, with the difference between the actual 127.95 cm and probe corrected 152.95 cm results being essentially undetectable.

A directive probe can be simulated by an endfire array of dipoles. It is sufficient to demonstrate that a single shifted dipole properly accounted for with probe correction correctly produces the far-field pattern of the test antenna. Since the contribution of each element of the dipole array will produce a correct far-field pattern, the sum of these patterns will, since the mathematical process is linear, still be the correct pattern.

The test of the probe correction algorithm and its implementation in the programs SPHERE and TRPRCF is thus deemed to be successful.

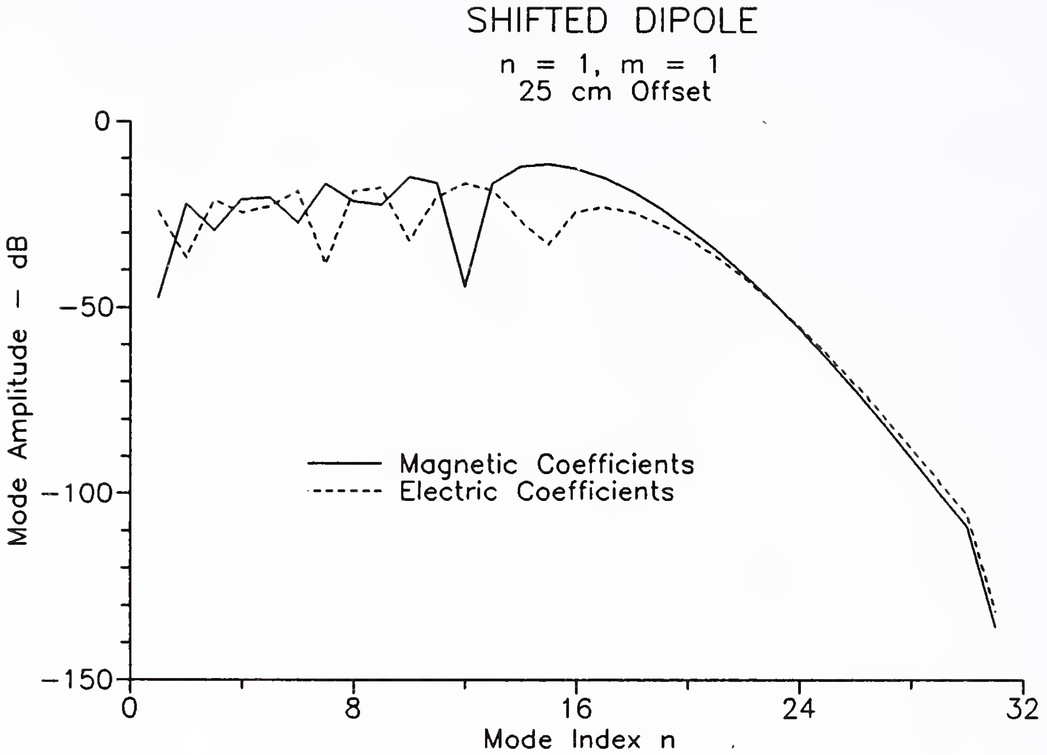

Figure 4.1 Mode amplitudes for a y directed electric dipole offset 25 cm in the +z direction. Normalization is such that amplitude of $t^E_{1,\pm1}$ is -3 dB for the dipole at the origin.

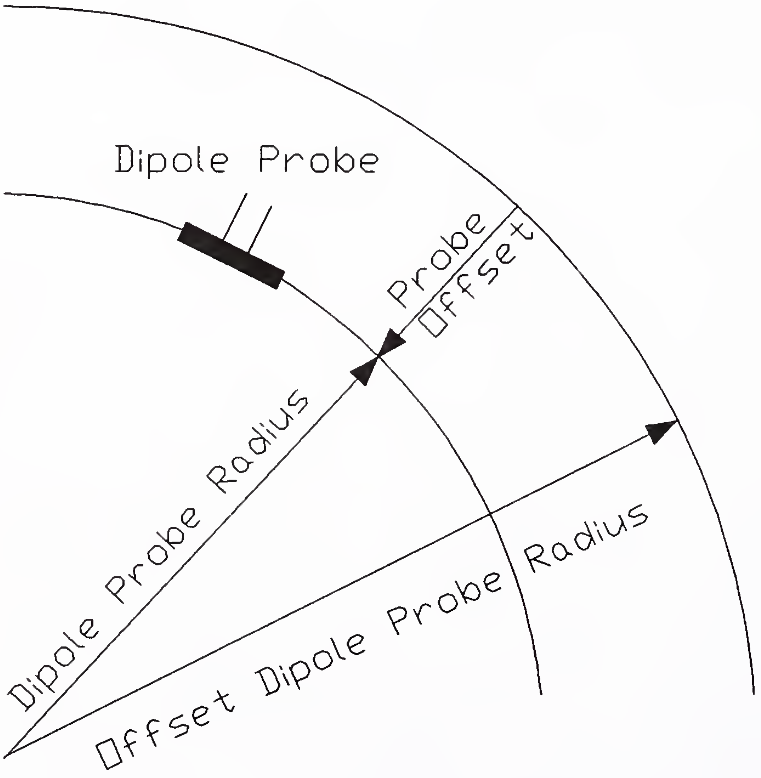
Dipole Probe
Probe Offset
Dipole Probe Radius
Offset Dipole Probe Radius

Figure 4.2 Geometry of the shifted dipole test. The actual scan radius was 127.95 cm. The dipole was thus offset 25 cm from the fictitious radius of 152.95 cm.

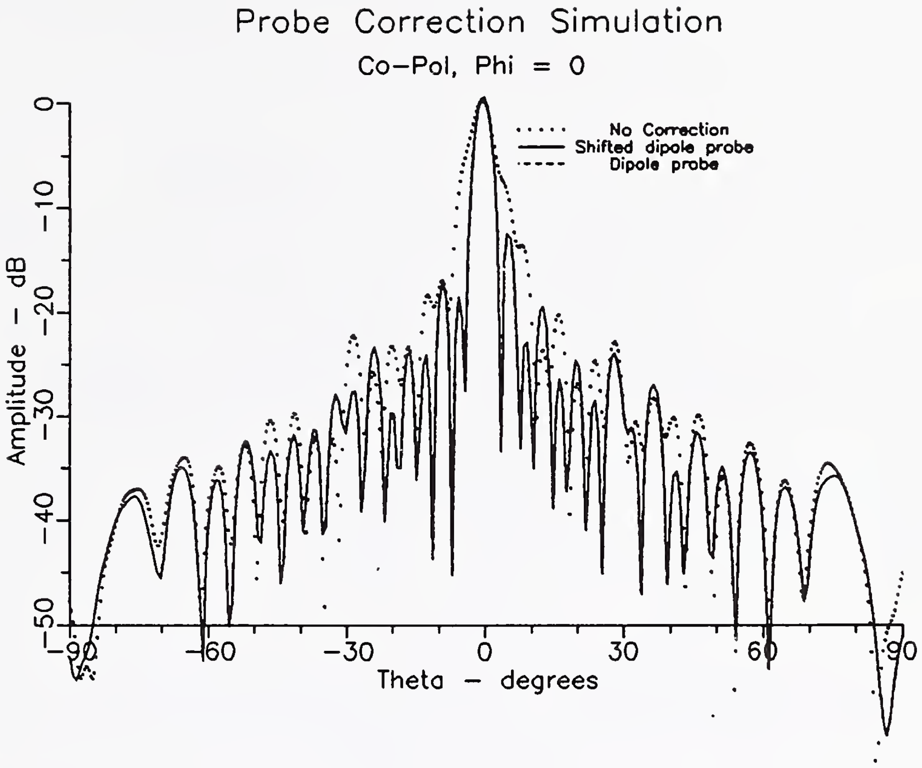

Figure 4.3 Comparison of far-field patterns calculated from data acquired at 127.95 cm and calculated assuming that (a) radius = 152.95 cm (dotted line), (b) radius = 152.95 cm but with probe correction (solid line), and (c) radius = 127.95 cm (dashed line). Main polarization, ϕ = 0° cut.

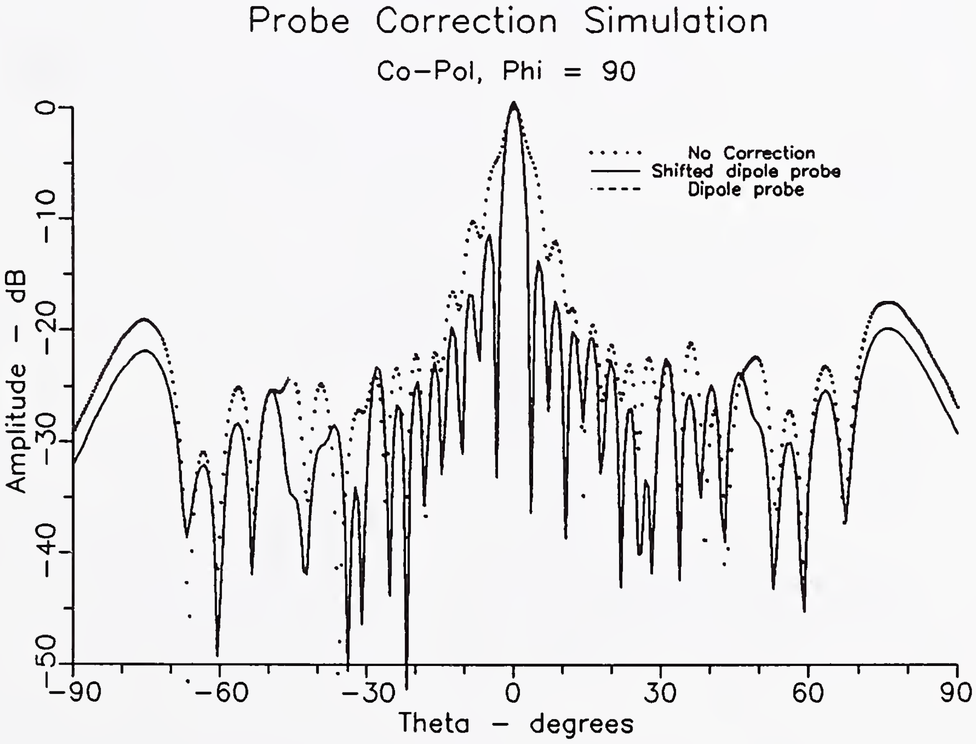

Figure 4.4 Comparison of far-field patterns calculated from data acquired at 127.95 cm and calculated assuming that (a) radius = 152.95 cm (dotted line), (b) radius = 152.95 cm but with probe correction (solid line), and (c) radius = 127.95 cm (dashed line). Main polarization, ϕ = 90° cut.

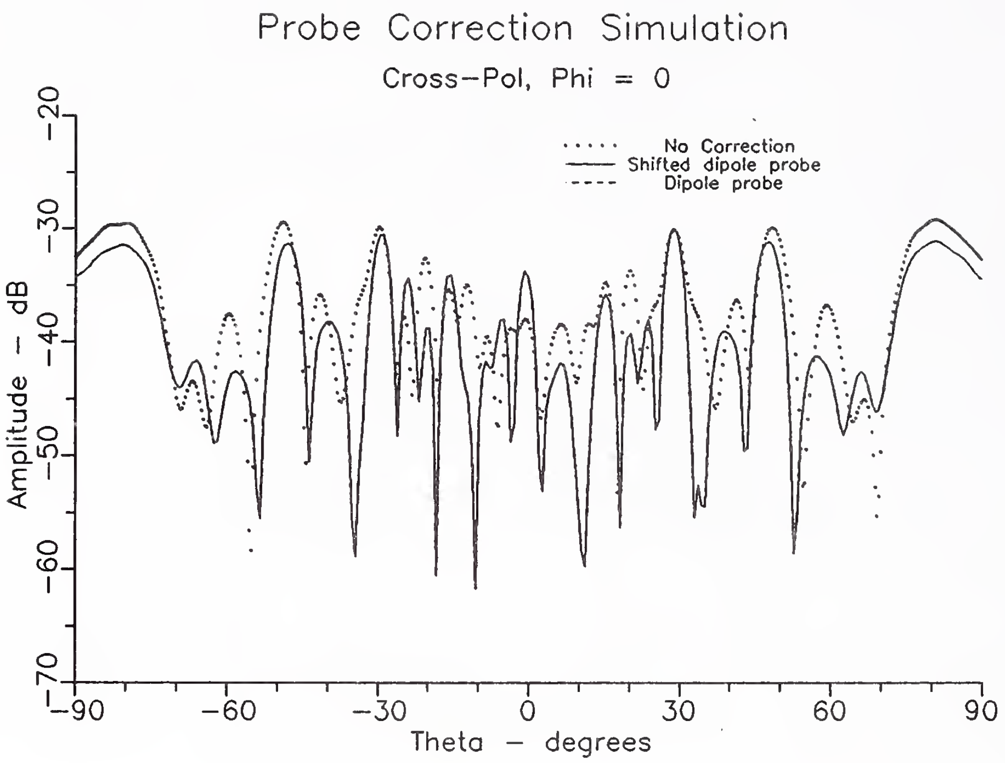

Figure 4.5 Comparison of far-field patterns calculated from data acquired at 127.95 cm and calculated assuming that (a) radius = 152.95 cm (dotted line), (b) radius = 152.95 cm but with probe correction (solid line), and (c) radius = 127.95 cm (dashed line). Cross polarization, $\phi = 0°$ cut.

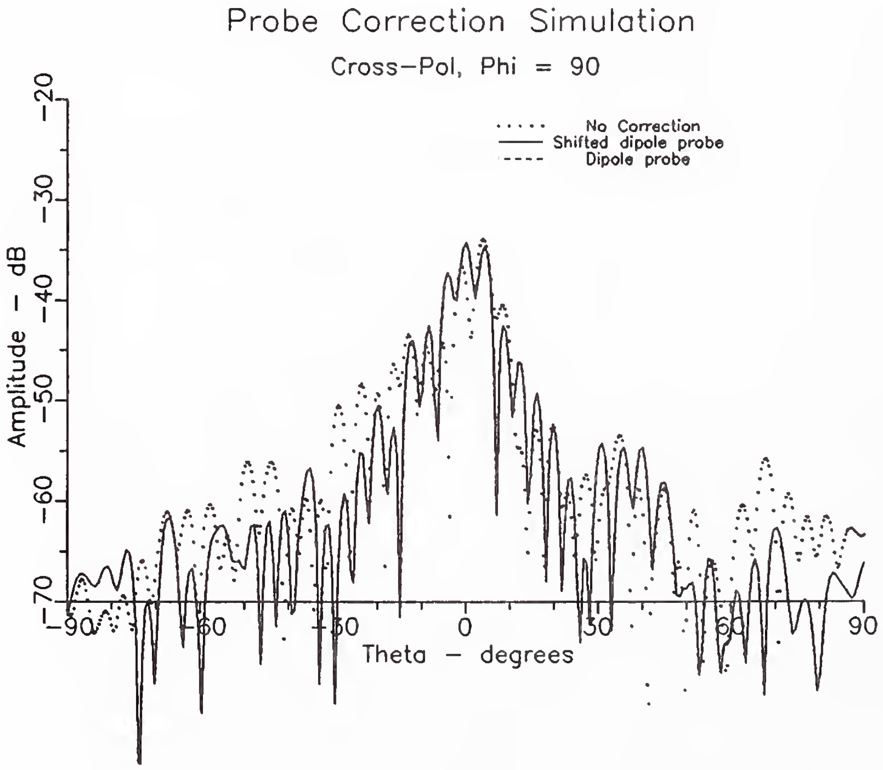

Figure 4.6 Comparison of far-field patterns calculated from data acquired at 127.95 cm and calculated assuming that (a) radius = 152.95 cm (dotted line), (b) radius = 152.95 cm but with probe correction (solid line), and (c) radius = 127.95 cm (dashed line). Cross polarization, $\phi = 90°$ cut.

5. SPHERICAL-WAVE EXPANSIONS FOR TRANSLATED DIPOLES

5.1 Theory

We consider the translation of a transverse electric or magnetic dipole in the z direction. For $r > \rho > 0$ [5]

$$\mathbf{m}_{nm}^{(3)}(\mathbf{r} \mp \rho\hat{\mathbf{z}}) = \sum_{\nu} \left[B(\nu m|nm;\pm\rho\hat{\mathbf{z}})\ \mathbf{m}_{\nu m}^{(3)}(\mathbf{r}) + C(\nu m|nm;\pm\rho\hat{\mathbf{z}})\ \mathbf{n}_{\nu m}^{(3)}(\mathbf{r}) \right] \tag{5-1}$$

$$\mathbf{n}_{nm}^{(3)}(\mathbf{r} \mp \rho\hat{\mathbf{z}}) = \sum_{\nu} \left[B(\nu m|nm;\pm\rho\hat{\mathbf{z}})\ \mathbf{n}_{\nu m}^{(3)}(\mathbf{r}) + C(\nu m|nm;\pm\rho\hat{\mathbf{z}})\ \mathbf{m}_{\nu m}^{(3)}(\mathbf{r}) \right] , \tag{5-2}$$

where $n = 1$ and $m = \pm 1$. The upper and lower signs correspond to translation in the positive and negative z directions, respectively, and ρ is defined as the magnitude of the displacement ($\rho > 0$).

The coefficients $B(\nu m|nm;\rho\hat{z})$ and $C(\nu m|nm;\rho\hat{z})$ are given by

$$B(\nu m|nm;\rho\hat{z}) = -\frac{L^2 - \nu(\nu+1) - n(n+1)}{2\sqrt{\nu(\nu+1)n(n+1)}} A(\nu m|nm;\rho\hat{z}) \tag{5-3}$$

$$C(\nu m|nm;\rho\hat{z}) = -\frac{imk\rho}{\sqrt{\nu(\nu+1)n(n+1)}} A(\nu m|nm;\rho\hat{z}) \tag{5-4}$$

$$A(\nu m|nm;\rho\hat{z}) = (-)^m \sqrt{4\pi}\ i^{-\nu+n} \sum_{\alpha} i^{\alpha} \sqrt{2\alpha+1}\ a(\alpha 0|\nu,-mnm)\ j_{\alpha}(k\rho) , \qquad \rho > 0 \tag{5-5}$$

$$a(\alpha 0|\nu,\mp 1n,\pm 1) = \frac{\alpha(\alpha+1) - \nu(\nu+1) - n(n+1)}{2\sqrt{\nu(\nu+1)n(n+1)}} a(\alpha 0|\nu 0n0) . \tag{5-6}$$

For displacement in the negative z direction use the relations

$$A(\nu m|nm;-\rho\hat{z}) = (-)^{\nu+n} A(\nu m|nm;\rho\hat{z}) \tag{5-7}$$

$$B(\nu m|nm;-\rho\hat{z}) = (-)^{\nu+n} B(\nu m|nm;\rho\hat{z}) \tag{5-8}$$

$$C(\nu m|nm;-\rho\hat{z}) = -(-)^{\nu+n} C(\nu m|nm;\rho\hat{z}) . \tag{5-9}$$

In terms of $a(\alpha 0|\nu 0 n 0)$

$$B(\nu 1|11;\rho\hat{z}) = B(\nu,-1|1,-1;\rho\hat{z})$$

$$= \frac{\sqrt{\pi}}{4\nu(\nu+1)} \sum_{\alpha} i^{\alpha-\nu+1} \sqrt{2\alpha+1}\, [\alpha(\alpha+1) - \nu(\nu+1) - 2]^2\, a(\alpha 0|\nu 010)\, j_{\alpha}(k\rho) \qquad (5\text{-}10)$$

$$C(\nu 1|11;\rho\hat{z}) = - C(\nu,-1|1,-1;\rho\hat{z})$$

$$= \frac{i\sqrt{\pi}}{2\nu(\nu+1)} \sum_{\alpha} i^{\alpha-\nu+1} \sqrt{2\alpha+1}\, [\alpha(\alpha+1) - \nu(\nu+1) - 2]\, a(\alpha 0|\nu 010)\, k\rho\, j_{\alpha}(k\rho) \,. \qquad (5\text{-}11)$$

Since $\alpha+\nu+1$ must be even, the B's will be real and the C's will be imaginary. There are only two nonzero terms in the sum; they correspond to $\alpha = \nu+1$ and $\alpha = \nu-1$. From Table 6.1

$$a(\nu-1,0|\nu 010) = \nu \sqrt{\frac{3}{4\pi(2\nu-1)(2\nu+1)}} \,. \qquad (5\text{-}12)$$

$$a(\nu+1,0|\nu 010) = (\nu+1) \sqrt{\frac{3}{4\pi(2\nu+1)(2\nu+3)}} \qquad (5\text{-}13)$$

Finally, we have $(\rho > 0)$

$$B(\nu 1|11;\rho\hat{z}) = B(\nu,-1|1,-1;\rho\hat{z})$$

$$= \frac{1}{2}\sqrt{\frac{3}{2\nu+1}}\, [-\nu\, j_{\nu+1}(k\rho) + (\nu+1)\, j_{\nu-1}(k\rho)] \qquad (5\text{-}14)$$

$$C(\nu 1|11;\rho\hat{z}) = - C(\nu,-1|1,-1;\rho\hat{z})$$

$$= -\frac{i}{2}\sqrt{\frac{3}{2\nu+1}}\, k\rho\, [j_{\nu+1}(k\rho) + j_{\nu-1}(k\rho)]$$

$$= -\frac{i}{2}\sqrt{3(2\nu+1)}\, j_{\nu}(k\rho) \,. \qquad (5\text{-}15)$$

These formulas check with general asymptotic expressions [5] for the translation coefficients.

For our application we are interested mainly in obtaining the vector spherical harmonic expansion of the far field of a translated dipole. We have

$$\mathbf{m}'_{1,\pm 1}(\mathbf{r}) \sim \mathbf{t}'_{1,\pm 1}(\hat{\mathbf{r}})\,\frac{\exp(ikr)}{ikr} \tag{5-16}$$

$$\mathbf{n}'_{1,\pm 1}(\mathbf{r}) \sim i\hat{\mathbf{r}} \times \mathbf{t}'_{1,\pm 1}(\hat{\mathbf{r}})\,\frac{\exp(ikr)}{ikr} \tag{5-17}$$

with

$$\mathbf{t}'_{1,\pm 1}(\hat{\mathbf{r}}) = \sum_{\nu} i^{-\nu}\,[B(\nu,\pm 1|1,\pm 1;\rho\hat{\mathbf{z}})\,\mathbf{X}_{\nu,\pm 1}(\hat{\mathbf{r}}) + C(\nu,\pm 1|1,\pm 1;\rho\hat{\mathbf{z}})\,i\hat{\mathbf{r}} \times \mathbf{X}_{\nu,\pm 1}(\hat{\mathbf{r}})]\ . \tag{5-18}$$

For x and y directed magnetic dipoles

$$\mathbf{t}'_{x} = \frac{1}{\sqrt{2}}\,[\mathbf{t}'_{1,-1} - \mathbf{t}'_{11}] \tag{5-19}$$

$$\mathbf{t}'_{y} = \frac{i}{\sqrt{2}}\,[\mathbf{t}'_{1,-1} + \mathbf{t}'_{11}]\ . \tag{5-20}$$

If dipole far field is represented as

$$\mathbf{t}'(\hat{\mathbf{r}}) = \sum_{\nu\mu} [B_{\nu\mu}\,\mathbf{X}_{\nu\mu}(\hat{\mathbf{r}}) + C_{\nu\mu}\,i\hat{\mathbf{r}} \times \mathbf{X}_{\nu\mu}(\hat{\mathbf{r}})]\ , \tag{5-21}$$

then we have:

(1) Magnetic dipole, x directed

$$\begin{aligned} B_{\nu 1} &= -\,B_{\nu,-1} = -\,\frac{1}{\sqrt{2}}\,i^{-\nu}\,B(\nu 1|11;\rho\hat{\mathbf{z}}) \\ C_{\nu 1} &= C_{\nu,-1} = -\,\frac{1}{\sqrt{2}}\,i^{-\nu}\,C(\nu 1|11;\rho\hat{\mathbf{z}})\ . \end{aligned} \tag{5-22}$$

(2) Magnetic dipole, y directed

$$B_{\nu 1} = B_{\nu,-1} = \frac{i}{\sqrt{2}}\, i^{-\nu}\, B(\nu 1|11;\rho\hat{z})$$
$$C_{\nu 1} = -\, C_{\nu,-1} = \frac{i}{\sqrt{2}}\, i^{-\nu}\, C(\nu 1|11;\rho\hat{z}) \ . \qquad (5\text{-}23)$$

(3) Electric dipole, x directed

$$B_{\nu 1} = B_{\nu,-1} = -\frac{1}{\sqrt{2}}\, i^{-\nu}\, C(\nu 1|11;\rho\hat{z})$$
$$C_{\nu 1} = -\, C_{\nu,-1} = -\frac{1}{\sqrt{2}}\, i^{-\nu}\, B(\nu 1|11;\rho\hat{z}) \ . \qquad (5\text{-}24)$$

(4) Electric dipole, y directed

$$B_{\nu 1} = -\, B_{\nu,-1} = \frac{i}{\sqrt{2}}\, i^{-\nu}\, C(\nu 1|11;\rho\hat{z})$$
$$C_{\nu 1} = C_{\nu,-1} = \frac{i}{\sqrt{2}}\, i^{-\nu}\, B(\nu 1|11;\rho\hat{z}) \ . \qquad (5\text{-}25)$$

Expressions for a displacement in the negative z direction follow from Eqs (22) through (25),(8), and (9).

A listing of a Pascal program, which calculates the coefficients in Eqs (22) through (25), is attached (Section 5.2). Representative output for kz = 10 is given in Tables 5.1 through 5.4.

5.2 **Computer Program**

The computer code is listed on the following pages.

```
{$R-,S+,I+,D+,F-,V+,B-,N+,L+ }
{$M 16384,0,655360 }

Program Dipole; {Calculate coefficients in the vector spherical harmonic
                 expansion of x and y directed magnetic and electric dipoles}
uses crt,dos;
type
  Vector0 =          array[0..1] of extended;
  Vector1 =          array[1..2] of extended;
  VectorPtr0 =       ^Vector0;
  VectorPtr1 =       ^Vector1;
var
  B,C:               VectorPtr1;
  Z:                 extended;
  MaxN:              integer;
  DipoleType:        char;


procedure shank3(Z: extended; j,y: VectorPtr0; MaxN: integer);

var
  U,V,W,Z2:          extended;
  N:                 integer;
begin {Shank3}
  Z2:=Z*Z;
  j^[0]:= sin(Z)/Z;
  y^[0]:=-cos(Z)/Z;
  Z2:=Z*Z;
  U:=1;
  V:=Z/(2.0*MaxN+1);
  W:=V;
  N:=MaxN;
  while abs(V/W)>1E-20 do begin
    inc(N);
    U:=1/(1-Z2*U/(4.0*N*N-1));
    V:=V*(U-1);
    W:=W+V
  end;

  j^[MaxN]:=W;        {Backward recursion for j}
  for N:=MaxN-1 downto 1 do j^[N]:=1/((2.0*N+1)/Z-j^[N+1]);

  U:=y^[0]/j^[0];     {Forward recursion for y}
  for N:=1 to MaxN do begin
    U:=(2.0*N-1)/Z-1/U;
    y^[N]:=U*y^[N-1];
    j^[N]:=j^[N]*j^[N-1]
  end
end; {Shank3}


procedure XCoef(B,C: VectorPtr1; Z: extended; MaxN: integer);

var
  Nu,
  Sign:              integer;
  j,y:               VectorPtr0;

begin {XCoef}
  j:=@C^[1]; {we hope this equivalence works!}
  y:=@B^[1];
  shank3(abs(Z),j,y,MaxN+1); {need j for orders 0 to MaxN+1}
  Sign:=1;
  for Nu:=1 to MaxN do begin
    B^[Nu]:=0.5*sqrt(3.0/(2.0*Nu+1))*(-Nu*j^[Nu+1]+(Nu+1.0)*j^[Nu-1]);
    C^[Nu]:=-0.5*sqrt(3.0*(2.0*Nu+1))*j^[Nu];
    if Z<0 then begin
      Sign:=-Sign;
      B^[Nu]:=-Sign*B^[Nu];
      C^[Nu]:= Sign*C^[Nu];
    end
  end {remember B is real, C is imaginary}
end; {XCoef}


procedure XMag;

var
  Ir,Ii,It:          integer;
  N:                 integer;
  Bxy,Cxy,K:         extended;
  ch:                char;
begin {XMag}
  ClrScr;
  writeln('                      Spherical Harmonic Expansion Coefficents');
  writeln('                       Far Field, X Directed Magnetic Dipole');
  writeln('                             [see XDIPOLE.WMC, eq (21)]');
  writeln;
  writeln('                                B(Nu,-1) = - B(Nu,1)');
  writeln('                                C(Nu,-1) =   C(Nu,1)');
  writeln;
  writeln('                                kz = ',Z:15:10);
  writeln;
  writeln('   Nu                   B(Nu,1)                              C(Nu,1)')
  => ;
  writeln;
  Ir:=1;
  Ii:=0;
  K:=0.5*sqrt(2);
  for N:=1 to MaxN do begin
    It:= Ii; Ii:=-Ir; Ir:= It; {(-i)^N}
    if Ii=0 then begin
      Bxy:=-K*Ir*B^[N];
      Cxy:=-K*Ir*C^[N];
      writeln(N:5,Bxy:35,' ',Cxy:35,'i')
    end;
    if Ir=0 then begin
      Bxy:=-K*Ii*B^[N];
      Cxy:= K*Ii*C^[N];
      writeln(N:5,Bxy:35,'i',Cxy:35,' ')
    end
  end;
  ch:=readkey;
end; {XMag}


procedure YMag;

var
  Ir,Ii,It:          integer;
  N:                 integer;
  Bxy,Cxy,K:         extended;
  ch:                char;
begin {YMag}
  ClrScr;
  writeln('                      Spherical Harmonic Expansion Coefficents');
  writeln('                       Far Field, Y Directed Magnetic Dipole');
  writeln('                             [see XDIPOLE.WMC, eq (21)]');
  writeln;
  writeln('                                B(Nu,-1) =   B(Nu,1)');
  writeln('                                C(Nu,-1) = - C(Nu,1)');
  writeln;
  writeln('                                  kz = ',Z:15:10);
  writeln;
  writeln('   Nu                    B(Nu,1)                          C(Nu,1)')
  => ;
  writeln;
  Ir:=1;
  Ii:=0;
  K:=0.5*sqrt(2);
  for N:=1 to MaxN do begin
    It:= Ii; Ii:=-Ir; Ir:= It; {(-i)^N}
    if Ii=0 then begin
      Bxy:= K*Ir*B^[N];
      Cxy:=-K*Ir*C^[N];
      writeln(N:5,Bxy:35,'i',Cxy:35,' ')
    end;
    if Ir=0 then begin
      Bxy:=-K*Ii*B^[N];
      Cxy:=-K*Ii*C^[N];
      writeln(N:5,Bxy:35,' ',Cxy:35,'i')
    end
  end;
  ch:=readkey;
end; {YMag}


procedure XEle;

var
  Ir,Ii,It:        integer;
  N:               integer;
  Bxy,Cxy,K:       extended;
  ch:              char;
begin {XEle}
  ClrScr;
  writeln('                        Spherical Harmonic Expansion Coefficents');
  writeln('                         Far Field, X Directed Electric Dipole');
  writeln('                               [see XDIPOLE.WMC, eq (21)]');
  writeln;
  writeln('                                    B(Nu,-1) =   B(Nu,1)');
  writeln('                                    C(Nu,-1) = - C(Nu,1)');
  writeln;
  writeln('                                    kz = ',Z:15:10);
  writeln;
  writeln('   Nu                    B(Nu,1)                          C(Nu,1)')
  => ;
  writeln;
  Ir:=1;
  Ii:=0;
  K:=0.5*sqrt(2);
  for N:=1 to MaxN do begin
    It:= Ii; Ii:=-Ir; Ir:= It; {(-i)^N}
    if Ii=0 then begin
      Bxy:=-K*Ir*C^[N];
      Cxy:=-K*Ir*B^[N];
      writeln(N:5,Bxy:35,'i',Cxy:35,' ')
    end;
    if Ir=0 then begin
      Bxy:= K*Ii*C^[N];
      Cxy:=-K*Ii*B^[N];
      writeln(N:5,Bxy:35,' ',Cxy:35,'i')
    end
  end;
  ch:=readkey;
 end; {XEle}
```

```
procedure YEle;

var
  Ir,Ii,It:        integer;
  N:               integer;
  Bxy,Cxy,K:       extended;
  ch:              char;
begin {YEle}
  ClrScr;
  writeln('                        Spherical Harmonic Expansion Coefficents');
  writeln('                         Far Field, Y Directed Electric Dipole');
  writeln('                               [see XDIPOLE.WMC, eq (21)]');
  writeln;
  writeln('                                    B(Nu,-1) = - B(Nu,1)');
  writeln('                                    C(Nu,-1) =   C(Nu,1)');
  writeln;
  writeln('                                    kz = ',Z:15:10);
  writeln;
  writeln('   Nu                    B(Nu,1)                          C(Nu,1)')
  => ;
  writeln;
  Ir:=1;
  Ii:=0;
  K:=0.5*sqrt(2);
  for N:=1 to MaxN do begin
    It:= Ii; Ii:=-Ir; Ir:= It; {(-i)^N}
    if Ii=0 then begin
      Bxy:=-K*Ir*C^[N];
      Cxy:= K*Ir*B^[N];
      writeln(N:5,Bxy:35,' ',Cxy:35,'i')
    end;
    if Ir=0 then begin
      Bxy:=-K*Ii*C^[N];
      Cxy:=-K*Ii*B^[N];
      writeln(N:5,Bxy:35,'i',Cxy:35,' ')
    end
  end;
  ch:=readkey;
end; {YEle}


begin {XDipole}
  write('Enter kz coordinate for dipole  '); read(Z);
  write('Enter the number of coefficients to calculate '); read(MaxN);
  getmem(B,10*MaxN+20);
  getmem(C,10*MaxN+20);
  XCoef(B,C,Z,MaxN);
  DipoleType:='x';
  while DipoleType<>#27 do begin
    writeln;
    writeln('Enter dipole type (A..D)');
    writeln('  A.  x directed magnetic dipole');
    writeln('  B.  y directed magnetic dipole');
    writeln('  C.  x directed electric dipole');
    writeln('  D.  y directed electric dipole');
    writeln('  ESC to quit');
    DipoleType:=readkey;
    case upcase(DipoleType) of
      'A': XMag;
      'B': YMag;
      'C': XEle;
      'D': YEle
    else write(chr(7))
    end;
  end
end.
```

Table 5.1 Expansion coefficients for the far-field pattern of an x directed magnetic dipole on the z axis, kz = 10 (see Eqs (5-21) and (5-22)).

Nu	B(Nu,1)	C(Nu,1)
1	-i 6.60248 28489 50692 46E-2	8.32267 59967 30105 50E-2
2	8.60999 36288 15349 90E-2	-i 1.06726 74407 94977 15E-1
3	-i 1.45477 96134 36174 74E-1	6.39905 82502 21619 83E-2
4	- 5.03346 08740 67401 85E-3	-i 1.93979 90313 26956 72E-1
5	-i 1.58057 28870 41234 05E-1	- 1.12791 12629 88448 94E-1
6	- 1.81570 63718 07568 78E-1	-i 9.82562 59272 52380 02E-2
7	i 8.26991 87592 27027 56E-2	- 2.68919 05813 00916 23E-1
8	- 3.26310 25112 85262 05E-2	i 3.17068 96749 96400 32E-1
9	i 9.47357 26873 73178 67E-2	2.67184 29937 41520 03E-1
10	9.95970 87484 41351 04E-2	-i 1.81297 76514 80810 73E-1
11	-i 7.48108 74271 28279 94E-2	- 1.04476 18784 84089 69E-1
12	- 4.56683 33279 96282 14E-2	i 5.27130 18483 89711 03E-2
13	i 2.38990 28098 49686 85E-2	2.37553 44340 12262 99E-2
14	1.10410 34950 67201 12E-2	-i 9.69887 19556 28861 67E-3
15	-i 4.58844 44084 57078 61E-3	- 3.62619 71961 04263 17E-3
16	- 1.73813 74419 47636 63E-3	i 1.25200 35565 35636 78E-3
17	i 6.06119 35233 64076 01E-4	4.01920 97138 29737 22E-4
18	1.96085 07463 19153 51E-4	-i 1.20644 34991 61994 15E-4
19	-i 5.92182 88821 40788 16E-5	- 3.40230 57038 97834 83E-5
20	- 1.67818 36832 71975 83E-5	i 9.05134 98768 97675 79E-6

Table 5.2 Expansion coefficients for the far-field pattern of a y directed magnetic dipole on the z axis, kz = 10 (see Eqs (5-21) and (5-23)).

Nu	B(Nu,1)	C(Nu,1)
1	- 6.60248 28489 50692 46E-2	-i 8.32267 59967 30105 50E-2
2	-i 8.60999 36288 15349 90E-2	- 1.06726 74407 94977 15E-1
3	- 1.45477 96134 36174 74E-1	-i 6.39905 82502 21619 83E-2
4	i 5.03346 08740 67401 85E-3	- 1.93979 90313 26956 72E-1
5	- 1.58057 28870 41234 05E-1	i 1.12791 12629 88448 94E-1
6	i 1.81570 63718 07568 78E-1	- 9.82562 59272 52380 02E-2
7	8.26991 87592 27027 56E-2	i 2.68919 05813 00916 23E-1
8	i 3.26310 25112 85262 05E-2	3.17068 96749 96400 32E-1
9	9.47357 26873 73178 67E-2	-i 2.67184 29937 41520 03E-1
10	-i 9.95970 87484 41351 04E-2	- 1.81297 76514 80810 73E-1
11	- 7.48108 74271 28279 94E-2	i 1.04476 18784 84089 69E-1
12	i 4.56683 33279 96282 14E-2	5.27130 18483 89711 03E-2
13	2.38990 28098 49686 85E-2	-i 2.37553 44340 12262 99E-2
14	-i 1.10410 34950 67201 12E-2	- 9.69887 19556 28861 67E-3
15	- 4.58844 44084 57078 61E-3	i 3.62619 71961 04263 17E-3
16	i 1.73813 74419 47636 63E-3	1.25200 35565 35636 78E-3
17	6.06119 35233 64076 01E-4	-i 4.01920 97138 29737 22E-4
18	-i 1.96085 07463 19153 51E-4	- 1.20644 34991 61994 15E-4
19	- 5.92182 88821 40788 16E-5	i 3.40230 57038 97834 83E-5
20	i 1.67818 36832 71975 83E-5	9.05134 98768 97675 79E-6

Table 5.3 Expansion coefficients for the far-field pattern of an x directed electric dipole on the z axis, kz = 10 (see Eqs (5-21) and (5-24)).

Nu	B(Nu,1)	C(Nu,1)
1	8.32267 59967 30105 50E-2	-i 6.60248 28489 50692 46E-2
2	-i 1.06726 74407 94977 15E-1	8.60999 36288 15349 90E-2
3	6.39905 82502 21619 83E-2	-i 1.45477 96134 36174 74E-1
4	-i 1.93979 90313 26956 72E-1	- 5.03346 08740 67401 85E-3
5	- 1.12791 12629 88448 94E-1	-i 1.58057 28870 41234 05E-1
6	-i 9.82562 59272 52380 02E-2	- 1.81570 63718 07568 78E-1
7	- 2.68919 05813 00916 23E-1	i 8.26991 87592 27027 56E-2
8	i 3.17068 96749 96400 32E-1	- 3.26310 25112 85262 05E-2
9	2.67184 29937 41520 03E-1	i 9.47357 26873 73178 67E-2
10	-i 1.81297 76514 80810 73E-1	9.95970 87484 41351 04E-2
11	- 1.04476 18784 84089 69E-1	-i 7.48108 74271 28279 94E-2
12	i 5.27130 18483 89711 03E-2	- 4.56683 33279 96282 14E-2
13	2.37553 44340 12262 99E-2	i 2.38990 28098 49686 85E-2
14	-i 9.69887 19556 28861 67E-3	1.10410 34950 67201 12E-2
15	- 3.62619 71961 04263 17E-3	-i 4.58844 44084 57078 61E-3
16	i 1.25200 35565 35636 78E-3	- 1.73813 74419 47636 63E-3
17	4.01920 97138 29737 22E-4	i 6.06119 35233 64076 01E-4
18	-i 1.20644 34991 61994 15E-4	1.96085 07463 19153 51E-4
19	- 3.40230 57038 97834 83E-5	-i 5.92182 88821 40788 16E-5
20	i 9.05134 98768 97675 79E-6	- 1.67818 36832 71975 83E-5

Table 5.4 Expansion coefficients for the far-field pattern of a y directed electric dipole on the z axis, kz = 10 (see Eqs (5-21) and (5-25)).

Nu	B(Nu,1)	C(Nu,1)
1	-i 8.32267 59967 30105 50E-2	- 6.60248 28489 50692 46E-2
2	- 1.06726 74407 94977 15E-1	-i 8.60999 36288 15349 90E-2
3	-i 6.39905 82502 21619 83E-2	- 1.45477 96134 36174 74E-1
4	- 1.93979 90313 26956 72E-1	i 5.03346 08740 67401 85E-3
5	i 1.12791 12629 88448 94E-1	- 1.58057 28870 41234 05E-1
6	- 9.82562 59272 52380 02E-2	i 1.81570 63718 07568 78E-1
7	i 2.68919 05813 00916 23E-1	8.26991 87592 27027 56E-2
8	3.17068 96749 96400 32E-1	i 3.26310 25112 85262 05E-2
9	-i 2.67184 29937 41520 03E-1	9.47357 26873 73178 67E-2
10	- 1.81297 76514 80810 73E-1	-i 9.95970 87484 41351 04E-2
11	i 1.04476 18784 84089 69E-1	- 7.48108 74271 28279 94E-2
12	5.27130 18483 89711 03E-2	i 4.56683 33279 96282 14E-2
13	-i 2.37553 44340 12262 99E-2	2.38990 28098 49686 85E-2
14	- 9.69887 19556 28861 67E-3	-i 1.10410 34950 67201 12E-2
15	i 3.62619 71961 04263 17E-3	- 4.58844 44084 57078 61E-3
16	1.25200 35565 35636 78E-3	i 1.73813 74419 47636 63E-3
17	-i 4.01920 97138 29737 22E-4	6.06119 35233 64076 01E-4
18	- 1.20644 34991 61994 15E-4	-i 1.96085 07463 19153 51E-4
19	i 3.40230 57038 97834 83E-5	- 5.92182 88821 40788 16E-5
20	9.05134 98768 97675 79E-6	i 1.67818 36832 71975 83E-5

6. PRODUCTS OF SPHERICAL HARMONICS

6.1 Introduction

The major intent of these notes is to develop the following formulas for the expansion of scalar products of spherical harmonics:

$$Y_{\nu\mu}(\hat{\mathbf{r}})\ Y_{nm}(\hat{\mathbf{r}}) = \sum_{\alpha} a(\alpha,\mu+m|\nu\mu nm)\ Y_{\alpha,\mu+m}(\hat{\mathbf{r}}) \tag{6-1}$$

$$\mathbf{X}_{\nu\mu}(\hat{\mathbf{r}}) \cdot \mathbf{X}_{nm}(\hat{\mathbf{r}}) = \sum_{\alpha} b(\alpha,\mu+m|\nu\mu nm)\ Y_{\alpha,\mu+m}(\hat{\mathbf{r}}) \tag{6-2}$$

$$i\hat{\mathbf{r}} \times \mathbf{X}_{\nu\mu}(\hat{\mathbf{r}}) \cdot \mathbf{X}_{nm}(\hat{\mathbf{r}}) = \sum_{\alpha} c(\alpha,\mu+m|\nu\mu nm)\ Y_{\alpha,\mu+m}(\hat{\mathbf{r}}) \ , \tag{6-3}$$

where $|\nu - n| \le \alpha \le \nu + n$. In Eqs (1) and (2), the coefficients are 0 when $\alpha + \nu + n$ is odd. In Eq (3), the coefficients are 0 when $\alpha + \nu + n$ is even. (Other coefficients may be 0; for example, when $|\mu + m| > \alpha$ or in the expansion of $i\hat{\mathbf{r}} \times \mathbf{X}_{nm}(\hat{\mathbf{r}}) \cdot \mathbf{X}_{nm}(\hat{\mathbf{r}}) = 0$.) Notation for spherical harmonics follows Jackson [1, Chapters 3 and 16].

In Sections 6.2 to 6.4 we establish the form of Eqs (1) through (3) by a straightforward inductive process which leads to simple (but cumbersome) recursion formulas for calculating the coefficients. In Section 6.5 we summarize the results of a more sophisticated approach yielding practical formulas for computation. Several useful expansions of vector products of spherical harmonics are given in Section 6.6.

6.2 Expansion of $Y_{\nu\mu}(\hat{\mathbf{r}})\ Y_{nm}(\hat{\mathbf{r}})$

Scalar spherical harmonics are given by the formulas

$$\begin{aligned} Y_{nm}(\hat{\mathbf{r}}) &= (-)^m\ K_{nm}\ (x/r + iy/r)^m\ P_n^{(m)}(z/r) \ , \qquad m \ge 0 \\ Y_{n,-m}(\hat{\mathbf{r}}) &= (-)^m\ Y^*_{nm}(\hat{\mathbf{r}}) \ , \end{aligned} \tag{6-4}$$

where

$$K_{nm} = \sqrt{\frac{2n+1}{4\pi} \frac{(n-m)!}{(n+m)!}}$$

$$P_n^{(m)}(x) = \frac{d^m}{dx^m} P_n(x) \ .$$

Since the Legendre polynomial $P_n(x)$ is an nth order polynomial in x, $Y_{nm} = 0$ when $m > n$.

The fact that $\alpha + \nu + n$ must be even in Eq (1) can be verified by using the inversion symmetry

$$Y_{nm}(-\hat{r}) = (-)^n Y_{nm}(\hat{r}) \qquad (6\text{-}5)$$

which follows from Eq (4). If both sides of Eq (1) are to have the same parity, then

$$(-)^{\nu+n} = (-)^{\alpha} \quad \text{or} \quad (-)^{\alpha+\nu+n} = 1 \ .$$

If the number of terms in Eq (1) is finite, it is easy to show using Eq (4) that the highest order term must correspond to $\alpha = \nu + n$:

$$a(\nu+n,\mu+m|\nu\mu nm) = \frac{G_{\nu\mu} \ G_{nm}}{G_{\nu+n,\mu+m}} \ , \qquad (6\text{-}6)$$

where

$$G_{nm} = K_{nm} \frac{(2n)!}{n! \ (n-m)!} \ .$$

Note that $G_{n,-m} = G_{nm}$.

When $\alpha = |\nu - n|$, the coefficient can be calculated as follows:

$$a(|\nu-n|,\mu+m|\nu\mu nm) = \int Y^*_{|\nu-n|,\mu+m}(\hat{\mathbf{r}})\, Y_{\nu\mu}(\hat{\mathbf{r}})\, Y_{nm}(\hat{\mathbf{r}})\, d\hat{\mathbf{r}}$$

$$= 0 , \qquad |\nu-n| < |\mu + m| \qquad (6\text{-}7a)$$

$$= (-)^m \int Y^*_{\nu,-\mu}(\hat{\mathbf{r}})\, Y_{\nu-n,-\mu-m}(\hat{\mathbf{r}})\, Y_{nm}(\hat{\mathbf{r}})\, d\hat{\mathbf{r}} = (-)^m \frac{G_{\nu-n,\mu+m}\, G_{nm}}{G_{\nu\mu}} ,$$

$$\nu \geq n \qquad (6\text{-}7b)$$

$$= (-)^\mu \int Y^*_{n,-m}(\hat{\mathbf{r}})\, Y_{n-\nu,-\mu-m}(\hat{\mathbf{r}})\, Y_{\nu\mu}(\hat{\mathbf{r}})\, d\hat{\mathbf{r}} = (-)^\mu \frac{G_{n-\nu,\mu+m}\, G_{\nu\mu}}{G_{nm}} ,$$

$$\nu \leq n . \qquad (6\text{-}7c)$$

The smallest value of α allowed in Eq (1) is $\alpha = |\nu - n|$. Otherwise, from Eq (7b), we see that a term with $\alpha = |\nu - n| - 1$ in the expansion of $Y_{\nu\mu}(\hat{\mathbf{r}})\, Y_{nm}(\hat{\mathbf{r}})$ would imply the existence of a term with $\alpha = \nu$ in the expansion of $Y_{\nu-n-1,-\mu-m}(\hat{\mathbf{r}})\, Y_{nm}(\hat{\mathbf{r}})$.

Using Eqs (6) and (7) we can write down the low-order expansions

$$Y_{00}\, Y_{nm} = \frac{1}{\sqrt{4\pi}}\, Y_{nm} \qquad (6\text{-}8)$$

and for $n \geq 1$

$$Y_{1,-1}\, Y_{nm} = -\frac{G_{n-1,m-1}\, G_{11}}{G_{nm}}\, Y_{n-1,m-1} + \frac{G_{11}\, G_{nm}}{G_{n+1,m-1}}\, Y_{n+1,m-1} \qquad (6\text{-}9a)$$

$$Y_{10}\, Y_{nm} = \frac{G_{n-1,m}\, G_{10}}{G_{nm}}\, Y_{n-1,m} + \frac{G_{10}\, G_{nm}}{G_{n+1,m}}\, Y_{n+1,m} \qquad (6\text{-}9b)$$

$$Y_{11}\, Y_{nm} = -\frac{G_{n-1,m+1}\, G_{11}}{G_{nm}}\, Y_{n-1,m+1} + \frac{G_{11}\, G_{nm}}{G_{n+1,m+1}}\, Y_{n+1,m+1} . \qquad (6\text{-}9c)$$

Equations (9), which are equivalent to elementary recursion formulas for the Legendre functions, are written explicitly in Table 6.1.

Table 6.1 $Y_{1\mu}(\hat{\mathbf{r}})\ Y_{nm}(\hat{\mathbf{r}}) = \sum_{\alpha} a(\alpha,\mu+m|1\mu nm)\ Y_{\alpha,\mu+m}(\hat{\mathbf{r}})$

$$Y_{1,-1}\ Y_{nm} = -\sqrt{\frac{3(n+m-1)(n+m)}{8\pi(2n-1)(2n+1)}}\ Y_{n-1,m-1} + \sqrt{\frac{3(n-m+1)(n-m+2)}{8\pi(2n+1)(2n+3)}}\ Y_{n+1,m-1}$$

$$Y_{10}\ \ Y_{nm} = \sqrt{\frac{3(n-m)(n+m)}{4\pi(2n-1)(2n+1)}}\ Y_{n-1,m} + \sqrt{\frac{3(n-m+1)(n+m+1)}{4\pi(2n+1)(2n+3)}}\ Y_{n+1,m}$$

$$Y_{11}\ \ Y_{nm} = -\sqrt{\frac{3(n-m-1)(n-m)}{8\pi(2n-1)(2n+1)}}\ Y_{n-1,m+1} + \sqrt{\frac{3(n+m+1)(n+m+2)}{8\pi(2n+1)(2n+3)}}\ Y_{n+1,m+1}$$

Consider the product $Y_{\nu'0}Y_{nm}$. We see from Eqs (8) and (9b) that Eq (1) holds when $\nu' = 1$ or 0. Now, we show that if

$$Y_{\nu'0}(\hat{\mathbf{r}})\ Y_{nm}(\hat{\mathbf{r}}) = \sum_{\alpha} a(\alpha m|\nu' 0nm)\ Y_{\alpha m}(\hat{\mathbf{r}}) \tag{6-10}$$

for all n and m when $\nu' \leq \nu-1$, then Eq (10) also holds for $\nu' = \nu$.

We expand the product $Y_{10}Y_{\nu-1,0}Y_{nm}$ in two ways to get

$$Y_{10}Y_{\nu-1,0}Y_{nm} = [a(\nu 0|10,\nu-1,0)\ Y_{\nu 0} + a(\nu-2,0|10,\nu-1,0)\ Y_{\nu-2,0}]Y_{nm}$$

$$= Y_{\nu-1,0}[a(n+1,m|10nm)\ Y_{n+1,m} + a(n-1,m|10nm)Y_{n-1,m}]\ .$$

Thus,

$$\begin{aligned} a(\nu 0|10,\nu-1,0)\ Y_{\nu 0}\ Y_{nm} &= a(n+1,m|10nm)\ Y_{\nu-1,0}\ Y_{n+1,m} + a(n-1,m|10nm)\ Y_{\nu-1,0}\ Y_{n-1,m} \\ &\quad - a(\nu-2,0|10,\nu-1,0)\ Y_{\nu-2,0}\ Y_{nm}\ . \end{aligned} \tag{6-11}$$

By hypothesis, the products on the right side of Eq (11) can be expanded using Eq (10). Therefore, Eq (11) provides a means for calculating the coefficients and verifying the basic properties of the expansion of $Y_{\nu 0}\ Y_{nm}$. That is, there are no terms with $\alpha + \nu + n$ odd, $\alpha > \nu + n$ or $\alpha < |\nu - n|$. When $\nu - n > 1$, there is a potential difficulty. In this case, if $\nu - n > |m| + 1$, there will be terms in $Y_{\nu-n-2,m}$ on the right side of Eq (11). For these to cancel, we must have

$$a(n+1,m|10nm)\ a(\nu-n-2,m|\nu-1,0,n+1,m)$$

$$= a(\nu-2,0|10,\nu-1,0)\ a(\nu-n-2,m|\nu-2,0nm)\ ,$$

a fact easily verified using Eqs (6) and (7b). (Alternatively, we could have included the hypothesis $\nu \leq n$ without loss of generality.)

In establishing Eq (1) for $\mu \neq 0$, the raising and lowering operators are most useful:

$$L_{\pm}\ Y_{nm} = \lambda^{\pm}_{nm}\ Y_{n,m\pm1}\ , \tag{6-12}$$

where

$$L_{\pm} = L_x \pm iL_y\ , \qquad \mathbf{L} = -i\mathbf{r} \times \nabla$$

$$\lambda^{\pm}_{nm} = \sqrt{(n\mp m)(n\pm m+1)}\ .$$

Consider the product $Y_{\nu\mu'}\ Y_{nm}$. We have established that Eq (1) holds when $\mu' = 0$. Now, we show that if

$$Y_{\nu\mu'}(\hat{\mathbf{r}})\ Y_{nm}(\hat{\mathbf{r}}) = \sum_{\alpha} a(\alpha m|\nu\mu' nm)\ Y_{\alpha,\mu'+m}(\hat{\mathbf{r}}) \tag{6-13}$$

for all ν, n and m when $\mu-1 \geq \mu' \geq 0$, then Eq (13) is valid for $\mu' = \mu$, as well. Apply the raising operator to $Y_{\nu,\mu-1}\ Y_{nm}$ to get

$$L_+\ (Y_{\nu,\mu-1}\ Y_{nm}) = \lambda^{+}_{\nu,\mu-1}\ Y_{\nu\mu}\ Y_{nm} + \lambda^{+}_{nm}\ Y_{\nu,\mu-1}\ Y_{n,m+1}$$

$$= \sum_{\alpha} \lambda^{+}_{\alpha,\mu+m-1}\ a(\alpha,\mu+m-1|\nu,\mu-1,nm)\ Y_{\alpha,\mu+m}$$

or

$$\lambda^+_{\nu,\mu-1}\ Y_{\nu\mu}\ Y_{nm}$$

$$= \sum_\alpha \lambda^+_{\alpha,\mu+m-1}\ a(\alpha,\mu+m-1|\nu,\mu-1,nm)\ Y_{\alpha,\mu+m} - \lambda^+_{nm}\ Y_{\nu,\mu-1}\ Y_{n,m+1}\ . \qquad (6\text{-}14)$$

Equation (14) provides a means for calculating the coefficients and verifying the basic properties of the expansion of $Y_{\nu\mu}\ Y_{nm}$. (As a check, Eq (14) can be used to derive Eq (9c) from Eq (9b).)

A similar argument using the lowering operator can be applied when μ is negative. On the other hand, we can take the complex conjugate of Eq (13) and use the symmetry

$$Y^*_{nm} = (-)^m\ Y_{n,-m}\ . \qquad (6\text{-}15)$$

At this point Eq (1) has been established inductively. The coefficients can be determined from Eqs (11) and (14).

6.3 Expansion of $\mathbf{X}_{\nu\mu}(\hat{\mathbf{r}}) \cdot \mathbf{X}_{nm}(\hat{\mathbf{r}})$

The identity

$$\sqrt{\nu(\nu+1)n(n+1)}\ \mathbf{X}_{\nu\mu} \cdot \mathbf{X}_{nm} = \frac{1}{2}\ [L^2 - \nu(\nu+1) - n(n+1)]\ Y_{\nu\mu}\ Y_{nm} \qquad (6\text{-}16)$$

can be obtained by evaluating $L^2(Y_{\nu\mu}\ Y_{nm})$. Equation (16) is dependent on the differential equation

$$L^2\ Y_{nm} = n(n+1)\ Y_{nm} \qquad (6\text{-}17)$$

and the definition

$$\mathbf{X}_{nm} \equiv \mathbf{L}\ Y_{nm}/\sqrt{n(n+1)}\ . \qquad (6\text{-}18)$$

The expansion Eq (2) is easily obtained when Eq (1) is substituted into Eq (16). We find that

$$b(\alpha,\mu+m|\nu\mu nm) = \frac{\alpha(\alpha+1) - \nu(\nu+1) - n(n+1)}{2\sqrt{\nu(\nu+1)n(n+1)}}\ a(\alpha,\mu+m|\nu\mu nm)\ . \qquad (6\text{-}19)$$

Equations (2) for $\nu = 1$ are written explicitly in Table 6.2.

Table 6.2 $\mathbf{X}_{1\mu}(\hat{\mathbf{r}}) \cdot \mathbf{X}_{nm}(\hat{\mathbf{r}}) = \sum_{\alpha} b(\alpha,\mu+m|1\mu nm)\ Y_{\alpha,\mu+m}(\hat{\mathbf{r}})$

$$\mathbf{X}_{1,-1} \cdot \mathbf{X}_{nm} = \sqrt{\frac{3(n+1)(n+m-1)(n+m)}{8\pi(2n-1)2n(2n+1)}}\ Y_{n-1,m-1} + \sqrt{\frac{3n(n-m+1)(n-m+2)}{8\pi(2n+1)(2n+2)(2n+3)}}\ Y_{n+1,m-1}$$

$$\mathbf{X}_{10} \cdot \mathbf{X}_{nm} = -\sqrt{\frac{3(n+1)(n-m)(n+m)}{4\pi(2n-1)2n(2n+1)}}\ Y_{n-1,m} + \sqrt{\frac{3n(n-m+1)(n+m+1)}{4\pi(2n+1)(2n+2)(2n+3)}}\ Y_{n+1,m}$$

$$\mathbf{X}_{11} \cdot \mathbf{X}_{nm} = \sqrt{\frac{3(n+1)(n-m-1)(n-m)}{8\pi(2n-1)2n(2n+1)}}\ Y_{n-1,m+1} + \sqrt{\frac{3n(n+m+1)(n+m+2)}{8\pi(2n+1)(2n+2)(2n+3)}}\ Y_{n+1,m+1}$$

6.4 **Expansion of** $i\hat{\mathbf{r}} \times \mathbf{X}_{\nu\mu}(\hat{\mathbf{r}}) \cdot \mathbf{X}_{nm}(\hat{\mathbf{r}})$

Using the definition Eq (18), we can easily establish Eq (3) for $\nu = 1$:

$$i\hat{\mathbf{r}} \times \mathbf{X}_{1\mu}(\hat{\mathbf{r}}) \cdot \mathbf{X}_{nm}(\hat{\mathbf{r}}) = -\sqrt{\frac{3}{8\pi n(n+1)}}\ L_{\mu}\ Y_{nm}\ , \tag{6-20}$$

where

$$L_1 = -(L_x + iL_y)/\sqrt{2}\ , \qquad L_0 = L_z\ , \qquad L_{-1} = (L_x - iL_y)/\sqrt{2}\ .$$

With the help of Eq (12), the formulas Eq (20) have been written explicitly in Table 6.3.

Table 6.3 $i\hat{\mathbf{r}} \times \mathbf{X}_{1\mu}(\hat{\mathbf{r}}) \cdot \mathbf{X}_{nm}(\hat{\mathbf{r}}) = \sum_{\alpha} c(\alpha,\mu+m|1\mu nm)\ Y_{\alpha,\mu+m}(\hat{\mathbf{r}})$

$$i\hat{\mathbf{r}} \times \mathbf{X}_{1,-1} \cdot \mathbf{X}_{nm} = -\sqrt{\frac{3(n+m)(n-m+1)}{16\pi n(n+1)}}\ Y_{n,m-1}$$

$$i\hat{\mathbf{r}} \times \mathbf{X}_{10} \cdot \mathbf{X}_{nm} = -\sqrt{\frac{3}{8\pi n(n+1)}}\ m\ Y_{nm}$$

$$i\hat{\mathbf{r}} \times \mathbf{X}_{11} \cdot \mathbf{X}_{nm} = \sqrt{\frac{3(n-m)(n+m+1)}{16\pi n(n+1)}}\ Y_{n,m+1}$$

The expansion

$$Y_{10}\,\mathbf{X}_{nm} = \frac{\sqrt{n(n+2)}}{n+1}\,a(n+1,m|10nm)\,\mathbf{X}_{n+1,m} + \frac{\sqrt{(n-1)(n+1)}}{n}\,a(n-1,m|10nm)\,\mathbf{X}_{n-1,m}$$

$$- \sqrt{\frac{2}{n(n+1)}}\,c(nm|10nm)\,\hat{\mathbf{ir}} \times \mathbf{X}_{nm} \tag{6-21}$$

can be established by rearranging the orthogonality integrals for the coefficients so that they correspond to our definitions of a and c. With Eq (21) and the value of c(nm|10nm) from Table 6.3, we find that

$$\sqrt{\frac{3}{4\pi}}\,\frac{\mu}{\nu(\nu+1)}\,\hat{\mathbf{ir}} \times \mathbf{X}_{\nu\mu} \cdot \mathbf{X}_{nm} = -\,\frac{\sqrt{\nu(\nu+2)}}{\nu+1}\,a(\nu+1,\mu|10\nu\mu)\,\mathbf{X}_{\nu+1,\mu} \cdot \mathbf{X}_{nm}$$

$$-\,\frac{\sqrt{(\nu-1)(\nu+1)}}{\nu}\,a(\nu-1,\mu|10\nu\mu)\,\mathbf{X}_{\nu-1,\mu} \cdot \mathbf{X}_{nm} + Y_{10}\,\mathbf{X}_{\nu\mu} \cdot \mathbf{X}_{nm}\ . \tag{6-22}$$

The terms on the right side of Eq (22) may be expanded using Eqs (1) and (2). We can verify that there are no terms with $\alpha + \nu + n$ even, $\alpha > \nu + n$ or $\alpha < |\nu - n|$. (Equations (6), (7) and (19) can be used to show that terms with $\alpha = \nu + n + 1$ and $\alpha = |\nu - n| - 1$ cancel on the right side of Eq (22).) The case $\mu = 0$ must be treated separately: When $\mu = m = 0$, $\hat{\mathbf{ir}} \times \mathbf{X}_{\nu 0} \cdot \mathbf{X}_{n0} = 0$ and all of the c's are 0. Otherwise we can use Eq (22) (with $\nu\mu$ and nm exchanged) and the fact that

$$\hat{\mathbf{ir}} \times \mathbf{X}_{\nu\mu} \cdot \mathbf{X}_{nm} = -\,\hat{\mathbf{ir}} \times \mathbf{X}_{nm} \cdot \mathbf{X}_{\nu\mu}\ .$$

6.5 **Explicit Formulas for the Coefficients**

In this section we will obtain explicit expressions for the coefficients in Eqs (1) through (3):

$$a(\alpha,\mu+m|\nu\mu nm) = (-)^{\mu+m}\sqrt{\frac{(2\alpha+1)(2\nu+1)(2n+1)}{4\pi}}$$

$$\times \begin{pmatrix} \alpha & \nu & n \\ 0 & 0 & 0 \end{pmatrix} \begin{pmatrix} \alpha & \nu & n \\ -\mu-m & \mu & m \end{pmatrix} \tag{6-23}$$

$$b(\alpha,\mu+m|\nu\mu nm) = \frac{(-)^{\mu+m}}{2}\sqrt{\frac{(2\alpha+1)(2\nu+1)(2n+1)}{4\pi\nu(\nu+1)n(n+1)}}$$

$$\times\ [\alpha(\alpha+1) - \nu(\nu+1) - n(n+1)] \begin{pmatrix} \alpha & \nu & n \\ 0 & 0 & 0 \end{pmatrix} \begin{pmatrix} \alpha & \nu & n \\ -\mu-m & \mu & m \end{pmatrix} \tag{6-24}$$

$$c(\alpha,\mu+m|\nu\mu nm) = -\frac{(-)^{\mu+m}}{2}\sqrt{\frac{(2\alpha+1)(2\nu+1)(2n+1)}{4\pi\nu(\nu+1)n(n+1)}}$$

$$\times\sqrt{[\alpha^2-(\nu-n)^2][(\nu+n+1)^2-\alpha^2]}\begin{pmatrix}\alpha-1 & \nu & n\\ 0 & 0 & 0\end{pmatrix}\begin{pmatrix}\alpha & \nu & n\\ -\mu-m & \mu & m\end{pmatrix} . \qquad (6\text{-}25)$$

Some basic properties of the 3-j symbols $\begin{pmatrix}\alpha & \nu & n\\ \beta & \mu & m\end{pmatrix}$ are given in Section 6.8. Equations (23) through (25) are contained implicitly in the work of Cruzan [6], although he writes them awkwardly. Bruning and Lo [7], and others have noted Eqs (23) and (24) but have apparently overlooked Eq (25). The relation between Eqs (23) and (24) has already been demonstrated by elementary means in Section 6.3.

Equation (23) is actually a special case of the Clebsch-Gordan series discussed in Section 6.8 (see Eqs (57) through (59)). Slightly more work is required for Eqs (24) and (25). We begin with polar expressions for the spherical harmonics [3, 8]:

$$\mathbf{X}_{nm}(\hat{\mathbf{r}}) = \sqrt{\frac{2n+1}{4\pi}}\left[\frac{\hat{\boldsymbol{\theta}}+i\hat{\boldsymbol{\phi}}}{2}\,d^n_{m1}(\theta)+\frac{\hat{\boldsymbol{\theta}}-i\hat{\boldsymbol{\phi}}}{2}\,d^n_{m,-1}(\theta)\right]\exp(im\phi) \qquad (6\text{-}26a)$$

$$i\hat{\mathbf{r}}\times\mathbf{X}_{nm}(\hat{\mathbf{r}}) = \sqrt{\frac{2n+1}{4\pi}}\left[\frac{\hat{\boldsymbol{\theta}}+i\hat{\boldsymbol{\phi}}}{2}\,d^n_{m1}(\theta)-\frac{\hat{\boldsymbol{\theta}}-i\hat{\boldsymbol{\phi}}}{2}\,d^n_{m,-1}(\theta)\right]\exp(im\phi) . \qquad (6\text{-}26b)$$

The rotation functions $d^n_{m\mu}(\theta)$ are generalizations of the associated Legendre functions. From Eq (26) we have

$$\mathbf{X}_{\nu\mu}\cdot\mathbf{X}_{nm} = \frac{\sqrt{(2\nu+1)(2n+1)}}{8\pi}\,[d^\nu_{\mu1}\,d^n_{m,-1}+d^\nu_{\mu,-1}\,d^n_{m1}]\,\exp[i(\mu+m)\phi] \qquad (6\text{-}27a)$$

$$i\mathbf{r}\times\mathbf{X}_{\nu\mu}\cdot\mathbf{X}_{nm} = \frac{\sqrt{(2\nu+1)(2n+1)}}{8\pi}\,[d^\nu_{\mu1}\,d^n_{m,-1}-d^\nu_{\mu,-1}\,d^n_{m1}]\,\exp[i(\mu+m)\phi] . \qquad (6\text{-}27b)$$

The Clebsch-Gordan series Eq (58) can be used to obtain

$$d^\nu_{\mu,\pm1}\,d^n_{m,\mp1}\exp i(\mu+m)\phi$$

$$= (-)^{\mu+m}\sum_\alpha\sqrt{4\pi(2\alpha+1)}\begin{pmatrix}\alpha & \nu & n\\ 0 & \pm1 & \mp1\end{pmatrix}\begin{pmatrix}\alpha & \nu & n\\ -\mu-m & \mu & m\end{pmatrix}Y_{\alpha,\mu+m} . \qquad (6\text{-}28)$$

Substitution of Eq (28) into Eq (27) leads to

$$b(\alpha,\mu+m|\nu\mu nm) = (-)^{\mu+m}\sqrt{\frac{(2\alpha+1)(2\nu+1)(2n+1)}{4\pi}}\left[\frac{1+(-)^{\alpha+\nu+n}}{2}\right]$$

$$\times\begin{pmatrix}\alpha & \nu & n\\ 0 & 1 & -1\end{pmatrix}\begin{pmatrix}\alpha & \nu & n\\ -\mu-m & \mu & m\end{pmatrix} \qquad (6\text{-}29)$$

$$c(\alpha,\mu+m|\nu\mu nm) = (-)^{\mu+m}\sqrt{\frac{(2\alpha+1)(2\nu+1)(2n+1)}{4\pi}}\left[\frac{1-(-)^{\alpha+\nu+n}}{2}\right]$$

$$\times\begin{pmatrix}\alpha & \nu & n\\ 0 & 1 & -1\end{pmatrix}\begin{pmatrix}\alpha & \nu & n\\ -\mu-m & \mu & m\end{pmatrix}, \qquad (6\text{-}30)$$

where we have used the property (justified in Eqs (35) and (36)) that

$$\begin{pmatrix}\alpha & \nu & n\\ 0 & -1 & 1\end{pmatrix} = (-)^{\alpha+\nu+n}\begin{pmatrix}\alpha & \nu & n\\ 0 & 1 & -1\end{pmatrix}. \qquad (6\text{-}31)$$

The symmetric expressions Eqs (29) and (30) clearly show that b is 0 if $\alpha + \nu + n$ is odd and c is 0 if $\alpha + \nu + n$ is even.

To obtain Eqs (24) and (25) it is necessary to write the 3-j symbol

$$\begin{pmatrix}\alpha & \nu & n\\ 0 & -1 & 1\end{pmatrix}$$

in terms of 3-j symbols with the three lower indices equal to 0 (which have the simple closed-form expression Eq (64)). This may be done using

$$[\alpha(\alpha+1) - \nu(\nu+1) - n(n+1)]\begin{pmatrix}\alpha & \nu & n\\ 0 & 0 & 0\end{pmatrix}$$

$$= \sqrt{\nu(\nu+1)n(n+1)}\left[\begin{pmatrix}\alpha & \nu & n\\ 0 & 1 & -1\end{pmatrix} + \begin{pmatrix}\alpha & \nu & n\\ 0 & -1 & 1\end{pmatrix}\right], \qquad (6\text{-}32)$$

$$\pm(4\alpha+2)\begin{pmatrix}\alpha & \nu & n\\ 0 & \pm1 & \mp1\end{pmatrix} = \sqrt{\xi_\alpha}\begin{pmatrix}\alpha-1 & \nu & n\\ 0 & \pm1 & \mp1\end{pmatrix} + \sqrt{\xi_{\alpha+1}}\begin{pmatrix}\alpha+1 & \nu & n\\ 0 & \pm1 & \mp1\end{pmatrix}, \qquad (6\text{-}33)$$

and

$$0 = \sqrt{\xi_\alpha}\begin{pmatrix}\alpha-1 & \nu & n\\ 0 & 0 & 0\end{pmatrix} + \sqrt{\xi_{\alpha+1}}\begin{pmatrix}\alpha+1 & \nu & n\\ 0 & 0 & 0\end{pmatrix} \qquad (6\text{-}34)$$

$$\xi_\alpha = [\alpha^2 - (\nu-n)^2][(\nu+n+1)^2 - \alpha^2].$$

Equations (32) through (34) are special cases of the recursion formulas Eqs (61) and (62) in Section 6.8.

We find that when $\alpha + \nu + n$ is even

$$\begin{pmatrix} \alpha & \nu & n \\ 0 & 1 & -1 \end{pmatrix} = \begin{pmatrix} \alpha & \nu & n \\ 0 & -1 & 1 \end{pmatrix}$$

$$= \frac{1}{2} \frac{\alpha(\alpha+1) - \nu(\nu+1) - n(n+1)}{\sqrt{\nu(\nu+1)n(n+1)}} \begin{pmatrix} \alpha & \nu & n \\ 0 & 0 & 0 \end{pmatrix} , \tag{6-35}$$

while when $\alpha + \nu + n$ is odd

$$\begin{pmatrix} \alpha & \nu & n \\ 0 & 1 & -1 \end{pmatrix} = - \begin{pmatrix} \alpha & \nu & n \\ 0 & -1 & 1 \end{pmatrix}$$

$$= - \frac{1}{2} \sqrt{\frac{[\alpha^2 - (\nu-n)^2][(\nu+n+1)^2 - \alpha^2]}{\nu(\nu+1)n(n+1)}} \begin{pmatrix} \alpha-1 & \nu & n \\ 0 & 0 & 0 \end{pmatrix} . \tag{6-36}$$

Substitution of Eqs (35) and (36) into Eqs (29) and (30) yields Eqs (24) and (25). For spherical near-field scanning, the simple case $\mu = -m = \pm 1$ is most important:

$$b(\alpha 0|\nu,\pm 1,n,\mp 1) = \sqrt{\frac{(2\alpha+1)(2\nu+1)(2n+1)}{4\pi}}$$

$$\times \frac{[\alpha(\alpha+1) - \nu(\nu+1) - n(n+1)]^2}{4\nu(\nu+1)n(n+1)} \begin{pmatrix} \alpha & \nu & n \\ 0 & 0 & 0 \end{pmatrix}^2 \tag{6-37}$$

$$c(\alpha 0|\nu,\pm 1,n,\mp 1) = \pm \sqrt{\frac{(2\alpha+1)(2\nu+1)(2n+1)}{4\pi}}$$

$$\times \frac{[\alpha^2 - (\nu-n)^2][(\nu+n+1)^2 - \alpha^2]}{4\nu(\nu+1)n(n+1)} \begin{pmatrix} \alpha-1 & \nu & n \\ 0 & 0 & 0 \end{pmatrix}^2 . \tag{6-38}$$

Equations (35) and (36) may also be written in terms of 6-j symbols: When $\alpha + \nu + n$ is even,

$$\begin{pmatrix} \alpha & \nu & n \\ 0 & 1 & -1 \end{pmatrix} = \sqrt{(2\nu+1)(2n+1)} \begin{pmatrix} \alpha & \nu & n \\ 0 & 0 & 0 \end{pmatrix} \begin{Bmatrix} \alpha & \nu & n \\ 1 & n & \nu \end{Bmatrix} , \tag{6-39}$$

and when $\alpha + \nu + n$ is odd,

$$\begin{pmatrix} \alpha & \nu & n \\ 0 & 1 & -1 \end{pmatrix} = \sqrt{\frac{(2\nu-1)(2\nu+1)(2n+1)}{\nu+1}} \begin{pmatrix} \alpha & \nu-1 & n \\ 0 & 0 & 0 \end{pmatrix} \begin{Bmatrix} \alpha & \nu-1 & n \\ 1 & n & \nu \end{Bmatrix} \tag{6-40a}$$

$$\begin{pmatrix}\alpha & \nu & n\\ 0 & 1 & -1\end{pmatrix} = \sqrt{\frac{\alpha(2\alpha-1)(2\alpha+1)(2n+1)}{\nu(\nu+1)}}\begin{pmatrix}\alpha-1 & \nu & n\\ 0 & 0 & 0\end{pmatrix}\begin{Bmatrix}\alpha-1 & \nu & n\\ n & 1 & \alpha\end{Bmatrix} . \qquad (6\text{-}40b)$$

Although these are special cases of a more general relationship between 3-j and 6-j symbols [9, Eq (6.2.8)], we may regard Eqs (39) and (40) as definitions. Explicit expressions, obtained by comparing Eqs (35) and (36) with Eqs (39) and (40), agree with formulas for 6-j symbols given by Edmonds [9, Table 5]. Equations (40a) and (40b) can be related by interchanging α and ν in one of them and using the fact that

$$\begin{pmatrix}\alpha & \nu & n\\ 0 & 1 & -1\end{pmatrix} = -\sqrt{\frac{\alpha(\alpha+1)}{\nu(\nu+1)}}\begin{pmatrix}\alpha & \nu & n\\ 1 & 0 & -1\end{pmatrix} , \qquad (\alpha + \nu + n \text{ odd})$$

which follows from Eq (60).

With Eqs (39) and (40), Eqs (29) and (30) become

$$b(\alpha,\mu+m|\nu\mu nm) = (-)^{\mu+m}\sqrt{\frac{2\alpha+1}{4\pi}}(2\nu+1)(2n+1)$$

$$\times\begin{pmatrix}\alpha & \nu & n\\ 0 & 0 & 0\end{pmatrix}\begin{Bmatrix}\alpha & \nu & n\\ 1 & n & \nu\end{Bmatrix}\begin{pmatrix}\alpha & \nu & n\\ -\mu-m & \mu & m\end{pmatrix} \qquad (6\text{-}41)$$

$$c(\alpha,\mu+m|\nu\mu nm) = (-)^{\mu+m}\sqrt{\frac{2\alpha+1}{4\pi}\frac{2\nu-1}{\nu+1}}(2\nu+1)(2n+1)$$

$$\times\begin{pmatrix}\alpha & \nu-1 & n\\ 0 & 0 & 0\end{pmatrix}\begin{Bmatrix}\alpha & \nu-1 & n\\ 1 & n & \nu\end{Bmatrix}\begin{pmatrix}\alpha & \nu & n\\ -\mu-m & \mu & m\end{pmatrix} \qquad (6\text{-}42a)$$

$$c(\alpha,\mu+m|\nu\mu nm) = (-)^{\mu+m}\sqrt{\frac{2\nu+1}{4\pi}\frac{\alpha(2\alpha-1)}{\nu(\nu+1)}}(2\alpha+1)(2n+1)$$

$$\times\begin{pmatrix}\alpha-1 & \nu & n\\ 0 & 0 & 0\end{pmatrix}\begin{Bmatrix}\alpha-1 & \nu & n\\ n & 1 & \alpha\end{Bmatrix}\begin{pmatrix}\alpha & \nu & n\\ -\mu-m & \mu & m\end{pmatrix} . \qquad (6\text{-}42b)$$

Tough [10] gives the form Eq (42a) while Cruzan [6] gives Eq (42b). The difference between Eqs (42a) and (42b) reflects the relationship

$$c(\alpha\beta|\nu,-\mu nm) = (-)^{m+1}\sqrt{\frac{\alpha(\alpha+1)}{\nu(\nu+1)}}\, c(\nu\mu|\alpha,-\beta nm) \qquad (6\text{-}43)$$

which can be found from elementary manipulation of the integral definition

$$c(\alpha\beta|\nu\mu nm) = \int Y^{*}_{\alpha\beta}(\hat{\mathbf{r}})\ i\hat{\mathbf{r}} \times \mathbf{X}_{\nu\mu}(\hat{\mathbf{r}}) \cdot \mathbf{X}_{nm}(\hat{\mathbf{r}})\ d\hat{\mathbf{r}}\ .$$

When $\mu = -m$, we have several useful summation formulas:

$$\sum_{\alpha} \sqrt{2\alpha+1}\ a(\alpha 0|\nu,-mnm) = \sqrt{\frac{(2\nu+1)(2n+1)}{4\pi}}\ \delta_{m0} \qquad (6\text{-}44)$$

$$\sum_{\alpha} \sqrt{2\alpha+1}\ b(\alpha 0|\nu,-mnm) = \sqrt{\frac{(2\nu+1)(2n+1)}{16\pi}}\ \delta_{m,\pm 1} \qquad (6\text{-}45)$$

$$\sum_{\alpha} \sqrt{2\alpha+1}\ c(\alpha 0|\nu,-mnm) = \mp \sqrt{\frac{(2\nu+1)(2n+1)}{16\pi}}\ \delta_{m,\pm 1}\ . \qquad (6\text{-}46)$$

These follow from Eqs (1) through (3) noting that on the z axis

$$Y_{nm}(\hat{\mathbf{z}}) = \sqrt{\frac{2n+1}{4\pi}}\ \delta_{m0} \qquad (6\text{-}47)$$

$$\mathbf{X}_{nm}(\hat{\mathbf{z}}) = \sqrt{\frac{2n+1}{16\pi}}\ (\hat{\mathbf{x}} \pm i\hat{\mathbf{y}})\ \delta_{m,\pm 1}\ . \qquad (6\text{-}48)$$

Using Eq (23) we find that Eq (44) is equivalent to

$$\sum_{\alpha} (2\alpha+1) \begin{pmatrix} \alpha & \nu & n \\ 0 & 0 & 0 \end{pmatrix} \begin{pmatrix} \alpha & \nu & n \\ 0 & -m & m \end{pmatrix} = \delta_{m0}\ , \qquad (6\text{-}49)$$

a special case of the "orthogonality" relation Eq (66). If b and c are taken from Eqs (29) and (30) then Eqs (45) and (46) also reduce to cases of Eq (66). On the other hand, if we use Eqs (41) and (42) in Eqs (45) and (46), we find formulas such as

$$\sum_{\alpha} (2\alpha+1) \begin{pmatrix} \alpha & \nu & n \\ 0 & 0 & 0 \end{pmatrix} \begin{Bmatrix} \alpha & \nu & n \\ 1 & n & \nu \end{Bmatrix} \begin{pmatrix} \alpha & \nu & n \\ 0 & -m & m \end{pmatrix}$$

$$= (-)^{\nu+n} \begin{pmatrix} 1 & \nu & \nu \\ m & -m & 0 \end{pmatrix} \begin{pmatrix} 1 & n & n \\ m & -m & 0 \end{pmatrix} \qquad (6\text{-}50)$$

which are further examples of general relationships between 3-j and 6-j symbols [9, Eq (6.2.6)].

6.6 **Expansion of Vector Products**

The useful expansions

$$\mathbf{X}_{\nu\mu}(\hat{\mathbf{r}}) \times \mathbf{X}_{nm}(\hat{\mathbf{r}}) = -i \sum_{\alpha} c(\alpha,\mu+m|\nu\mu nm)\ Y_{\alpha,\mu+m}(\hat{\mathbf{r}})\ \hat{\mathbf{r}} \tag{6-51}$$

$$[i\hat{\mathbf{r}} \times \mathbf{X}_{\nu\mu}(\hat{\mathbf{r}})] \times \mathbf{X}_{nm}(\hat{\mathbf{r}}) = -i \sum_{\alpha} b(\alpha,\mu+m|\nu\mu nm)\ Y_{\alpha,\mu+m}(\hat{\mathbf{r}})\ \hat{\mathbf{r}} \tag{6-52}$$

$$\begin{aligned} Y_{\nu\mu}(\hat{\mathbf{r}})\ \mathbf{X}_{nm}(\hat{\mathbf{r}}) = \sum_{\alpha} \Bigg[& \frac{\alpha(\alpha+1) - \nu(\nu+1) + n(n+1)}{2\sqrt{\alpha(\alpha+1)n(n+1)}}\ a(\alpha,\mu+m|\nu\mu nm)\ \mathbf{X}_{\alpha,\mu+m}(\hat{\mathbf{r}}) \\ & - \sqrt{\frac{\nu(\nu+1)}{\alpha(\alpha+1)}}\ c(\alpha,\mu+m|\nu\mu nm)\ i\hat{\mathbf{r}} \times \mathbf{X}_{\alpha,\mu+m}(\hat{\mathbf{r}}) \Bigg] \end{aligned} \tag{6-53}$$

follow easily from the definitions of the coefficients. Equation (53) is a generalization of Eq (21).

6.7 **Other Notations for Vector Spherical Harmonics**

Danos and Maximon [11], James [8], and others use different definitions for vector spherical harmonics. Many of these definitions are variants of that used by Edmonds [9]. Edmonds' and Jackson's spherical harmonics are related by the formulas [9, pp. 83-84]

$$\begin{aligned} \mathbf{X}_{nm} &= \mathbf{Y}_{nnm} \\ i\hat{\mathbf{r}} \times \mathbf{X}_{nm} &= -\sqrt{\frac{n+1}{2n+1}}\ \mathbf{Y}_{n,n-1,m} - \sqrt{\frac{n}{2n+1}}\ \mathbf{Y}_{n,n+1,m} \\ \hat{\mathbf{r}}\ Y_{nm} &= \sqrt{\frac{n}{2n+1}}\ \mathbf{Y}_{n,n-1,m} - \sqrt{\frac{n+1}{2n+1}}\ \mathbf{Y}_{n,n+1,m} \end{aligned} \tag{6-54}$$

and, conversely,

$$\mathbf{Y}_{nnm} = \mathbf{X}_{nm}$$

$$\mathbf{Y}_{n,n-1,m} = -\sqrt{\frac{n+1}{2n+1}}\, i\hat{\mathbf{r}} \times \mathbf{X}_{nm} + \sqrt{\frac{n}{2n+1}}\, \hat{\mathbf{r}}\, Y_{nm} \tag{6-55}$$

$$\mathbf{Y}_{n,n+1,m} = -\sqrt{\frac{n}{2n+1}}\, i\hat{\mathbf{r}} \times \mathbf{X}_{nm} - \sqrt{\frac{n+1}{2n+1}}\, \hat{\mathbf{r}}\, Y_{nm} .$$

Jackson's spherical harmonics are perhaps better suited to electromagnetics since they facilitate division of the fields into radial and transverse components.

6.8 **The Clebsch-Gordan Series and the Wigner 3-j Symbols**

Here we can only summarize some useful results. Details may be found in References [9, 12-16].

Generalized spherical harmonics or rotation functions are defined by

$$D^n_{mm'}(\phi,\theta,\chi) = \exp(-im\phi)\, d^n_{mm'}(\theta)\, \exp(-im'\chi) , \tag{6-56}$$

where $d^n_{mm'}(\theta)$ is a real function, n is nonnegative and may be integral or half-integral,

$$n = 0,\ 1/2,\ 1,\ 3/2,\ \ldots ,$$

and m and m' range over the values

$$-n,\ -n+1,\ -n+2,\ \ldots ,\ n .$$

Applications with nonintegral values of n rarely occur outside of quantum mechanics.

A connection between the rotation functions and the scalar spherical harmonics is

$$Y_{nm}(\hat{\mathbf{r}}) = \sqrt{\frac{2n+1}{4\pi}}\, D^{n*}_{m0}(\phi,\theta,\chi) . \tag{6-57}$$

Products of rotation functions can be expanded using the Clebsch-Gordan series [9, Eq (4.3.2)]

$$D^{\nu}_{\mu\mu'}\, D^{n}_{mm'} = \sum_{\alpha\beta\beta'} (2\alpha+1) \begin{pmatrix} \alpha & \nu & n \\ \beta & \mu & m \end{pmatrix} D^{\alpha *}_{\beta\beta'} \begin{pmatrix} \alpha & \nu & n \\ \beta' & \mu' & m' \end{pmatrix} , \qquad (6\text{-}58)$$

an extremely powerful, yet elementary result. The sum over β and β' is trivial since the 3-j symbols in Eq (58) vanish unless $\beta + \mu + m = 0$ and $\beta' + \mu' + m' = 0$.

Equations (57) and (58) immediately give

$$Y_{\nu\mu}\, Y_{nm} = (-)^{\mu+m} \sum_{\alpha} \sqrt{\frac{(2\alpha+1)(2\nu+1)(2n+1)}{4\pi}}$$

$$\times \begin{pmatrix} \alpha & \nu & n \\ 0 & 0 & 0 \end{pmatrix} \begin{pmatrix} \alpha & \nu & n \\ -\mu-m & \mu & m \end{pmatrix} Y_{\alpha,\mu+m} , \qquad (6\text{-}59)$$

which is equivalent to Eqs (1) and (23).

Explicit formulas for some of the simpler 3-j symbols may be found in Edmonds [9, Section 3.7 and Table 2]. Useful relations and properties of 3-j symbols are compiled in the remainder of this section.

The 3-j symbols are real. $\begin{pmatrix} \alpha & \nu & n \\ \beta & \mu & m \end{pmatrix}$ is 0 if:

(1) $|\beta| > \alpha$, $|\mu| > \nu$, or $|m| > n$.

(2) $\beta + \mu + m \neq 0$.

(3) α, ν and n do not satisfy the triangle inequality; for example, if $\alpha > \nu + n$ or $\alpha < |\nu - n|$.

We have the symmetries:

(1) 3-j symbols are invariant under a cyclic (even) permutation of columns,

$$\begin{pmatrix} \alpha & \nu & n \\ \beta & \mu & m \end{pmatrix} = \begin{pmatrix} n & \alpha & \nu \\ m & \beta & \mu \end{pmatrix} , \text{ etc.}$$

(2) An anti-cyclic (odd) permutation of columns may change the sign,

$$\begin{pmatrix} \alpha & \nu & n \\ \beta & \mu & m \end{pmatrix} = (-)^{\alpha+\nu+n} \begin{pmatrix} \alpha & n & \nu \\ \beta & m & \mu \end{pmatrix} , \text{ etc.}$$

(3) Reversal of lower index signs may change the sign,

$$\begin{pmatrix}\alpha & \nu & n\\ -\beta & -\mu & -m\end{pmatrix} = (-)^{\alpha+\nu+n}\begin{pmatrix}\alpha & n & \nu\\ \beta & m & \mu\end{pmatrix} .$$

The following recursion formulas are used in the main text:

$$\lambda^{\pm}_{\alpha\beta}\begin{pmatrix}\alpha & \nu & n\\ \beta\pm1 & \mu & m\end{pmatrix} + \lambda^{\pm}_{\nu\mu}\begin{pmatrix}\alpha & \nu & n\\ \beta & \mu\pm1 & m\end{pmatrix} + \lambda^{\pm}_{nm}\begin{pmatrix}\alpha & \nu & n\\ \beta & \mu & m\pm1\end{pmatrix} = 0 \qquad (6\text{-}60)$$

$$[\alpha(\alpha+1) - \nu(\nu+1) - n(n+1) - 2\mu m]\begin{pmatrix}\alpha & \nu & n\\ \beta & \mu & m\end{pmatrix}$$

$$= \lambda^{+}_{\nu\mu}\lambda^{-}_{nm}\begin{pmatrix}\alpha & \nu & n\\ \beta & \mu+1 & m-1\end{pmatrix} + \lambda^{-}_{\nu\mu}\lambda^{+}_{nm}\begin{pmatrix}\alpha & \nu & n\\ \beta & \mu-1 & m+1\end{pmatrix} \qquad (6\text{-}61)$$

$$\zeta_\alpha\begin{pmatrix}\alpha & \nu & n\\ \beta & \mu & m\end{pmatrix} = \sqrt{\xi_\alpha}\begin{pmatrix}\alpha-1 & \nu & n\\ \beta & \mu & m\end{pmatrix} + \sqrt{\xi_{\alpha+1}}\begin{pmatrix}\alpha+1 & \nu & n\\ \beta & \mu & m\end{pmatrix} , \qquad (6\text{-}62)$$

where

$$\lambda^{\pm}_{nm} = \sqrt{(n\mp m)(n\pm m+1)}$$

$$\zeta_\alpha = [(\mu-m) + \beta\,\frac{\nu(\nu+1) - n(n+1)}{\alpha(\alpha+1)}](2\alpha+1)$$

$$\xi_\alpha = [\alpha^2 - (\nu-n)^2][(\nu+n+1)^2 - \alpha^2](\alpha^2 - \beta^2)/\alpha^2 .$$

Equation (61) follows from Eq (60).

When $\beta = \mu = m = 0$, Eq (62) reduces to the two term recursion formula Eq (34) which is easily solved: When $\alpha + \nu + n$ is odd

$$\begin{pmatrix}\alpha & \nu & n\\ 0 & 0 & 0\end{pmatrix} = 0 . \qquad (6\text{-}63)$$

When $\alpha + \nu + n$ is even

$$\begin{pmatrix}\alpha & \nu & n\\ 0 & 0 & 0\end{pmatrix} = (-)^{(\alpha+\nu+n)/2}\sqrt{\frac{(\alpha+\nu-n)!\ (\alpha-\nu+n)!\ (-\alpha+\nu+n)!}{(\alpha+\nu+n+1)!}}$$

$$\times\ \frac{(\frac{\alpha+\nu+n}{2})!}{(\frac{\alpha+\nu-n}{2})!\ (\frac{\alpha-\nu+n}{2})!\ (\frac{-\alpha+\nu+n}{2})!} . \qquad (6\text{-}64)$$

The magnitude of the term

$$\begin{pmatrix} \nu+n & \nu & n \\ 0 & 0 & 0 \end{pmatrix} = (-)^{\nu+n} \sqrt{\frac{(2\nu)!(2n)!}{(2\nu+2n)!}} \frac{(\nu+n)!}{\nu!\ n!} \tag{6-65}$$

can be verified with Eqs (23) and (6). The phase is determined by convention.

The "orthogonality" relations are also useful:

$$\sum_{\alpha\beta} (2\alpha+1) \begin{pmatrix} \alpha & \nu & n \\ \beta & \mu & m \end{pmatrix} \begin{pmatrix} \alpha & \nu & n \\ \beta & \mu' & m' \end{pmatrix} = \delta_{\mu\mu'} \delta_{mm'} \tag{6-66}$$

$$(2\alpha+1) \sum_{\mu m} \begin{pmatrix} \alpha & \nu & n \\ \beta & \mu & m \end{pmatrix} \begin{pmatrix} \alpha' & \nu & n \\ \beta' & \mu & m \end{pmatrix} = \delta_{\alpha\alpha'} \delta_{\beta\beta'} \ . \tag{6-67}$$

Formulas given in this section are often written in terms of Clebsch-Gordan coefficients (also called vector-coupling or Wigner coefficients). These are simply related to the 3-j symbols:

$$<\alpha\beta|\nu\mu nm> = \sqrt{2\alpha+1}\ (-)^{-\nu+n-\beta} \begin{pmatrix} \alpha & \nu & n \\ -\beta & \mu & m \end{pmatrix} . \tag{6-68}$$

Although Clebsch-Gordan coefficients are used interchangeably with 3-j symbols, it is often easier to deal with the latter because of the simpler symmetries.

7. CALCULATION OF TRANSLATED PROBE COEFFICIENTS IN SPHERICAL NEAR-FIELD SCANNING

7.1 Introduction

While we present an overview of the role of translated probe coefficients in spherical near-field scanning, our intent is to describe an algorithm for efficient calculation. We make no attempt to describe notation unless it is needed for this purpose. The interested reader will find a more complete development elsewhere [5].

7.2 Transmission Formula

For a receiving probe, the Jensen transmission formula [17] for spherical near-field scanning is (see Eq (8-16))

$$W(r_0,\phi,\theta,\chi) = \sum_{\mu nm} \left[R^H_{n\mu}(r_0)\, t^H_{nm} + R^E_{n\mu}(r_0)\, t^E_{nm} \right] D^n_{\mu m}(-\chi,-\theta,-\phi) \ , \qquad (7\text{-}1)$$

where r_0 is the radius of the measurement sphere and (ϕ,θ,χ) are the Euler angles describing the position/orientation of the probe. The goal is to determine the coefficients of the far-field (transmitting) pattern

$$\mathbf{t}(\hat{\mathbf{r}}) = \sum_{\nu\mu} \left[t^H_{\nu\mu}\, \mathbf{X}_{\nu\mu}(\hat{\mathbf{r}}) + t^E_{\nu\mu}\, i\hat{\mathbf{k}} \times \mathbf{X}_{\nu\mu}(\hat{\mathbf{r}}) \right]$$

using the measured data $W(r_0,\phi,\theta,\chi)$ and the orthogonality properties of the rotation functions $D^n_{\mu m}(-\chi,-\theta,-\phi)$.

The translated probe coefficients

$$\begin{aligned} R^H_{nm}(r) &= \int \mathbf{r}(\hat{\mathbf{k}}) \cdot \mathbf{X}_{nm}(\hat{\mathbf{k}}) \exp(i\gamma r) \frac{d\mathbf{K}}{\gamma k} \\ R^E_{nm}(r) &= \int \mathbf{r}(\hat{\mathbf{k}}) \cdot i\hat{\mathbf{k}} \times \mathbf{X}_{nm}(\hat{\mathbf{k}}) \exp(i\gamma r) \frac{d\mathbf{K}}{\gamma k} \end{aligned} \qquad (7\text{-}2)$$

are functions of the measurement radius r_0 and the probe receiving pattern $\mathbf{r}(\hat{\mathbf{k}})$ (which must be measured separately).

The probe receiving pattern may be expanded in terms of vector spherical harmonics as

$$\mathbf{r}(\hat{\mathbf{k}}) = \sum_{\nu\mu}\left[r^H_{\nu\mu}\ \mathbf{X}_{\nu\mu}(\hat{\mathbf{k}}) + r^E_{\nu\mu}\ i\hat{\mathbf{k}} \times \mathbf{X}_{\nu\mu}(\hat{\mathbf{k}})\right] . \tag{7-3}$$

The object of these notes is to describe a simple method for computing the translated probe coefficients Eq (2) from the inputs $r^H_{\nu\mu}$, $r^E_{\nu\mu}$ and r_0.

7.3 **Calculation of the Translated Probe Coefficients**

If Eq (3) is substituted into Eq (2) we find that

$$\begin{aligned} R^H_{nm}(r) &= \sum_{\nu}\left[r^H_{\nu,-m}\ B(\nu,-m|nm;r) + r^E_{\nu,-m}\ C(\nu,-m|nm;r)\right] \\ R^E_{nm}(r) &= -\sum_{\nu}\left[r^H_{\nu,-m}\ C(\nu,-m|nm;r) + r^E_{\nu,-m}\ B(\nu,-m|nm;r)\right] , \end{aligned} \tag{7-4}$$

where

$$\begin{aligned} B(\nu,-m|nm;r) &= B(\nu m|n,-m;r) \\ &= \int \mathbf{X}_{\nu,-m}(\hat{\mathbf{k}}) \cdot \mathbf{X}_{nm}(\hat{\mathbf{k}})\ \exp(i\gamma r)\ \frac{d\mathbf{K}}{\gamma k} \end{aligned} \tag{7-5a}$$

$$\begin{aligned} C(\nu,-m|nm;r) &= -C(\nu m|n,-m;r) \\ &= \int i\hat{\mathbf{k}} \times \mathbf{X}_{\nu,-m}(\hat{\mathbf{k}}) \cdot \mathbf{X}_{nm}(\hat{\mathbf{k}})\ \exp(i\gamma r)\ \frac{d\mathbf{K}}{\gamma k} . \end{aligned} \tag{7-5b}$$

B and C are closely related to coefficients occurring in translation formulas for spherical waves [5].

The dot products of vector spherical harmonics may be expanded in terms of scalar spherical harmonics as

$$\mathbf{X}_{\nu,-m}(\hat{\mathbf{k}}) \cdot \mathbf{X}_{nm}(\hat{\mathbf{k}}) = \sum_{\alpha} b(\alpha 0|\nu,-mnm)\ Y_{\alpha 0}(\hat{\mathbf{k}}) \tag{7-6a}$$

$$i\hat{\mathbf{k}} \times \mathbf{X}_{\nu,-m}(\hat{\mathbf{k}}) \cdot \mathbf{X}_{nm}(\hat{\mathbf{k}}) = \sum_{\alpha} c(\alpha 0|\nu,-mnm)\ Y_{\alpha 0}(\hat{\mathbf{k}}) . \tag{7-6b}$$

In Eq (6), α ranges over the interval $|\nu-n| \le \alpha \le \nu+n$. Additionally, $b(\alpha 0|\nu,-mnm)$ is 0 if $\alpha + \nu + n$ is odd and $c(\alpha 0|\nu,-mnm)$ is 0 if $\alpha + \nu + n$ is even.

If Eq (6) is substituted into Eq (5) the integrals can be done analytically to yield [5]

$$B(\nu,-m|nm;r) = \sqrt{\pi} \sum_{\alpha} i^{\alpha} \sqrt{2\alpha+1}\, b(\alpha 0|\nu,-mnm)\, h_{\alpha}^{(1)}(kr)$$

$$C(\nu,-m|nm;r) = \sqrt{\pi} \sum_{\alpha} i^{\alpha} \sqrt{2\alpha+1}\, c(\alpha 0|\nu,-mnm)\, h_{\alpha}^{(1)}(kr) \quad . \qquad (7\text{-}7)$$

$h_{\alpha}^{(1)}(kr)$ is a spherical Hankel function of the first kind.

In practical spherical scanning applications, special probes are used for which m assumes only the values ±1. Under these conditions, b and c have especially simple forms (see Eqs (6-37) and (6-38)):

$$b(\alpha 0|\nu,\pm 1,n,\mp 1) = \sqrt{\frac{(2\alpha+1)(2\nu+1)(2n+1)}{4\pi}} \times \frac{[\alpha(\alpha+1) - \nu(\nu+1) - n(n+1)]^2}{4\nu(\nu+1)n(n+1)} \begin{pmatrix} \alpha & \nu & n \\ 0 & 0 & 0 \end{pmatrix}^2 \qquad (7\text{-}8a)$$

$$c(\alpha 0|\nu,\pm 1,n,\mp 1) = \pm \sqrt{\frac{(2\alpha+1)(2\nu+1)(2n+1)}{4\pi}} \times \frac{[\alpha^2 - (\nu-n)^2][(\nu+n+1)^2 - \alpha^2]}{4\nu(\nu+1)n(n+1)} \begin{pmatrix} \alpha-1 & \nu & n \\ 0 & 0 & 0 \end{pmatrix}^2 \quad . \qquad (7\text{-}8b)$$

For a given choice of m, b and c will have a constant sign independent of α.

There are closed-form expressions for the 3-j symbols in Eq (8) (see Eqs (6-63) and (6-64)), but it is probably better to calculate them recursively

$$\xi_{\alpha} \begin{pmatrix} \alpha-1 & \nu & n \\ 0 & 0 & 0 \end{pmatrix}^2 = \xi_{\alpha+1} \begin{pmatrix} \alpha+1 & \nu & n \\ 0 & 0 & 0 \end{pmatrix}^2 , \qquad (7\text{-}9)$$

where

$$\xi_{\alpha} = [\alpha^2 - (\nu-n)^2]\,[(\nu+n+1)^2 - \alpha^2] \ .$$

Remember that $|\nu-n| \le \alpha \le \nu+n$ and that the 3-j symbol is 0 unless the sum of the indices is even (assuming the lower indices are 0.)

The 3-j symbols may be normalized using

$$\sum_{\alpha} (2\alpha+1) \begin{pmatrix} \alpha & \nu & n \\ 0 & 0 & 0 \end{pmatrix}^2 = 1 \ . \qquad (7\text{-}10)$$

7.4 **Summary**

The crucial formulas for calculation of the translated probe coefficients are listed below:

$$\begin{aligned} R^H_{nm}(r) &= \sum_{\nu} \left[r^H_{\nu,-m} \, B(\nu,-m|nm;r) + r^E_{\nu,-m} \, C(\nu,-m|nm;r) \right] \\ R^E_{nm}(r) &= - \sum_{\nu} \left[r^H_{\nu,-m} \, C(\nu,-m|nm;r) + r^E_{\nu,-m} \, B(\nu,-m|nm;r) \right] \end{aligned} \qquad (7\text{-}4)$$

$$\begin{aligned} B(\nu,-m|nm;r) &= \sqrt{\pi} \sum_{\alpha} i^{\alpha} \sqrt{2\alpha+1} \, b(\alpha 0|\nu,-mnm) \, h^{(1)}_{\alpha}(kr) \\ C(\nu,-m|nm;r) &= \sqrt{\pi} \sum_{\alpha} i^{\alpha} \sqrt{2\alpha+1} \, c(\alpha 0|\nu,-mnm) \, h^{(1)}_{\alpha}(kr) \end{aligned} \qquad (7\text{-}7)$$

$$b(\alpha 0|\nu,\pm 1,n,\mp 1) = \sqrt{\frac{(2\alpha+1)(2\nu+1)(2n+1)}{4\pi}} \times \frac{[\alpha(\alpha+1) - \nu(\nu+1) - n(n+1)]^2}{4\nu(\nu+1)n(n+1)} \begin{pmatrix} \alpha & \nu & n \\ 0 & 0 & 0 \end{pmatrix}^2 \qquad (7\text{-}8a)$$

$$c(\alpha 0|\nu,\pm 1,n,\mp 1) = \pm \sqrt{\frac{(2\alpha+1)(2\nu+1)(2n+1)}{4\pi}} \times \frac{[\alpha^2 - (\nu-n)^2][(\nu+n+1)^2 - \alpha^2]}{4\nu(\nu+1)n(n+1)} \begin{pmatrix} \alpha-1 & \nu & n \\ 0 & 0 & 0 \end{pmatrix}^2 \qquad (7\text{-}8b)$$

$$\xi_{\alpha} \begin{pmatrix} \alpha-1 & \nu & n \\ 0 & 0 & 0 \end{pmatrix}^2 = \xi_{\alpha+1} \begin{pmatrix} \alpha+1 & \nu & n \\ 0 & 0 & 0 \end{pmatrix}^2 \qquad (7\text{-}9)$$

$$\sum_{\alpha} (2\alpha+1) \begin{pmatrix} \alpha & \nu & n \\ 0 & 0 & 0 \end{pmatrix}^2 = 1 \ . \qquad (7\text{-}10)$$

8. SPHERICAL NEAR-FIELD SCANNING TRANSMISSION EQUATIONS: RECEIVING PROBE, TRANSMITTING TEST ANTENNA; TRANSMITTING PROBE, RECEIVING TEST ANTENNA

8.1 Introduction

In these notes spherical near-field transmission equations are derived for both receiving and transmitting probes. The connection between the two cases is discussed in terms of reciprocity. The approach adopted is heavily dependent on concepts introduced in a recent paper [5].

8.2 Initial Definitions

The electric field of a finite source may be represented in terms of plane waves as

$$\mathbf{E}(\mathbf{r}) = \frac{1}{2\pi} \int \mathbf{t}(\hat{\mathbf{r}}) \exp(i\mathbf{k} \cdot \mathbf{r}) \frac{d\mathbf{K}}{\gamma k}, \qquad z > 0 . \tag{8-1}$$

Equation (1) is a two-dimensional Fourier transform on transverse $\mathbf{k}$:

$$\int d\mathbf{K} = \int_{-\infty}^{\infty} dk_x \int_{-\infty}^{\infty} dk_y , \qquad \mathbf{K} = k_x\hat{\mathbf{x}} + k_y\hat{\mathbf{y}} , \qquad K = |\mathbf{K}| .$$

Due to the restriction $k = |\mathbf{k}| = \omega/c$, the z component of the propagation vector is not independent, but is given by

$$\gamma = k_z = \begin{cases} \sqrt{k^2 - K^2} , & k \geq K \\ i\sqrt{K^2 - k^2} , & k < K . \end{cases}$$

The function $\mathbf{t}(\hat{\mathbf{r}})$ is known as the far-field (transmitting) pattern as a consequence of the asymptotic relationship

$$\mathbf{E}(\mathbf{r}) \xrightarrow[r\to\infty]{} \mathbf{t}(\hat{\mathbf{r}})\, G(\mathbf{r}) , \tag{8-2}$$

where

$$G(\mathbf{r}) = \frac{\exp(ikr)}{ikr} . \tag{8-3}$$

$\mathbf{t}(\hat{\mathbf{k}})$ is a function of direction only and $\mathbf{t}(\hat{\mathbf{k}}) \cdot \mathbf{k} = 0$; therefore the far-field pattern may be expanded in vector spherical harmonics as

$$\mathbf{t}(\hat{\mathbf{k}}) = \sum_{\nu\mu} \left[t^{H}_{\nu\mu} \, \mathbf{X}_{\nu\mu}(\hat{\mathbf{k}}) + t^{E}_{\nu\mu} \, i\hat{\mathbf{k}} \times \mathbf{X}_{\nu\mu}(\hat{\mathbf{k}}) \right] . \tag{8-4}$$

The response $W(\mathbf{r})$ of a receiver to the incident field $\mathbf{E}(\mathbf{r})$ may be written

$$W(\mathbf{r}) = \int \mathbf{r}(\hat{\mathbf{k}}) \cdot \mathbf{t}(\hat{\mathbf{k}}) \exp(i\mathbf{k} \cdot \mathbf{r}) \frac{d\mathbf{K}}{\gamma k} , \qquad z > 0 . \tag{8-5}$$

(The receiver is not allowed to rotate as it is moved from place to place.) This is Kerns' transmission formula of planar near-field scanning [18]. The receiving pattern $\mathbf{r}(\hat{\mathbf{k}})$ is defined so that the response to the plane wave

$$\frac{\mathbf{t}(\hat{\mathbf{k}})}{2\pi} \exp(i\mathbf{k} \cdot \mathbf{r})$$

is

$$\mathbf{r}(\hat{\mathbf{k}}) \cdot \mathbf{t}(\hat{\mathbf{k}}) \exp(i\mathbf{k} \cdot \mathbf{r}_0)$$

when the receiver is located at $\mathbf{r}_0$. Like $\mathbf{t}(\hat{\mathbf{k}})$, $\mathbf{r}(\hat{\mathbf{k}})$ is a function of direction only and $\mathbf{r}(\hat{\mathbf{k}}) \cdot \mathbf{k}$ can be taken equal to 0; therefore, the receiving pattern may be expanded in vector spherical harmonics as

$$\mathbf{r}(\hat{\mathbf{k}}) = \sum_{\nu\mu} \left[r^{H}_{\nu\mu} \, \mathbf{X}_{\nu\mu}(\hat{\mathbf{k}}) + r^{E}_{\nu\mu} \, i\hat{\mathbf{k}} \times \mathbf{X}_{\nu\mu}(\hat{\mathbf{k}}) \right] . \tag{8-6}$$

The far-field and receiving patterns are standard quantities which can be measured directly on a far-field range (at least to within a constant overall phase factor).

8.3 Transmitting and Receiving Operators

The receiving and transmitting operators are defined as follows:

$$\mathbf{R} = 2\pi \sum_{\nu\mu} \left[r^{H}_{\nu\mu}\, \boldsymbol{\mathcal{P}}_{\nu\mu} + r^{E}_{\nu\mu}\, \frac{1}{k} \nabla \times \boldsymbol{\mathcal{P}}_{\nu\mu} \right] \tag{8-7}$$

$$\mathbf{T} = \sum_{\nu\mu} \left[t^{H}_{\nu\mu}\, \boldsymbol{\mathcal{P}}_{\nu\mu} + t^{E}_{\nu\mu}\, \frac{1}{k} \nabla \times \boldsymbol{\mathcal{P}}_{\nu\mu} \right] . \tag{8-8}$$

The spherical-wave operator $\boldsymbol{\mathcal{P}}_{nm}$ is an nth order differential operator in ∂_x, ∂_y and ∂_z [5].

The electric field Eq (1) may be written in terms of the transmitting operator as

$$\mathbf{E}(\mathbf{r}) = \mathbf{T}\, G(\mathbf{r}) \tag{8-9}$$

and because **T** is translationally invariant, the field translated by a vector displacement $\boldsymbol{\rho}$ is given by

$$\mathbf{E}(\mathbf{r} - \boldsymbol{\rho}) = [\mathbf{T}\, G](\mathbf{r} - \boldsymbol{\rho}) = \mathbf{T}\, [G(\mathbf{r} - \boldsymbol{\rho})] . \tag{8-10}$$

With the receiving and transmitting operators, Kerns' transmission formula Eq (5) may be written

$$W(\mathbf{r}) = \mathbf{R} \cdot \mathbf{T}\, G(\mathbf{r}) . \tag{8-11}$$

Although derived assuming a transmitter located at the origin, it is clear that Eq (11) holds when **r** is interpreted as the relative displacement from the transmitter to the receiver.

8.4 Rotation of the Vector Spherical Harmonics

Equations (5) and (11) provide a way of calculating the probe response as the probe is moved through an incident field without rotation. To discuss rotated probes and test antennas, as is required in spherical near-field scanning, it is necessary to be able to rotate the transmitting and receiving patterns. This can be done using the following result: Let $\mathbf{V}_{nm}$ represent $\mathbf{X}_{nm}$, $\hat{\mathbf{ir}} \times \mathbf{X}_{nm}$, $\boldsymbol{\mathcal{P}}_{nm}$, or $\frac{1}{k}\, \boldsymbol{\nabla} \times \boldsymbol{\mathcal{P}}_{nm}$, then

$$\mathbf{V}'_{nm}(\hat{\mathbf{r}}) = \sum_{\mu=-n}^{n} D^{n}_{\mu m}(\phi,\theta,\chi)\; \mathbf{V}_{n\mu}(\hat{\mathbf{r}}) \; . \tag{8-12}$$

Here $\mathbf{V}'_{nm}$ is the result of rotating $\mathbf{V}_{nm}$ through the Euler angles (ϕ,θ,χ). According to convention [15], the rotation is accomplished as follows: First $\mathbf{V}$ is rotated by χ about the laboratory z axis, then by θ about the laboratory y axis, and, finally, by ϕ again about the laboratory z axis. The specific form of the rotation functions $D^{n}_{\mu m}$ need not concern us here. The fact that rotated spherical harmonics can be expressed as superpositions of unrotated spherical harmonics may be viewed as a consequence of the completeness of the vector spherical harmonic basis.

8.5 Spherical Scanning: Receiving Probe

In spherical near-field scanning we may view the test antenna as fixed at the origin of the laboratory coordinate system in a given reference orientation. The location and orientation of the probe is specified in terms of the Euler angles (ϕ,θ,χ). The Euler angles (0,0,0) are taken to correspond to the probe reference orientation with the probe located at $r_0\hat{\mathbf{z}}$. The radius of the measurement sphere is, of course, r_0. Under these conditions, the angles θ and ϕ correspond to the usual spherical angles giving the position of the probe in the laboratory coordinate system. The angle χ corresponds to rotation of the probe about the radius vector joining the probe and test antenna.

Equivalently, we may leave the probe in its reference position/orientation on the z axis and rotate the test antenna through the Euler angles $(-\chi,-\theta,-\phi)$. Taking this approach we may write the transmission equation as

$$W_{pa}(r_0,\phi,\theta,\chi) = \mathbf{R}_p \cdot \mathbf{T}'_a \, G(r_0\hat{\mathbf{z}}) \,, \qquad (8\text{-}13)$$

where in their reference orientations, the probe and test antenna are represented by the receiving and transmitting operators $\mathbf{R}_p$ and $\mathbf{T}_a$. With Eq (12) we have

$$\mathbf{T}'_a = \sum_{\beta nm} D^n_{\beta m}(-\chi,-\theta,-\phi) \left[t^{aH}_{nm} \, \boldsymbol{\mathcal{P}}_{n\beta} + t^{aE}_{nm} \, \frac{1}{k} \nabla \times \boldsymbol{\mathcal{P}}_{n\beta} \right] . \qquad (8\text{-}14)$$

The Euler angles (ϕ,θ,χ) refer to the effective position/orientation of the probe.

Substitution of expansions for the operators in Eq (13) gives

$$\begin{aligned} W_{pa}(r_0,\phi,\theta,\chi) &= \sum_{\nu\mu nm} D^n_{\mu m}(-\chi,-\theta,-\phi) \\ &\times \left\{ \left[r^{pH}_{\nu,-\mu} \, t^{aH}_{nm} - r^{pE}_{\nu,-\mu} \, t^{aE}_{nm} \right] B(\nu,-\mu|n\mu;r_0) \right. \\ &+ \left. \left[r^{pE}_{\nu,-\mu} \, t^{aH}_{nm} - r^{pH}_{\nu,-\mu} \, t^{aE}_{nm} \right] C(\nu,-\mu|n\mu;r_0) \right\} . \end{aligned} \qquad (8\text{-}15)$$

B and C are given by

$$B(\nu,-m|nm;r_0) = 2\pi \, \boldsymbol{\mathcal{P}}_{\nu,-m} \cdot \boldsymbol{\mathcal{P}}_{nm} \, G(r_0\hat{\mathbf{z}})$$

$$C(\nu,-m|nm;r_0) = 2\pi \, \frac{1}{k} \nabla \times \boldsymbol{\mathcal{P}}_{n,-m} \cdot \boldsymbol{\mathcal{P}}_{nm} \, G(r_0\hat{\mathbf{z}})$$

and are closely related to translation coefficients for spherical waves [5, Eqs (49) and (50)].

Equation (15) can be written more compactly as

$$W_{pa}(r_0,\phi,\theta,\chi) = \sum_{\mu nm} D^n_{\mu m}(-\chi,-\theta,-\phi) \left[R^{pH}_{n\mu}(r_0) \, t^{aH}_{nm} + R^{pE}_{n\mu}(r_0) \, t^{aE}_{nm} \right] , \qquad (8\text{-}16)$$

where the translated probe receiving coefficients are given by

$$R^{pH}_{nm}(r_0) = \mathbf{R}_p \cdot \boldsymbol{\mathcal{P}}_{nm}\, G(r_0\hat{\mathbf{z}}) \tag{8-17a}$$

$$= \sum_{\nu} \left[r^{pH}_{\nu,-m}\, B(\nu,-m|nm;r_0) + r^{pE}_{\nu,-m}\, C(\nu,-m|nm;r_0) \right]$$

$$R^{pE}_{nm}(r_0) = \mathbf{R}_p \cdot \frac{1}{k}\, \boldsymbol{\nabla} \times \boldsymbol{\mathcal{P}}_{nm}\, G(r_0\hat{\mathbf{z}}) \tag{8-17b}$$

$$= - \sum_{\nu} \left[r^{pH}_{\nu,-m}\, C(\nu,-m|nm;r_0) + r^{pE}_{\nu,-m}\, B(\nu,-m|nm;r_0) \right] .$$

The translated receiving coefficients are basically the response of the probe in its reference position/orientation to ideal multipole transmitters located at the origin. Equation (12) guarantees that this information is sufficient to give the response as a function of the Euler angles locating the probe.

8.6 **Spherical Scanning: Transmitting Probe**

Up to this point we have considered the probe to be a receiver. The case of a transmitting probe is also important and will be considered here. If the probe and test antenna (in their reference orientations) are represented by the transmitting and receiving operators $\mathbf{T}_p$ and $\mathbf{R}_a$, the transmission equation can be written

$$W_{ap}(r_0,\phi,\theta,\chi) = \mathbf{R}'_a \cdot \mathbf{T}_p\, G(-r_0\hat{\mathbf{z}}) \ , \tag{8-18}$$

where

$$\mathbf{R}'_a = 2\pi \sum_{\beta nm} D^{n}_{\beta m}(-\chi,-\theta,-\phi) \left[r^{aH}_{nm}\, \boldsymbol{\mathcal{P}}_{n\beta} + r^{aE}_{nm}\, \frac{1}{k}\, \boldsymbol{\nabla} \times \boldsymbol{\mathcal{P}}_{n\beta} \right] . \tag{8-19}$$

As in the case of the receiving probe, the test antenna has been rotated so that the probe remains in its reference position/orientation on the z axis. Note that $-r_0\hat{\mathbf{z}}$ is the relative displacement from the transmitter (the probe) to the receiver (the test antenna). The Euler angles (ϕ,θ,χ) again refer to the effective position/orientation of the probe.

Substitution of expansions for the operators in Eq (18) gives

$$W_{ap}(r_0,\phi,\theta,\chi) = \sum_{\nu\mu nm} (-)^{\nu+n}\, D^{n}_{\mu m}(-\chi,-\theta,-\phi)$$

$$\times \left\{ \left[r^{aH}_{nm}\, t^{pH}_{\nu,-\mu} - r^{aE}_{nm}\, t^{pE}_{\nu,-\mu} \right] B(\nu,-\mu|n\mu;r_0) \right.$$

$$\left. + \left[r^{aE}_{nm}\, t^{pH}_{\nu,-\mu} - r^{aH}_{nm}\, t^{pE}_{\nu,-\mu} \right] C(\nu,-\mu|n\mu;r_0) \right\} . \qquad (8\text{-}20)$$

We have used the fact that under the change of variables $\mathbf{r} \longrightarrow -\mathbf{r}$, $\mathcal{P}_{nm} \longrightarrow (-)^{n}\mathcal{P}_{nm}$. Equation (20) can be written more compactly as

$$W_{ap}(r_0,\phi,\theta,\chi) = \sum_{\mu nm} D^{n}_{\mu m}(-\chi,-\theta,-\phi) \left[r^{aH}_{nm}\, T^{pH}_{n\mu} + r^{aE}_{nm}\, T^{pE}_{n\mu} \right] , \qquad (8\text{-}21)$$

where the translated probe transmitting coefficients are given by

$$T^{pH}_{nm}(r_0) = 2\pi\, \mathcal{P}_{nm} \cdot \mathbf{T}_p\, G(-r_0\hat{\mathbf{z}}) \qquad (8\text{-}22a)$$

$$= \sum_{\nu} (-)^{\nu+n} \left[t^{pH}_{\nu,-m}\, B(\nu,-m|nm;r_0) - t^{pE}_{\nu,-m}\, C(\nu,-m|nm;r_0) \right]$$

$$T^{pE}_{nm}(r_0) = 2\pi \frac{1}{k} \nabla \times \mathcal{P}_{nm} \cdot \mathbf{T}_p\, G(-r_0\hat{\mathbf{z}}) \qquad (8\text{-}22b)$$

$$= \sum_{\nu} (-)^{\nu+n} \left[t^{pH}_{\nu,-m}\, C(\nu,-m|nm;r_0) - t^{pE}_{\nu,-m}\, B(\nu,-m|nm;r_0) \right] .$$

The translated transmitting coefficients can be interpreted as responses of ideal multipole receivers located at the origin to the transmitting probe in its reference position/orientation.

8.7 **Reciprocity and the Transmission Equations**

For a reciprocal antenna the far-field and receiving patterns are related by

$$\mathbf{r}(\hat{\mathbf{k}}) = \mathbf{t}(-\hat{\mathbf{k}})/K . \qquad (8\text{-}23)$$

The constant of proportionality K depends on calibration (and may be different for test antenna and probe) [18]. Equation (23) implies

$$\begin{aligned} r^{H}_{nm} &= (-)^{n}\, t^{H}_{nm}/K \\ r^{E}_{nm} &= (-)^{n+1}\, t^{E}_{nm}/K \end{aligned} \tag{8-24}$$

for the expansion coefficients in Eqs (4) and (6).

If both the probe and antenna are reciprocal then Eq (24) with Eqs (15) and (20) can be used to show that

$$W_{pa}(r_0,\phi,\theta,\chi) \propto W_{ap}(r_0,\phi,\theta,\chi) \tag{8-25}$$

as expected.

If the probe is reciprocal, then

$$\begin{aligned} R^{pH}_{nm} &= (-)^{n}\, T^{pH}_{nm}/K \\ R^{pE}_{nm} &= (-)^{n+1}\, T^{pE}_{nm}/K\ . \end{aligned} \tag{8-26}$$

In this case the same transmission formula, Eq (16) or Eq (21), may be used with minor modification with the probe receiving or transmitting.

9. RECIPROCITY FROM AN OPERATIONAL VIEWPOINT

9.1 Introduction

In this chapter we develop relations between transmitting and receiving patterns by evaluating the Lorentz reciprocity integral using the operational methods developed in Chapter 8.

9.2 Representation of the Electromagnetic Fields

We consider a closed surface Σ which lies in free space outside the minimum sphere enclosing an antenna (see Figure 9.1). In the vicinity of this surface, the electromagnetic fields are given by the plane-wave representation,

$$
\begin{aligned}
\mathbf{E}(\mathbf{r}) &= \frac{1}{4\pi} \int \mathbf{a}(\hat{\mathbf{k}}) \exp(i\mathbf{k} \cdot \mathbf{r})\, d\hat{\mathbf{k}} \\
&+ \frac{1}{2\pi} \int \mathbf{b}(\hat{\mathbf{k}}) \exp(i\mathbf{k} \cdot \mathbf{r}) \frac{d\mathbf{K}}{\gamma k} , \qquad z > 0 . \qquad (9\text{-}1)
\end{aligned}
$$

The patterns $\mathbf{a}(\hat{\mathbf{k}})$ and $\mathbf{b}(\hat{\mathbf{k}})$ describe fields from sources outside and inside Σ, respectively. In particular $\mathbf{b}(\hat{\mathbf{k}})$ is the antenna far-field pattern. In cases of practical importance (external sources at finite distances, for example) $\mathbf{a}(\hat{\mathbf{k}})$ must be interpreted as a distribution.
The operator identities

$$
\begin{aligned}
\mathbf{a}(\nabla/ik) \exp(i\mathbf{k} \cdot \mathbf{r}) &= \mathbf{a}(\hat{\mathbf{k}}) \exp(i\mathbf{k} \cdot \mathbf{r}) \\
\mathbf{b}(\nabla/ik) \exp(i\mathbf{k} \cdot \mathbf{r}) &= \mathbf{b}(\hat{\mathbf{k}}) \exp(i\mathbf{k} \cdot \mathbf{r})
\end{aligned} \qquad (9\text{-}2)
$$

can be easily established by comparing terms in the Taylor expansions of each side. Substitution of Eq (2) into Eq (1) gives an operator expression for the fields:

$$
\mathbf{E}(\mathbf{r}) = \mathbf{a}(\nabla/ik)\, G^{(1)}(\mathbf{r}) + \mathbf{b}(\nabla/ik)\, G^{(3)}(\mathbf{r}) , \qquad (9\text{-}3)
$$

where

$$
G^{(1)}(\mathbf{r}) = j_0(kr) = \frac{\sin(kr)}{kr} = \frac{1}{4\pi} \int \exp(i\mathbf{k} \cdot \mathbf{r})\, d\hat{\mathbf{k}}
$$

$$G^{(3)}(\mathbf{r}) = h_0^{(1)}(kr) = \frac{\exp(ikr)}{ikr} = \frac{1}{2\pi}\int \exp(i\mathbf{k}\cdot\mathbf{r})\,\frac{d\mathbf{K}}{\gamma k}\,, \qquad z > 0\ . \qquad (9\text{-}4b)$$

Although Eq (1) is valid only for z > 0, Eq (3) holds in any spherical shell in free space outside the minimum sphere.

9.3 **The Lorentz Reciprocity Integral**

Let $(\mathbf{E}', \mathbf{H}')$ and $(\mathbf{E}'', \mathbf{H}'')$ be two electromagnetic fields which can exist in the vicinity of Σ. (These may be obtained by adjusting sources.) In this section we establish that

$$I_\Sigma = \int_\Sigma [\mathbf{E}'(\mathbf{r}) \times \mathbf{H}''(\mathbf{r}) - \mathbf{E}''(\mathbf{r}) \times \mathbf{H}'(\mathbf{r})] \cdot d\mathbf{S}$$

$$= \frac{1}{k^2 Z_0}\int [\mathbf{a}'(\hat{\mathbf{k}}) \cdot \mathbf{b}''(-\hat{\mathbf{k}}) - \mathbf{b}'(-\hat{\mathbf{k}}) \cdot \mathbf{a}''(\hat{\mathbf{k}})]\, d\hat{\mathbf{k}}\ . \qquad (9\text{-}5)$$

This is not an evaluation of the integral but merely a restatement. The pattern functions determine the fields and any relation expressed in terms of fields can, in principle, be re-expressed in terms of pattern functions. We will demonstrate Eq (5) using operational techniques.

Let $\mathbf{A}$ be a solenoidal vector field, that is,

$$\nabla \cdot \mathbf{A} = 0\ .$$

Then Gauss' theorem may be applied to obtain Green's second identity

$$\int [\mathbf{A}' \times (\nabla \times \mathbf{A}'') - \mathbf{A}'' \times (\nabla \times \mathbf{A}')] \cdot d\mathbf{S}$$

$$= \int [\mathbf{A}' \cdot \nabla^2\mathbf{A}'' - \mathbf{A}'' \cdot \nabla^2\mathbf{A}']\, dV\ . \qquad (9\text{-}6)$$

The integrals are over a closed surface S and the enclosed volume V. On substituting $\mathbf{E}$ from Eq (3), we find that

$$I_\Sigma = \frac{4\pi}{k^2 Z_0}\int \{[\mathbf{a}'(\nabla/ik)\, G^{(1)}(\mathbf{r})] \cdot [\mathbf{b}''(\nabla/ik)\, \delta(\mathbf{r})]$$

$$- [\mathbf{b}'(\nabla/ik)\, \delta(\mathbf{r})] \cdot [\mathbf{a}''(\nabla/ik)\, G^{(1)}(\mathbf{r})]\}\, dV\,, \qquad (9\text{-}7)$$

where we have used the facts that

$$(\nabla^2 + k^2)\ G^{(1)}(\mathbf{r}) = 0$$

$$(\nabla^2 + k^2)\ G^{(3)}(\mathbf{r}) = \frac{4\pi i}{k}\ \delta(\mathbf{r})\ .$$

Equation (7) contains only terms of the type $\mathbf{a} \cdot \mathbf{b}$. Terms with $\mathbf{a}' \cdot \mathbf{a}''$ drop out. It is less obvious that terms with $\mathbf{b}' \cdot \mathbf{b}''$ also cancel; however, this follows from application of Eq (8).

The identity

$$\int f(\mathbf{r})\ [g(\boldsymbol{\nabla})\ \delta(\mathbf{r})]\ dV = \int [g(-\boldsymbol{\nabla})\ f(\mathbf{r})]\ \delta(\mathbf{r})\ dV \tag{9-8}$$

can be established by taking a general term in the Taylor series expansion of g and integrating by parts. Using Eqs (8), (2) and (4a) with Eq (7) gives

$$I_\Sigma = \frac{1}{k^2\ Z_0} \int d\hat{\mathbf{k}}\ [\mathbf{a}'(\hat{\mathbf{k}}) \cdot \mathbf{b}''(-\hat{\mathbf{k}}) - \mathbf{b}'(-\hat{\mathbf{k}}) \cdot \mathbf{a}''(\hat{\mathbf{k}})]$$

$$\times \int \exp(i\mathbf{k} \cdot \mathbf{r})\ \delta(\mathbf{r})\ dV\ ,$$

which integrates immediately to give Eq (5).

9.4 **Reciprocity Relations**

The basic theorem is that I_S will vanish whenever S is a closed surface containing no sources (assuming ϵ and μ are scalars). The geometry is shown in Figure 9.1. The amplitudes of the outgoing and incoming waves in the (single-moded) feed are a_0 and b_0. The source region in the antenna is enclosed by the surfaces S_0 and S_a. S_a lies within the shielding and makes no contribution to the integral. The reciprocity theorem may now be stated as

$$-2\eta_0(a_0'\ b_0'' - b_0'\ a_0'')$$

$$= \frac{1}{k^2\ Z_0} \int d\hat{\mathbf{k}}\ [\mathbf{a}'(\hat{\mathbf{k}}) \cdot \mathbf{b}''(-\hat{\mathbf{k}}) - \mathbf{b}'(-\hat{\mathbf{k}}) \cdot \mathbf{a}''(\hat{\mathbf{k}})]\ . \tag{9-9}$$

The term on the left side represents the integral over S_0 and reflects normalizations used by Kerns [18], whose work should be consulted for details. The right side, of course, comes from Eq (5).

To find the relationship between transmitting and receiving patterns, we assume the excitations

$$a_0' = a_0 , \quad \mathbf{a}'(\hat{\mathbf{k}}) = 0 \tag{9-10a}$$

$$a_0'' = 0 , \quad \mathbf{a}''(\hat{\mathbf{k}}) = 2\mathbf{E}_0 \, \delta(\hat{\mathbf{k}} - \hat{\mathbf{k}}_0) . \tag{9-10b}$$

By definition, Eq (10a) implies that

$$\mathbf{b}'(\hat{\mathbf{k}}) = \mathbf{t}(\hat{\mathbf{k}}) \tag{9-11}$$

and, since by Eq (1) the incident wave is $\mathbf{E}_0 \exp(i\mathbf{k}_0 \cdot \mathbf{r})/(2\pi)$, Eq (10b) implies that

$$b_0'' = \mathbf{r}(\hat{\mathbf{k}}_0) \cdot \mathbf{E}_0 . \tag{9-12}$$

(The condition $a_0'' = 0$ requires a matched load.)

Substitution of Eqs (10) through (12) into Eq (9) gives

$$\frac{-2}{k^2 Z_0} \mathbf{t}(-\hat{\mathbf{k}}_0) \cdot \mathbf{E}_0 = -2\eta_0 \, a_0 \, \mathbf{r}(\hat{\mathbf{k}}_0) \cdot \mathbf{E}_0$$

or, since $\mathbf{E}_0$ is arbitrary,

$$\mathbf{r}(\hat{\mathbf{k}}_0) = \mathbf{t}(-\hat{\mathbf{k}}_0)/(a_0 \, k^2 \, \eta_0 \, Z_0) . \tag{9-13}$$

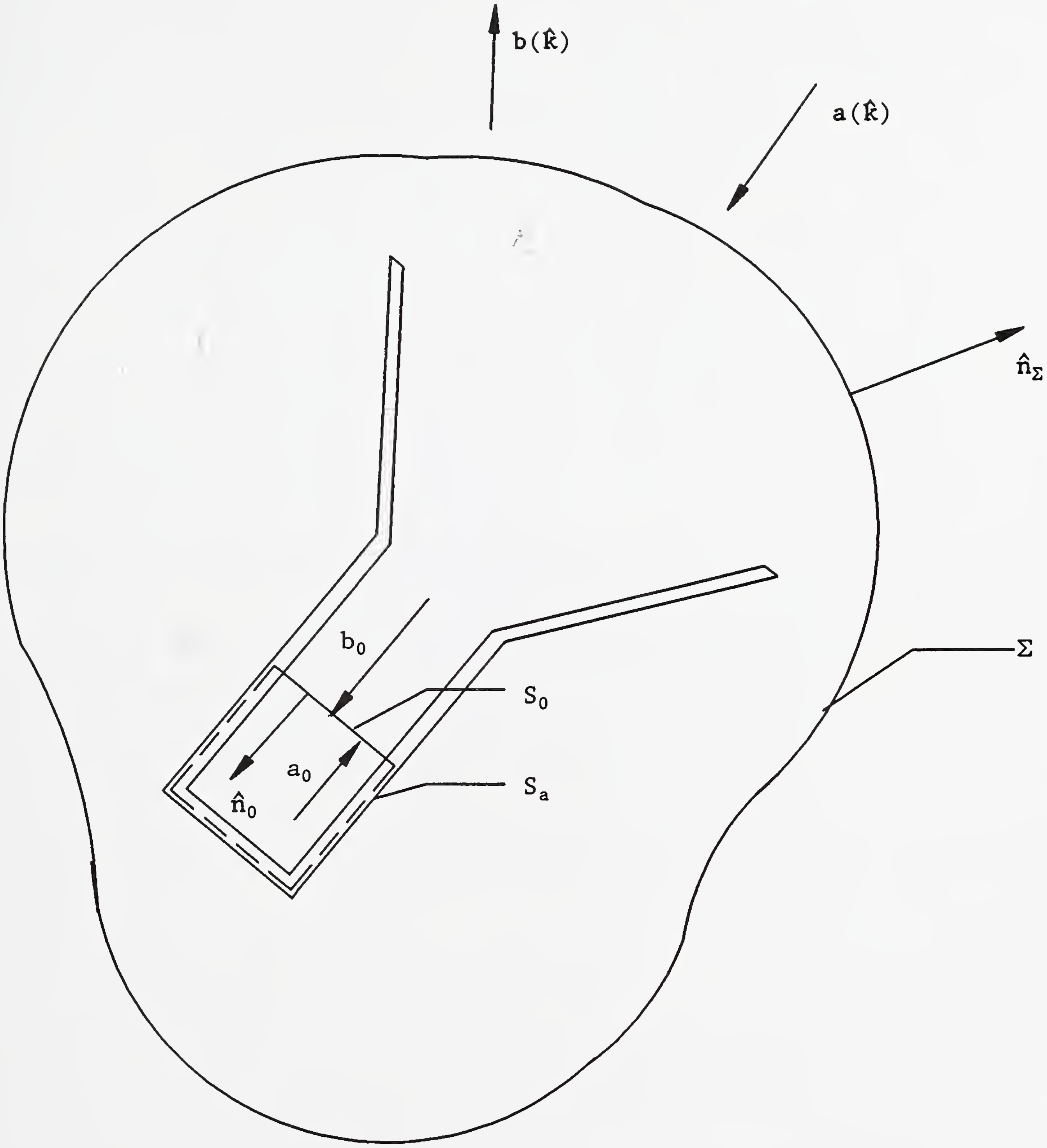
$b(\hat{k})$
$a(\hat{k})$
$\hat{n}_\Sigma$
Σ
b_0
S_0
a_0
$\hat{n}_0$
S_a

Figure 9.1 Geometry for the application of the reciprocity theorem.

10. THE UNIFORMLY EXCITED CIRCULAR APERTURE: SPHERICAL-WAVE FIELD EXPANSIONS

10.1 Introduction

Finding a spherical-wave expansion for a planar aperture transducer is simple in principle: (1) The far field is computed in terms of the Fourier transform of the aperture field. (2) The expansion coefficients are calculated using orthogonality integrals for the spherical modes. In practice, however, it is generally not possible to obtain closed-form expressions. An exception is the case of the uniformly excited circular aperture treated here. This problem was suggested by A. D. Yaghjian who kindly provided notes [19] on the subject. In this chapter we provide a "simplified" treatment for scalar (acoustic) fields and give a more complete treatment of the vector (electromagnetic) case. Besides the obvious pedagogic value, it is useful to have an analytic solution for a model which closely approximates a practical transducer. The near field of this model can be computed accurately and efficiently.

10.2 Scalar Spectrum and Far-Field Pattern

If there are no sources for $z > 0$ an scalar field $u(\mathbf{r})$ may be written in terms of its spectrum $b(\hat{\mathbf{k}})$ as

$$u(\mathbf{r}) = \frac{1}{2\pi} \int b(\hat{\mathbf{k}}) \exp(i\mathbf{k} \cdot \mathbf{r}) \, d\mathbf{K} , \qquad z > 0 . \tag{10-1}$$

Conversely, the spectrum is determined from the field in the aperture plane ($z = 0$)

$$b(\hat{\mathbf{k}}) = \frac{1}{2\pi} \int u(\mathbf{R}) \exp(-i\mathbf{k} \cdot \mathbf{R}) \, d\mathbf{R} . \tag{10-2}$$

The far-field pattern is easily related to the spectrum:

$$u(\mathbf{r}) \underset{r\longrightarrow\infty}{\sim} t(\hat{\mathbf{r}}) \frac{\exp(ikr)}{ikr}$$

$$t(\hat{\mathbf{k}}) = \gamma k \, b(\hat{\mathbf{k}}) . \tag{10-3}$$

For a uniform circular aperture of radius a (centered at the origin), the spectrum is, according to Eq (2),

$$b(\hat{\mathbf{k}}) = a^2 u_0 I(\hat{\mathbf{k}}) , \tag{10-4}$$

where u_0 is the (constant) field amplitude in the aperture and

$$I(\hat{\mathbf{k}}) = \frac{1}{2\pi a^2} \int_A \exp(-i\mathbf{k} \cdot \mathbf{R})\, d\mathbf{R} = \frac{J_1(Ka)}{Ka} . \tag{10-5}$$

10.3 **Expansion of $I(\hat{\mathbf{k}})$ in Spherical Harmonics**

$I(\hat{\mathbf{k}})$ may be expanded in spherical harmonics as

$$I(\hat{\mathbf{k}}) = \sum_{\nu=0}^{\infty} I_\nu Y_{\nu 0}(\hat{\mathbf{k}}) . \tag{10-6}$$

The azimuthal index is 0 as a consequence of the symmetry of the aperture field. Furthermore, because $I(-\hat{\mathbf{k}}) = I(\hat{\mathbf{k}})$, only even-numbered multipoles will be present. The coefficients are given by

$$I_n = \int Y^*_{n0}(\hat{\mathbf{k}})\, I(\hat{\mathbf{k}})\, d\hat{\mathbf{k}} . \tag{10-7}$$

Substituting for $I(\hat{\mathbf{k}})$ from Eq (5) leads to

$$\begin{aligned} I_n &= \frac{2i^{-n}}{a^2} \int d\mathbf{R} \frac{1}{4\pi i^{-n}} \int Y^*_{n0}(\hat{\mathbf{k}}) \exp(-i\mathbf{k} \cdot \mathbf{R})\, d\hat{\mathbf{k}} \\ &= \frac{2i^{-n}}{a^2} \int u^{(1)}_{n0}(\mathbf{R})\, d\mathbf{R} . \end{aligned} \tag{10-8}$$

Reference [5] may be consulted for integral representations of

$$u^{(1)}_{nm}(\mathbf{r}) = j_n(kr)\, Y_{nm}(\hat{\mathbf{r}}) \tag{10-9}$$

and other spherical-wave functions. Continuing from Eq (8)

$$\begin{aligned} I_n &= \frac{4\pi\, i^n}{(ka)^2} Y_{n0}(\hat{\mathbf{R}}) \int_0^{ka} x\, j_n(x)\, dx \\ &= \sqrt{4\pi(2n+1)}\; i^n\, P_n(0)\, \alpha_n(ka)/(ka)^2 . \end{aligned} \tag{10-10}$$

Here

$$\alpha_n(x) = \int_0^x t\, j_n(t)\, dt \tag{10-11}$$

and P_n is a Legendre polynomial. I_n is 0 when n is odd since

$$\begin{aligned} P_n(0) &= 0 , & n &= 1, 3, 5, \ldots \\ P_n(0) &= \frac{i^{-n}}{2^n} \frac{n!}{(\frac{n}{2}!)^2} , & n &= 0, 2, 4, \ldots \end{aligned} \tag{10-12}$$

α_n obeys the recursion formulas

$$\begin{aligned} \alpha_0(x) &= 1 - \cos(x) \\ \alpha_n(x) &= \frac{n}{n-1} \alpha_{n-2}(x) - \frac{2n-1}{n-1} x\, j_{n-1}(x) , \quad n = 2, 4, 6, \ldots \end{aligned} \tag{10-13}$$

In closed form

$$\alpha_{2n}(x) = \frac{2^{2n} (n!)^2}{(2n)!} \left[1 - x \sum_{\nu=0}^{n} \frac{(2\nu)!}{2^{2\nu}(\nu!)^2} \frac{4\nu-1}{2\nu-1} j_{2\nu-1}(x)\right] . \tag{10-14}$$

It is easy to show that Eq (10) follows from Eq (10.1.48) of Abramowitz and Stegun [20]. Also it is possible to obtain closed-form results for certain aperture tapers such as, for example, $u(\mathbf{R}) = R^n$, $n = 0, 1, \ldots$

Yaghjian [19] obtains I_n in a somewhat different form. The difference may be traced to the method used to evaluate the orthogonality integral. Our result is equivalent to

$$\int_0^\pi P_n(\cos\theta)\, J_1(x \sin\theta)\, d\theta = 2i^n\, P_n(0)\, \alpha_n(x)/x .$$

Yaghjian evaluates this integral by expanding $P_n(\cos\theta)$ in a Fourier series [21, Eq 8.911(4)] and integrating term by term [21, Eq 6.681(9)]. The two approaches agree if

$$\alpha_{2n}(2x) = 2x^2 \sum_{\nu=-n}^{n} (-)^{n+\nu} \frac{P_{2n-2\nu}(0)\, P_{2n+2\nu}(0)}{P_{2n}(0)} j_{-\nu}(x)\, j_\nu(x) \ , \tag{10-15}$$

a formula which can be checked by direct substitution for small values of n.

10.4 **The Scalar Field Expanded in Spherical Waves**

We have previously considered a one-sided problem ($z > 0$). To construct a spherical-wave expansion it is necessary to devise a finite source which produces the same fields when $z > 0$. To this end let us replace the aperture with a doublet (that is, two apertures back to back) such that the excitation is $+u_0$ on the $z > 0$ side and $-u_0$ on the $z < 0$ side. (If $u(\mathbf{r})$ is the excess pressure, this may be visualized in terms of a diaphragm oscillating back and forth about an equilibrium position at the origin.) The field is described by the spectrum given in Eq (4) with the direction of $\hat{\mathbf{k}}$ unrestricted. We also note that because $u(-\mathbf{r}) = -u(\mathbf{r})$, only odd-numbered multipoles will occur in the expansion.

According to Eq (3) the far field is

$$t(\hat{\mathbf{k}}) = \gamma k\, b(\hat{\mathbf{k}}) = \gamma k\, a^2\, u_0\, I(\hat{\mathbf{k}}) \ .$$

Now $\gamma = k \cos\theta = k \sqrt{\frac{4\pi}{3}}\, Y_{10}(\hat{\mathbf{k}})$. Consequently, using the expansion Eq (6) for $I(\hat{\mathbf{k}})$ and the formula for the product $Y_{10}\, Y_{nm}$ from Table 6.1, it follows that

$$t(\hat{\mathbf{k}}) = u_0 \sum_{\nu=1}^{\infty} t_\nu\, Y_{\nu 0}(\hat{\mathbf{k}}) \ , \tag{10-16}$$

where

$$t_n = \sqrt{4\pi(2n+1)}\; i^{n-1}\, P_{n-1}(0)\, [\alpha_{n-1}(ka) - ka\, j_n(ka)] \ . \tag{10-17}$$

The spherical-wave expansion for the field is simply

$$u(\mathbf{r}) = u_0 \sum_{\nu=1}^{\infty} i^\nu\, t_\nu\, u_{\nu 0}^{(3)}(\mathbf{r}) \ , \qquad r > a \ , \tag{10-18}$$

where

$$u_{nm}^{(3)}(\mathbf{r}) = h_n^{(1)}(kr)\ Y_{nm}(\hat{\mathbf{r}}) \ . \tag{10-19}$$

Because $Y_{n0}(\hat{\mathbf{R}}) = 0$ when n is odd, the field vanishes in the aperture plane, $r > a$, as required by the boundary conditions.

10.5 **A Piston Radiator in a Rigid Baffle**

Consider a circular piston vibrating harmonically in a rigid baffle. The z component of the fluid velocity field is a solution of the Helmholtz equation obeying the boundary condition $v(\mathbf{R}) = v_0$, $R < a$, and $v(\mathbf{R}) = 0$, $R > a$. Spherical-wave expansions for $v(\mathbf{r})$ are given by the expressions in Section 10.4 (with v_0 substituted for u_0). An equivalent finite source is a doublet aperture with the excitation $+v_0$ on the $z > 0$ side and with the excitation $-v_0$ on the $z < 0$ side. (This may be viewed as a very short cylinder vibrating symmetrically about the $z = 0$ plane.)

Often it is useful to express the solution in terms of the excess pressure field $p(\mathbf{r})$ which is related to $v(\mathbf{r})$ by

$$\partial_z p(\mathbf{r}) = ikc\rho_0\ v(\mathbf{r}) \ , \tag{10-20}$$

where c is the velocity of propagation and ρ_0 is the density of the medium. From Eqs (20), (4) and (1), we find that

$$\partial_z p(\mathbf{r}) = ikc\rho_0\ v_0 a^2 \frac{1}{2\pi} \int I(\hat{\mathbf{k}}) \exp(i\mathbf{k} \cdot \mathbf{r})\ d\mathbf{K} \ .$$

Integrating with respect to z, we have

$$p(\mathbf{r}) = \rho_0\ cv_0\ (ka)^2 \frac{1}{2\pi} \int I(\hat{\mathbf{k}}) \exp(i\mathbf{k} \cdot \mathbf{r}) \frac{d\mathbf{K}}{\gamma k} + f(x,y) \ . \tag{10-21}$$

The "constant of integration" f(x,y) must be 0 to satisfy radiation conditions at infinity.

From Eq (21) the far field pattern is

$$t(\hat{\mathbf{k}}) = \rho_0 \, cv_0 \, (ka)^2 \, I(\hat{\mathbf{k}}) = \rho_0 \, cv_0 \, (ka)^2 \, J_1(Ka)/Ka$$

$$= \rho_0 \, cv_0 \, (ka)^2 \sum_{\nu=0}^{\infty} I_\nu \, Y_{\nu 0}(\hat{\mathbf{k}}) \ , \tag{10-22}$$

where I_n is given by Eq (10). The spherical-wave expansion for $p(\mathbf{r})$ is

$$p(\mathbf{r}) = \rho_0 \, cv_0 \, (ka)^2 \sum_{\nu=0}^{\infty} i^\nu \, I_\nu \, u_{\nu 0}^{(3)}(\mathbf{r}) \ , \qquad r > a \ . \tag{10-23}$$

Only even-numbered multipoles occur in Eq (23) since $p(\mathbf{r}) = p(-\mathbf{r})$.

10.6 **Vector Spectrum and Far-Field Pattern**

In the electromagnetic case, the transverse part of the spectrum may be found from the transverse fields in the aperture as follows

$$\mathbf{b}_t(\hat{\mathbf{k}}) = \frac{1}{2\pi} \int_A \mathbf{E}_t(\mathbf{R}) \exp(-i\mathbf{k} \cdot \mathbf{r}) \, d\mathbf{R}$$

$$= a^2 \, \mathbf{E}_t \, I(\hat{\mathbf{k}}) \ , \tag{10-24}$$

where $\mathbf{E}_t$, which is constant for a uniform excitation, has been taken outside the integral.

Because $\mathbf{k} \cdot \mathbf{b}(\hat{\mathbf{k}}) = 0$, it is possible to find $\mathbf{b}(\hat{\mathbf{k}})$ from $\mathbf{b}_t(\hat{\mathbf{k}})$:

$$\mathbf{b}(\hat{\mathbf{k}}) = [\hat{\mathbf{z}} \times \mathbf{b}_t(\hat{\mathbf{k}})] \times \mathbf{k}/\gamma \ .$$

The far-field pattern is given by

$$\mathbf{t}(\hat{\mathbf{k}}) = \gamma k \, \mathbf{b}(\hat{\mathbf{k}}) = (ka)^2 \, [\hat{\mathbf{z}} \times \mathbf{E}_t] \times \hat{\mathbf{k}} \, I(\hat{\mathbf{k}}) \ . \tag{10-25}$$

10.7 **The Vector Field Expanded in Spherical Waves**

Technically Eq (25) gives the far-field pattern in the forward hemisphere ($\hat{\mathbf{z}} \cdot \hat{\mathbf{k}} > 0$) only. However, if we view the source as a doublet aperture with excitation $\mathbf{E}_t$ on the $z > 0$ side and excitation $-\mathbf{E}_t$ on the $z < 0$ side, then $\mathbf{t}(\hat{\mathbf{k}})$ gives the far-field pattern for all directions. (This source may also be viewed as a sheet of magnetic current with density $\mathbf{E}_t \times \hat{\mathbf{z}}$.) Symmetry requires that $\mathbf{E}(-\mathbf{r}) = -\mathbf{E}(\mathbf{r})$; thus, only odd magnetic multipoles and even electric multipoles will be present in the spherical-wave expansion. In addition, the azimuthal index takes only the values $m = \pm 1$.

The far-field pattern Eq (25) may be re-expressed as

$$\mathbf{t}(\hat{\mathbf{k}}) = (ka)^2 \sqrt{\frac{16\pi}{3}} \, [E_- \mathbf{X}_{11}(\hat{\mathbf{k}}) + E_+ \mathbf{X}_{1,-1}(\hat{\mathbf{k}})] \, I(\hat{\mathbf{k}}) \tag{10-26}$$

$$E_\pm \equiv (E_x \pm iE_y)/2 \, ,$$

where

$$\mathbf{X}_{1,\pm 1}(\hat{\mathbf{k}}) = \mp \sqrt{\frac{3}{16\pi}} \, (\hat{\mathbf{x}} \pm i\hat{\mathbf{y}}) \times i\hat{\mathbf{k}} \, .$$

The formula

$$\sqrt{\frac{16\pi}{3}} \, Y_{n0}(\hat{\mathbf{k}}) \, \mathbf{X}_{1,\pm 1}(\hat{\mathbf{k}}) = \frac{n-1}{\sqrt{(2n-1)(2n+1)}} \mathbf{X}_{n-1,\pm 1} + \frac{n+2}{\sqrt{(2n+1)(2n+3)}} \mathbf{X}_{n+1,\pm 1} \pm i\hat{\mathbf{k}} \times \mathbf{X}_{n,\pm 1} \tag{10-27}$$

(see Eq (6-53) and Tables 6.1 and 6.3) and the spherical harmonic expansion for $I(\hat{\mathbf{k}})$ given in Eqs (6) and (10) allow computation of the spherical harmonic expansion for the far-field pattern:

$$\mathbf{t}(\hat{\mathbf{k}}) = \sum_{\nu=1}^{\infty} \sum_{\mu=-\nu}^{\nu} [t^H_{\nu\mu} \, \mathbf{X}_{\nu\mu}(\hat{\mathbf{k}}) + t^E_{\nu\mu} \, i\hat{\mathbf{k}} \times \mathbf{X}_{\nu\mu}(\hat{\mathbf{k}})] \, . \tag{10-28}$$

Let

$$t_n^H = \sqrt{4\pi(2n+1)}\; i^{n-1}\; P_{n-1}(0)\; [\alpha_{n-1}(ka) - \frac{n}{n+1}\, ka\; j_n(ka)] \qquad (10\text{-}29a)$$

$$t_n^E = \sqrt{4\pi(2n+1)}\; i^{n}\; P_{n}(0)\; \alpha_n(ka) \ . \qquad (10\text{-}29b)$$

Then the coefficients in Eq (28) are

$$\begin{aligned} t_{nm}^E &= t_{nm}^H = 0 \ , & m &\neq \pm 1 \\ t_{n1}^H &= E_-\; t_n^H \ , & t_{n,-1}^H &= \ \ E_+\; t_n^H \\ t_{n1}^E &= E_-\; t_n^E \ , & t_{n,-1}^E &= -\, E_+\; t_n^E \ . \end{aligned} \qquad (10\text{-}30)$$

The electric field is given by the expansion

$$\mathbf{E}(\mathbf{r}) = \sum_{\nu=1}^{\infty} \sum_{\mu=-\nu}^{\nu} i^{\nu}\; [t_{\nu\mu}^H\; \mathbf{m}_{\nu\mu}^{(3)}(\mathbf{r}) + t_{\nu\mu}^E\; \mathbf{n}_{\nu\mu}^{(3)}(\mathbf{r})] \ , \qquad r > a \ , \qquad (10\text{-}31)$$

where

$$\begin{aligned} \mathbf{m}_{nm}(\mathbf{r}) &= f_n(kr)\; \mathbf{X}_{nm}(\hat{\mathbf{r}}) \\ \mathbf{n}_{nm}(\mathbf{r}) &= g_n(kr)\; i\hat{\mathbf{r}} \times \mathbf{X}_{nm}(\hat{\mathbf{r}}) + i\sqrt{n(n+1)}\; \frac{f_n(kr)}{kr}\; Y_{nm}(\hat{\mathbf{r}})\; \hat{\mathbf{r}} \\ f_n^{(3)}(x) &= h_n^{(1)}(x) \ , \qquad g_n(x) = \frac{1}{ix}\frac{d}{dx}\, [x f_n(x)] \ . \end{aligned} \qquad (10\text{-}32)$$

It is easy to verify that the tangential field vanishes in the aperture plane, $r > a$, as required by the boundary conditions.

The t_{nm}'s may also be found directly from the expressions

$$\begin{aligned} t_{n,\pm 1}^H &= i^{-n}\; 2ik^2\; \hat{\mathbf{z}} \times \mathbf{E}_t \cdot \int_A \mathbf{n}_{n,\mp 1}^{(1)}(\mathbf{R})\; d\mathbf{R} \\ t_{n,\pm 1}^E &= i^{-n}\; 2ik^2\; \hat{\mathbf{z}} \times \mathbf{E}_t \cdot \int_A \mathbf{m}_{n,\mp 1}^{(1)}(\mathbf{R})\; d\mathbf{R} \end{aligned} \qquad (10\text{-}33)$$

which are the vector analogs of Eq (8). To evaluate Eq (33), use Eq (32) (with $f_n^{(1)}(x) = j_n(x)$) and the cartesian components of the vector spherical harmonics. Since cartesian components of the vector spherical harmonics are often useful in analysis, they are given in Section 10.10.

Yaghjian [19] obtained expressions for the transverse electric field by a procedure which amounts to taking the transverse part of Eq (25). (He actually applies the operator ∂_z/ik to Eq (23).)

10.8 **Computation of α_n**

Numerical evaluation with Eq (14) does not give accurate results when n is large because the subtraction in the square brackets involves terms which are equal in the limit $n \longrightarrow \infty$. (The same effect occurs when recursion is used in the direction of increasing n.) This normally is not serious since α tends to be small by the time the problem becomes noticeable; however, if more accuracy is required, the infinite series

$$\alpha_{2n}(x) = x \frac{2^{2n}(n!)^2}{(2n)!} \sum_{\nu=n+1}^{\infty} \frac{(2\nu)!}{2^{2\nu}(\nu!)^2} \frac{4\nu-1}{2\nu-1} j_{2\nu-1}(x) \qquad (10\text{-}34)$$

can be used for the largest n values. (The summation in Eq (34) converges rapidly when $2n > x$.) For other values of n, α may be computed by recursion in the direction of decreasing n.

The asymptotic behavior

$$\alpha_{2n}(x) \underset{x\longrightarrow\infty}{\sim} (-)^n[1/P_{2n}(0) - \cos(x)]$$

follows from Eq (14) or Eq (15). From Eq (34) we have

$$\alpha_n(x) \underset{n\longrightarrow\infty}{\sim} \frac{\sqrt{2}}{e^2} \left[\frac{ex}{2n}\right]^{n+2} .$$

10.9 **Numerical Results**

A sample case is given in Table 10.1 for the purpose of allowing numerical comparisons. The aperture radius is ka = 10. Equation (29) has been used to calculate t_n^H (when n is odd) and t_n^E (when n is even) for $n \le 100$. As expected, the coefficients fall off rapidly when $n > ka$.

Table 10.1 Expansion coefficients, aperture radius ka = 10 (see Eq (10-29))

n	t_n^H, n odd; t_n^E, n even	n	t_n^H, n odd; t_n^E, n even
1	8.88290 65641 61171 19E+00	51	8.98718 80459 67957 92E-31
2	5.24797 96151 57838 07E+00	52	1.58279 58097 92345 73E-32
3	7.59860 31940 26376 97E+00	53	8.12890 79948 42326 49E-33
4	1.07161 43031 63398 32E+01	54	1.32956 04907 32971 08E-34
5	1.38875 36890 89261 74E+01	55	6.81996 04746 49004 33E-35
6	1.77591 16173 84174 62E+01	56	1.03869 08041 05408 79E-36
7	1.48196 90941 37683 71E+01	57	5.32195 06315 22596 19E-37
8	1.05978 39450 55578 18E+01	58	7.56618 63118 54351 94E-39
9	7.39763 09276 50643 17E+00	59	3.87267 98528 84585 55E-39
10	3.33101 80004 09695 54E+00	60	5.15134 30425 37966 44E-41
11	2.12170 35247 28489 87E+00	61	2.63414 61253 57852 55E-41
12	6.60309 09198 47212 30E-01	62	3.28539 16864 16401 08E-43
13	3.98156 64624 96662 58E-01	63	1.67850 41279 73652 38E-43
14	9.11406 68543 68622 30E-02	64	1.96691 16447 27909 18E-45
15	5.30080 80848 27879 70E-02	65	1.00406 94731 80199 67E-45
16	9.32386 45266 13645 82E-03	66	1.10755 29974 96221 74E-47
17	5.28700 95274 37814 08E-03	67	5.64952 63454 66140 03E-48
18	7.38158 80348 71480 92E-04	68	5.87659 14072 02370 06E-50
19	4.10821 08822 55210 25E-04	69	2.99546 41183 75996 73E-50
20	4.66840 59411 44109 10E-05	70	2.94320 23410 10353 31E-52
21	2.56143 19224 05396 54E-05	71	1.49923 66521 92906 93E-52
22	2.41692 42624 50217 96E-06	72	1.39366 29915 10581 78E-54
23	1.31135 74894 22240 35E-06	73	7.09476 03519 55332 89E-55
24	1.04440 87939 36802 55E-07	74	6.24897 03284 43279 48E-57
25	5.61604 36929 29645 92E-08	75	3.17932 62473 06017 62E-57
26	3.82714 63509 10735 78E-09	76	2.65708 89025 38966 24E-59
27	2.04289 70643 38552 11E-09	77	1.35112 23849 62090 74E-59
28	1.20506 16440 09997 10E-10	78	1.07288 02213 10516 16E-61
29	6.39338 41510 81896 80E-11	79	5.45275 27152 70510 22E-62
30	3.29705 99880 86973 53E-12	80	4.11920 89011 69410 21E-64
31	1.74026 77545 66542 65E-12	81	2.09250 81647 34267 71E-64
32	7.91397 24725 02382 76E-14	82	1.50568 91335 04275 89E-66
33	4.15892 40477 88792 26E-14	83	7.64520 64386 44849 16E-67
34	1.68047 11043 34818 72E-15	84	5.24603 17712 41856 50E-69
35	8.79789 71886 50300 00E-16	85	2.66254 04531 76516 34E-69
36	3.17987 87703 56954 01E-17	86	1.74418 02602 79352 49E-71
37	1.65933 63086 28276 90E-17	87	8.84867 13169 34599 94E-72
38	5.39686 19906 75366 43E-19	88	5.53968 01669 32226 08E-74
39	2.80813 32391 74686 39E-19	89	2.80932 52919 48188 13E-74
40	8.26278 54990 42238 30E-21	90	1.68251 03275 71364 34E-76
41	4.28846 79371 66006 42E-21	91	8.52931 74106 49564 49E-77
42	1.14712 86321 00349 26E-22	92	4.89144 97363 04915 96E-79
43	5.94032 58840 16801 73E-23	93	2.47879 87782 91701 62E-79
44	1.45085 97789 54707 37E-24	94	1.36248 85888 31866 51E-81
45	7.49808 46786 77098 78E-25	95	6.90225 61239 22805 07E-82
46	1.67882 62385 03440 53E-26	96	3.63944 27474 18410 03E-84
47	8.66056 82994 70368 55E-27	97	1.84312 36654 79104 40E-84
48	1.78414 34144 86632 47E-28	98	9.33079 72406 30199 37E-87
49	9.18888 12733 77642 26E-29	99	4.72395 90557 92718 03E-87
50	1.74756 17622 96418 55E-30	100	2.29796 98907 92321 27E-89

Evaluation of Eqs (25) and (28) on the z axis leads to the sum

$$x^2 = \sum_{\nu=1}^{\infty} \sqrt{\frac{2\nu+1}{4\pi}}\, [t_\nu^H(x) + t_\nu^E(x)] \qquad (10\text{-}35)$$

which provides a useful check. Analytic verification that Eq (35) follows from Eq (29) is straightforward.

10.10 **Cartesian Components of the Vector Spherical Harmonics**

Using the decomposition

$$\mathbf{L} = \frac{1}{2}(L_+ + L_-)\,\hat{\mathbf{x}} + \frac{1}{2i}(L_+ - L_-)\,\hat{\mathbf{y}} + L_z\,\hat{\mathbf{z}}\,, \qquad L_\pm = L_x \pm iL_y\,,$$

we have

$$\sqrt{n(n+1)}\,\mathbf{X}_{nm} = \mathbf{L}\,Y_{nm}$$

$$= \sqrt{(n-m)(n+m+1)/2}\,Y_{n,m+1}\,\xi_{-1} + m\,Y_{nm}\,\xi_0 - \sqrt{(n+m)(n-m+1)/2}\,Y_{n,m-1}\,\xi_1\,,$$

where

$$\xi_{\pm1} = \mp(\hat{\mathbf{x}} \pm i\hat{\mathbf{y}})/\sqrt{2}\,, \qquad \xi_0 = \hat{\mathbf{z}}\,.$$

With the additional formulas

$$\hat{\mathbf{r}} = \sqrt{\frac{4\pi}{3}}\left[-\,Y_{11}\,\xi_{-1} + Y_{10}\,\xi_0 - Y_{1,-1}\,\xi_1\right]$$

and (from Table 6.1)

$$\sqrt{\frac{4\pi}{3}}\,Y_{1,-1}\,Y_{nm} = -\sqrt{\frac{(n+m-1)(n+m)}{2(2n-1)(2n+1)}}\,Y_{n-1,m-1} + \sqrt{\frac{(n-m+1)(n-m+2)}{2(2n+1)(2n+3)}}\,Y_{n+1,m-1}$$

$$\sqrt{\frac{4\pi}{3}}\,Y_{10}\,Y_{nm} = \sqrt{\frac{(n-m)(n+m)}{(2n-1)(2n+1)}}\,Y_{n-1,m} + \sqrt{\frac{(n-m+1)(n+m+1)}{(2n+1)(2n+3)}}\,Y_{n+1,m}$$

$$\sqrt{\frac{4\pi}{3}}\,Y_{11}\,Y_{nm} = -\sqrt{\frac{(n-m-1)(n-m)}{2(2n-1)(2n+1)}}\,Y_{n-1,m+1} + \sqrt{\frac{(n+m+1)(n+m+2)}{2(2n+1)(2n+3)}}\,Y_{n+1,m+1}\,,$$

we have

$$\begin{aligned}\hat{\mathbf{r}}\, Y_{nm} = {} & \left[\sqrt{\frac{(n-m-1)(n-m)}{2(2n-1)(2n+1)}}\, Y_{n-1,m+1} - \sqrt{\frac{(n+m+1)(n+m+2)}{2(2n+1)(2n+3)}}\, Y_{n+1,m+1}\right] \xi_{-1} \\ & + \left[\sqrt{\frac{(n-m)(n+m)}{(2n-1)(2n+1)}}\, Y_{n-1,m} + \sqrt{\frac{(n-m+1)(n+m+1)}{(2n+1)(2n+3)}}\, Y_{n+1,m}\right] \xi_{0} \\ & + \left[\sqrt{\frac{(n+m-1)(n+m)}{2(2n-1)(2n+1)}}\, Y_{n-1,m-1} - \sqrt{\frac{(n-m+1)(n-m+2)}{2(2n+1)(2n+3)}}\, Y_{n+1,m-1}\right] \xi_{1}\end{aligned}$$

and

$$\begin{aligned} & -\sqrt{n(n+1)}\; i\hat{\mathbf{r}} \times \mathbf{X}_{nm} \\ & = \left[(n+1)\sqrt{\frac{(n-m-1)(n-m)}{2(2n-1)(2n+1)}}\, Y_{n-1,m+1} + n\sqrt{\frac{(n+m+1)(n+m+2)}{2(2n+1)(2n+3)}}\, Y_{n+1,m+1}\right] \xi_{-1} \\ & + \left[(n+1)\sqrt{\frac{(n-m)(n+m)}{(2n-1)(2n+1)}}\, Y_{n-1,m} - n\sqrt{\frac{(n-m+1)(n+m+1)}{(2n+1)(2n+3)}}\, Y_{n+1,m}\right] \xi_{0} \\ & + \left[(n+1)\sqrt{\frac{(n+m-1)(n+m)}{2(2n-1)(2n+1)}}\, Y_{n-1,m-1} + n\sqrt{\frac{(n-m+1)(n-m+2)}{2(2n+1)(2n+3)}}\, Y_{n+1,m-1}\right] \xi_{1} \,.\end{aligned}$$

The cartesian forms for the vector spherical-wave functions **m**, **n** and **ℓ** follow from the above equations and the plane-wave integral representations [5].

Formulas for the cartesian components of vector spherical harmonics may also be obtained using Eq (6-54) and the definitions of Edmonds' vector spherical harmonics [9, Eq (5.9.10)].

11. SPHERICAL NEAR-FIELD SCANNING: DETERMINING THE INCIDENT FIELD NEAR A ROTATABLE PROBE

11.1 Introduction

Many RCS (Radar Cross Section), EMI/EMC (ElectroMagnetic Interference/Compatibility), and antenna measurements require a known incident field within a test volume. To evaluate systems designed to produce a specific incident field (compact ranges, for example), we must measure the actual illumination for comparison with design specifications. Beyond its diagnostic value, this incident-field data can also be used for error estimation and for calculating first order corrections.

In this chapter, we develop a spherical near-field scanning algorithm for determining incident fields inside a probe's "minimum sphere." This differs from the well-known spherical near-field scanning formulation which determines fields outside the source's minimum sphere [22]. The scanner size depends on the extent of the region of interest but not on the extent of the (possibly much larger) source. The data may be collected using a standard roll-over-azimuth positioner.

The discussion is divided into the acoustic (scalar) case (Sections 11.2 to 11.6) and the electromagnetic (vector) case (Sections 11.7 to 11.10).

11.2 Acoustic Probe Receiving Operator

The receiving probe may be modeled as a differential operator $\mathcal{P}$ such that the probe response $W(\mathbf{r})$ to an incident field $u_i(\mathbf{r})$ may be written

$$W(\mathbf{r}) = [\mathcal{P}\, u_i](\mathbf{r}) \ . \tag{11-1}$$

The probe operator may be expanded

$$\mathcal{P} = 2\pi \sum_{\nu=0}^{N} \sum_{\mu=-\nu}^{\nu} r_{\nu\mu}\, \mathcal{P}_{\nu\mu} \ , \tag{11-2}$$

where $\mathcal{P}_{nm}$ is a scalar spherical-wave operator [5] and r_{nm} is a coefficient in the spherical harmonic expansion of the probe receiving pattern:

$$r(\hat{\mathbf{k}}) = \sum_{\nu\mu} r_{\nu\mu} \, Y_{\nu\mu}(\hat{\mathbf{k}}) \ . \tag{11-3}$$

$Y_{nm}(\hat{\mathbf{r}})$ is a scalar spherical harmonic [1, Chapter 3].

The orientation of the probe is defined in terms of a fiducial coordinate system which is imbedded in the probe in some convenient fashion. The location of the probe is taken as the location of the fiducial origin in the laboratory coordinate system. With the probe located at $\mathbf{r}_p$ in a specified reference orientation, the receiving pattern is defined so that the probe response to the incident plane wave

$$\frac{1}{2\pi} \exp(i\mathbf{k} \cdot \mathbf{r})$$

is

$$r(\hat{\mathbf{k}}) \exp(i\mathbf{k} \cdot \mathbf{r}_p) \ .$$

For practical probes, we may take

$$N \sim ka \ , \tag{11-4}$$

where a is the radius of the minimum sphere (the smallest sphere centered on the probe's fiducial origin which encloses the "active" parts of the probe).

Equation (1) is Kerns' transmission formula [18] written in operator notation.

11.3 **Rotation of the Acoustic Probe**

Let $\mathcal{P}'$ denote the rotated probe; then

$$\mathcal{P}' = 2\pi \sum_{\nu=0}^{N} \sum_{\mu=-\nu}^{\nu} \sum_{\mu'=-\nu}^{\nu} D^{\nu}_{\mu'\mu}(\phi,\theta,\chi) \, r_{\nu\mu} \, \mathcal{P}_{\nu\mu'} \ . \tag{11-5}$$

The D's are rotation functions [14]. The Euler angles (ϕ,θ,χ), which specify the probe orientation, are defined as follows: Starting with the probe its reference orientation (1) rotate the probe by an angle χ about the z axis; (2) then rotate by θ about the y axis; (3) finally, rotate by ϕ about the z axis.

11.4 The Incident Acoustic Field

Assume that we wish to know the incident field in the vicinity of the origin. We have the expansion

$$u_i(\mathbf{r}) = \sum_{\nu=0}^{N} \sum_{\mu=-\nu}^{\nu} a_{\nu\mu}\, u_{\nu\mu}(\mathbf{r}) \tag{11-6}$$

$$u_{nm}(\mathbf{r}) \equiv j_n(kr)\, Y_{nm}(\hat{\mathbf{r}}) \ , \tag{11-7}$$

where $j_n(kr)$ is a spherical Bessel function. The limit on the multipole index means that (5) will describe the field for $r < a$ with

$$a \sim N/k \tag{11-8}$$

(compare with Eq (4)). The primary goal of these notes is to show how a_{nm} may be determined from measurements.

11.5 The Acoustic Transmission Formula

Using the fact that [5]

$$[\mathcal{P}_{\nu\mu}\, u_{nm}](\mathbf{0}) = \frac{(-)^{\mu}}{4\pi i^{\nu}}\, \delta_{\nu n}\, \delta_{-\mu m} \ , \tag{11-9}$$

the response $W(\phi,\theta,\chi)$ of the rotated probe (located at the origin) can be written

$$W(\phi,\theta,\chi) = \frac{1}{2} \sum_{\nu\mu\mu'} (-)^{\mu}\, i^{-\nu}\, D^{\nu}_{\mu\mu'}(\phi,\theta,\chi)\, r_{\nu\mu'}\, a_{\nu,-\mu} \ . \tag{11-10}$$

The rotation functions are orthogonal

$$\int_0^{2\pi} d\phi \int_0^{\pi} \sin(\theta)\, d\theta \int_0^{2\pi} d\chi\, D^{\nu}_{\mu\mu'}(\phi,\theta,\chi)\, D^{n*}_{mm'}(\phi,\theta,\chi) = \frac{8\pi^2}{2\nu+1}\, \delta_{\nu n}\, \delta_{\mu m}\, \delta_{\mu' m'} \tag{11-11}$$

so that it is possible to invert the transmission equation Eq (10) to solve for the coefficients a_{nm}. In general, it is necessary to integrate over χ, as well as over the usual spherical angles θ and ϕ.

11.6 **The "Symmetric" Acoustic Probe**

The degree of freedom associated with χ can be eliminated by the use of a "symmetric" probe which has the property

$$\mathcal{P} = 2\pi \sum_{\nu=0}^{N} r_\nu \, \mathcal{P}_{\nu 0} \ . \tag{11-12}$$

Such a probe can be practically constructed by incorporating a section of circular pipe which propagates only an azimuthally symmetric wave. If the reference orientation of the probe is chosen so that the axis of the pipe is coincident with the z-axis, then the probe output will be independent of χ.

With Eq (12) the transmission equation (10) becomes

$$W(\hat{\mathbf{r}}) = \sum_{\nu\mu} i^{-\nu} \sqrt{\frac{\pi}{2\nu+1}} \, r_\nu \, a_{\nu\mu} \, Y_{\nu\mu}(\hat{\mathbf{r}}) \ , \tag{11-13}$$

where we have used the relation

$$D^{m}_{m0}(\phi,\theta,\chi) = \sqrt{\frac{4\pi}{2n+1}} \, Y^{*}_{nm}(\theta,\phi) \ . \tag{11-14}$$

Equation (13) may be solved to give

$$a_{nm} = \frac{i^n}{r_n} \sqrt{\frac{2n+1}{\pi}} \int W(\hat{\mathbf{r}}) \, Y^{*}_{nm}(\hat{\mathbf{r}}) \, d\hat{\mathbf{r}} \ . \tag{11-15}$$

The a_{nm} can be determined, provided that the probe coefficients can be accurately measured. As n becomes greater than ka, r_n tends to drop exponentially into the noise. Thus, attempts to determine the incident field outside the minimum sphere of the probe are doomed to catastrophic failure! On the other hand, even with $n < ka$, there is the possibility that some r_n will be near 0. (An example is given in Section 11.10.) Data from an independent probe may be needed to resolve all of the coefficients.

11.7 The Electromagnetic Transmission Formula

Aside from complications introduced by polarization, the electromagnetic case is quite similar to the acoustic case. Therefore, we will only briefly summarize the results here.

The receiving probe may be modeled as a differential operator $\mathcal{P}$ such that the probe response $W(\mathbf{r})$ to an incident field $\mathbf{E}_i(\mathbf{r})$ may be written

$$W(\mathbf{r}) = [\mathcal{P} \cdot \mathbf{E}_i](\mathbf{r}) . \tag{11-16}$$

The probe operator may be expanded

$$\mathcal{P} = 2\pi \sum_{\nu=1}^{N} \sum_{\mu=-\nu}^{\nu} [r^H_{\nu\mu} \mathcal{P}_{\nu\mu} + r^E_{\nu\mu} \frac{1}{k} \nabla \times \mathcal{P}_{\nu\mu}] , \tag{11-17}$$

where $\mathcal{P}_{nm}$ is a vector spherical-wave operator [5] and r^H_{nm} and r^E_{nm} are coefficients in the spherical harmonic expansion of the probe receiving pattern:

$$\mathbf{r}(\hat{\mathbf{k}}) = \sum_{\nu\mu} [r^H_{\nu\mu} \mathbf{X}_{\nu\mu}(\hat{\mathbf{k}}) + r^E_{\nu\mu} i\hat{\mathbf{k}} \times \mathbf{X}_{\nu\mu}(\hat{\mathbf{k}})] . \tag{11-18}$$

$\mathbf{X}_{nm}(\hat{\mathbf{r}})$ is a vector spherical harmonic [1, Chapter 16]. The superscripts E and H refer to electric and magnetic multipoles.

Let $\mathcal{P}'$ denote the rotated probe, then

$$\mathcal{P}' = 2\pi \sum_{\nu=1}^{N} \sum_{\mu=-\nu}^{\nu} \sum_{\mu'=-\nu}^{\nu} D^{\nu}_{\mu'\mu}(\phi,\theta,\chi) [r^H_{\nu\mu} \mathcal{P}_{\nu\mu'} + r^E_{\nu\mu} \frac{1}{k} \nabla \times \mathcal{P}_{\nu\mu'}] . \tag{11-19}$$

Assume that we wish to know the incident electric field in the vicinity of the origin. We have the expansion

$$\mathbf{E}_i(\mathbf{r}) = \sum_{\nu=1}^{N} \sum_{\mu=-\nu}^{\nu} [a^H_{\nu\mu} \mathbf{m}_{\nu\mu}(\mathbf{r}) + a^E_{\nu\mu} \mathbf{n}_{\nu\mu}(\mathbf{r})] \tag{11-20}$$

$$\mathbf{m}_{nm}(\mathbf{r}) \equiv j_n(kr) \mathbf{X}_{nm}(\hat{\mathbf{r}}) , \quad \mathbf{n}_{nm}(\mathbf{r}) \equiv \frac{1}{k} \nabla \times \mathbf{m}_{nm}(\mathbf{r}) . \tag{11-21}$$

Using the facts that [5]

$$[\boldsymbol{\mathcal{P}}_{\nu\mu} \cdot \mathbf{m}_{nm}](\mathbf{0}) = \frac{(-)^{\mu+1}}{4\pi i^{\nu}} \delta_{\nu n} \delta_{-\mu m} \tag{11-22}$$

$$[\boldsymbol{\mathcal{P}}_{\nu\mu} \cdot \mathbf{n}_{nm}](\mathbf{0}) = 0 \ , \tag{11-23}$$

the response $W(\phi,\theta,\chi)$ of the rotated probe (located at the origin) can be written

$$W(\phi,\theta,\chi) = \frac{1}{2} \sum_{\nu\mu\mu'} (-)^{\mu+1} i^{-\nu} D^{\nu}_{\mu\mu'}(\phi,\theta,\chi) \, [r^{H}_{\nu\mu'} \, a^{H}_{\nu,-\mu} - r^{E}_{\nu\mu'} \, a^{E}_{\nu,-\mu}] \ . \tag{11-24}$$

Using the orthogonality properties of the rotation functions Eq (11), it is possible to solve the transmission equation (24) for the unknown coefficients r^{H}_{nm} and r^{E}_{nm}.

11.8 The "Symmetric" Electromagnetic Probe

Application of Eq (24) is simplified by the use of a specially designed ($\mu = \pm 1$) probe [23] for which

$$\boldsymbol{\mathcal{P}} = 2\pi \sum_{\nu=1}^{N} \sum_{\mu=-1}^{1}{}' [r^{H}_{\nu\mu} \boldsymbol{\mathcal{P}}_{\nu\mu} + r^{E}_{\nu\mu} \frac{1}{k} \nabla \times \boldsymbol{\mathcal{P}}_{\nu\mu}] \ . \tag{11-25}$$

The prime on the summation indicates that $\mu = 0$ is excluded from the sum. Such a probe can be practically constructed by incorporating a section of open-ended circular waveguide designed so that only the TE_{11} modes propagate (see Figure 1.1). If the reference orientation is taken with the axis of the guide coincident with the z axis, then the probe output will have a $\cos(\chi - \chi_0)$ dependence. (A transverse electric dipole ($\mathbf{p} \cdot \hat{\mathbf{r}} = 0$) is another example of a $\mu = \pm 1$ probe.)

With Eq (25) the transmission equation becomes

$$\mathbf{W}(\hat{\mathbf{r}}) = \sum_{\nu\mu} [A^{H}_{\nu\mu} \mathbf{X}_{\nu\mu}(\hat{\mathbf{r}}) + A^{E}_{\nu\mu} \, i\hat{\mathbf{r}} \times \mathbf{X}_{\nu\mu}(\hat{\mathbf{r}})] \tag{11-26}$$

$$\mathbf{W}(\hat{\mathbf{r}}) \equiv W(\phi,\theta,\chi{=}-\pi/2) \, \hat{\boldsymbol{\theta}} + W(\phi,\theta,\chi{=}0) \, \hat{\boldsymbol{\phi}}$$

$$A_{nm}^{H} \equiv i^{-n+1} \sqrt{\frac{\pi}{2n+1}} \left[(r_{n1}^{H} - r_{n,-1}^{H})\, a_{nm}^{H} - (r_{n1}^{E} - r_{n,-1}^{E})\, a_{nm}^{E} \right] \qquad (11\text{-}27a)$$

$$A_{nm}^{E} \equiv i^{-n-1} \sqrt{\frac{\pi}{2n+1}} \left[(r_{n1}^{H} + r_{n,-1}^{H})\, a_{nm}^{H} - (r_{n1}^{E} + r_{n,-1}^{E})\, a_{nm}^{E} \right] . \qquad (11\text{-}27b)$$

Equation (26) involves measurements in two "spin" orientations ($\chi = -\pi/2, 0$) for each pointing direction (θ, ϕ).

In deriving Eq (26), we have used

$$\mathbf{X}_{nm}(\hat{\mathbf{r}}) = \sqrt{\frac{2n+1}{4\pi}} \left[\frac{\hat{\boldsymbol{\theta}} + i\hat{\boldsymbol{\phi}}}{2}\, d_{m1}^{n}(\theta) + \frac{\hat{\boldsymbol{\theta}} - i\hat{\boldsymbol{\phi}}}{2}\, d_{m,-1}^{n}(\theta) \right] \exp(im\phi)$$

(see Eq (6-26)).

The transmission equation (26) may be inverted to give

$$A_{nm}^{H} = \int \mathbf{W}(\hat{\mathbf{r}}) \cdot \mathbf{X}_{nm}^{*}(\hat{\mathbf{r}})\, d\hat{\mathbf{r}} \qquad (11\text{-}28a)$$

$$A_{nm}^{E} = \int \mathbf{W}(\hat{\mathbf{r}}) \cdot [i\hat{\mathbf{r}} \times \mathbf{X}_{nm}(\hat{\mathbf{r}})]^{*}\, d\hat{\mathbf{r}} . \qquad (11\text{-}28b)$$

The modal coefficients a_{nm}^{H} and a_{nm}^{E} then can be found by solving the simultaneous equations (27). (When Eqs (27a) and (27b) are not independent, as for a circularly polarized probe, an additional probe must be used to obtain enough data.)

11.9 **Practical Implementation**

We have shown that it is possible to determine the incident field over a region roughly corresponding to the volume of the probe's minimum sphere. If the area of interest is larger, then it is necessary to make measurements with the probe in different locations, or to use a bigger probe. Increasing the size of the probe is not always practical; for example, multiple interactions with the source may become a problem. Figure 11.1 shows one way to construct a large probe with a small cross section. In this example, the probe consists of a small transducer on a rotating arm in an arrangement which resembles the usual spherical scanning geometry turned inside out. If the transducer has the $\mu = \pm 1$ symmetry, then so will the probe. (The fiducial origin for this probe is taken at the fixed point and the reference orientation has a z directed boresight.) Figure 11.2 shows a measurement setup that makes use of a roll-over-azimuth positioner which is often standard equipment on a compact range. A flare has been added to the transducer to increase the gain of the probe. This is helpful (or perhaps, essential) because (1) susceptibility to reflections from the supporting structure is reduced and (2) the narrower the receiving pattern, the less the main incident plane-wave component will saturate the probe response.

The receiving pattern for the probes of Figures 11.1 and 11.2 can be measured directly; however, it is often easier to measure the receiving pattern for the transducer alone and then mathematically translate it by the length of the arm: If $\mathbf{r}_0(\hat{\mathbf{k}})$ is the receiving pattern of the transducer, then

$$\mathbf{r}(\hat{\mathbf{k}}) = \mathbf{r}_0(\hat{\mathbf{k}}) \exp(i\mathbf{k} \cdot \rho\hat{\mathbf{z}}) \ , \tag{11-29}$$

where ρ is the radius of the measurement sphere. We have

$$r^H_{nm} = \int \mathbf{r}_0(\hat{\mathbf{k}}) \cdot \mathbf{X}^*_{nm}(\hat{\mathbf{k}}) \exp(i\mathbf{k} \cdot \rho\hat{\mathbf{z}}) \ d\hat{\mathbf{k}} \ . \tag{11-30a}$$

$$r^E_{nm} = \int \mathbf{r}_0(\hat{\mathbf{k}}) \cdot [i\hat{\mathbf{k}} \times \mathbf{X}_{nm}(\hat{\mathbf{k}})]^* \exp(i\mathbf{k} \cdot \rho\hat{\mathbf{z}}) \ d\hat{\mathbf{k}} \ . \tag{11-30b}$$

r^H_{nm} and r^E_{nm} may be calculated using the same numerical routines developed to evaluate Eq (28), or they may be calculated analytically from $r^H_{0\nu m}$ and $r^E_{0\nu m}$ as is done in Chapter 7.

11.10 **The Ideal Dipole Probe**

The probe operator

$$\mathcal{P}_0 = \sqrt{\frac{4\pi}{3}} \frac{1}{ik} \nabla \times (\mathcal{P}_{11} + \mathcal{P}_{1,-1}) = \frac{1}{k^2} (\hat{\mathbf{y}} \times \nabla) \times \nabla \tag{11-31}$$

measures the y component of the electric field:

$$\mathcal{P}_0 \cdot \mathbf{E}_i = \hat{\mathbf{y}} \cdot \mathbf{E}_i \ . \tag{11-32}$$

If this "ideal" probe is used on an arm of length ρ as described in Section 11.9, then it is an interesting exercise to verify that the transmission equation (26) becomes

$$\mathbf{E}_t(\rho\hat{\mathbf{r}}) = E_\theta(\rho\hat{\mathbf{r}})\,\hat{\boldsymbol{\theta}} + E_\phi(\rho\hat{\mathbf{r}})\,\hat{\boldsymbol{\phi}}$$

$$= \sum_{\nu\mu} [a^H_{\nu\mu}\, f_\nu(k\rho)\, \mathbf{X}_{\nu\mu}(\hat{\mathbf{r}}) + a^E_{\nu\mu}\, g_\nu(k\rho)\, i\hat{\mathbf{r}} \times \mathbf{X}_{\nu\mu}(\hat{\mathbf{r}})] \qquad (11\text{-}33)$$

$$f_n(x) \equiv j_n(x) \;, \qquad g_n(x) \equiv \frac{1}{ix}\frac{d}{dx}[x\, f_n(x)] \;.$$

Equation (33) exhibits a well-known problem associated with calculating fields in interior regions: If $g_n(\rho)$ or $f_n(\rho)$ is 0, then the tangential electric field $\mathbf{E}_t(\rho\hat{\mathbf{r}})$ is not sufficient to determine a^H_{nm} or a^E_{nm}, respectively. (This problem does not arise in standard spherical near-field scanning applications because the radial functions for the exterior region do not have zeros.)

Hill [24] gives an excellent discussion of boundary conditions appropriate for interior problems. It can be shown that a knowledge of the quantity

$$\mathbf{F}(\rho\hat{\mathbf{r}}) = \mathbf{E}_t(\rho\hat{\mathbf{r}}) - \alpha\, \hat{\mathbf{r}} \times \mathbf{H}(\rho\hat{\mathbf{r}}) \qquad (11\text{-}34)$$

is always sufficient to determine the field for $r < \rho$. (α is an arbitrary real constant.) Equation (34) suggests a "more ideal" dipole probe:

$$\mathcal{P}_0 = \sqrt{\frac{4\pi}{3}}\left[\frac{1}{ik}\nabla \times (\mathcal{P}_{11} + \mathcal{P}_{1,-1}) + i(\mathcal{P}_{11} - \mathcal{P}_{1,-1})\right] . \qquad (11\text{-}35)$$

With this probe on an arm of length ρ, the transmission equation (26) becomes

$$\mathbf{E}_t(\rho\hat{\mathbf{r}}) - Z_0\, \hat{\mathbf{r}} \times \mathbf{H}(\rho\hat{\mathbf{r}})$$

$$= \sum_{\nu\mu} [f_\nu(k\rho) + g_\nu(k\rho)][a^H_{\nu\mu}\, \mathbf{X}_{\nu\mu}(\hat{\mathbf{r}}) + a^E_{\nu\mu}\, i\hat{\mathbf{r}} \times \mathbf{X}_{\nu\mu}(\hat{\mathbf{r}})] \;. \qquad (11\text{-}36)$$

($Z_0 = \sqrt{\mu_0/\epsilon_0}$.) f_n is real, g_n is imaginary, and f_n and g_n cannot both be 0 at the same radius; therefore, $|f_n + g_n| \neq 0$ and Eq (36) can always be solved for the unknown modal coefficients.

Although this treatment of dipole probes has illustrated some potential difficulties, there probably is little practical difference between spherical r-field scanning in the interior and in the exterior formulations. The eral rule is: If the probe is insensitive to a given multipole field, then the corresponding coefficients cannot be obtained. For example, it is not experimentally feasible to determine a_{nm}^{H} or a_{nm}^{E} when $r_{n\mu}^{H} \approx 0$ or $r_{n\mu}^{E} \approx 0$.

One caveat is that electrically small probes tend to behave like dipoles. However, it appears that single-moded, open-ended waveguides are well approximated by crossed electric and magnetic dipoles which produce measurement vectors proportional to Eq (34) with α mostly real. (See [25], for example.) Thus in principle, it is feasible to use open-ended waveguide probes for the interior region formulation.

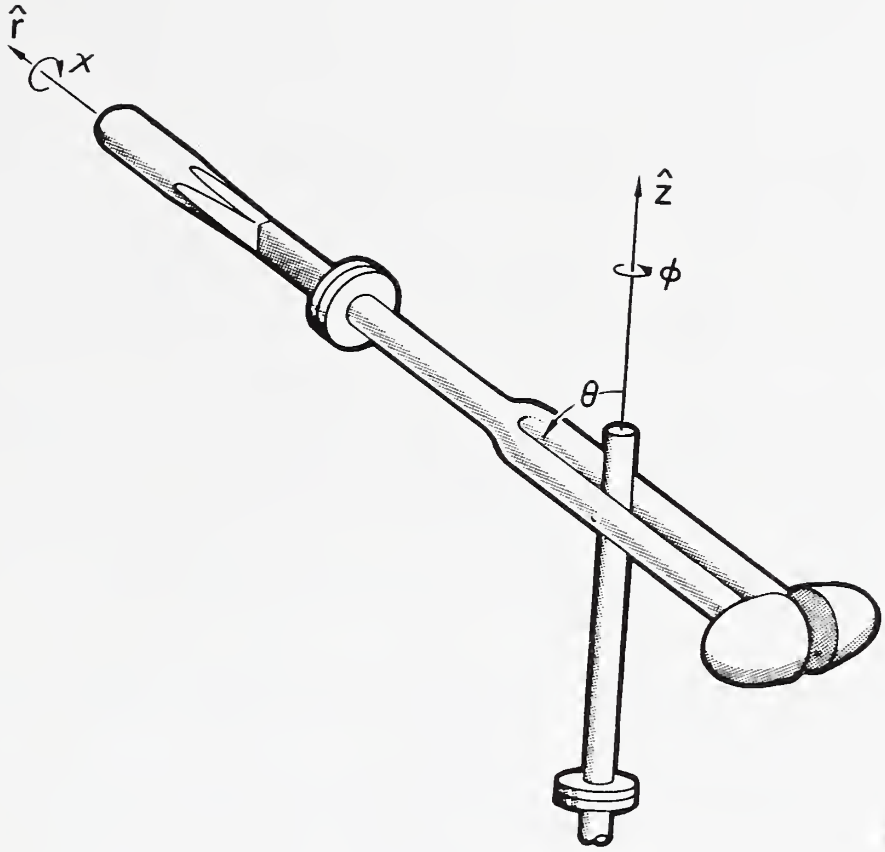
$\hat{r}$
χ
$\hat{z}$
ϕ
θ

Figure 11.1 A scanner for probing incident fields

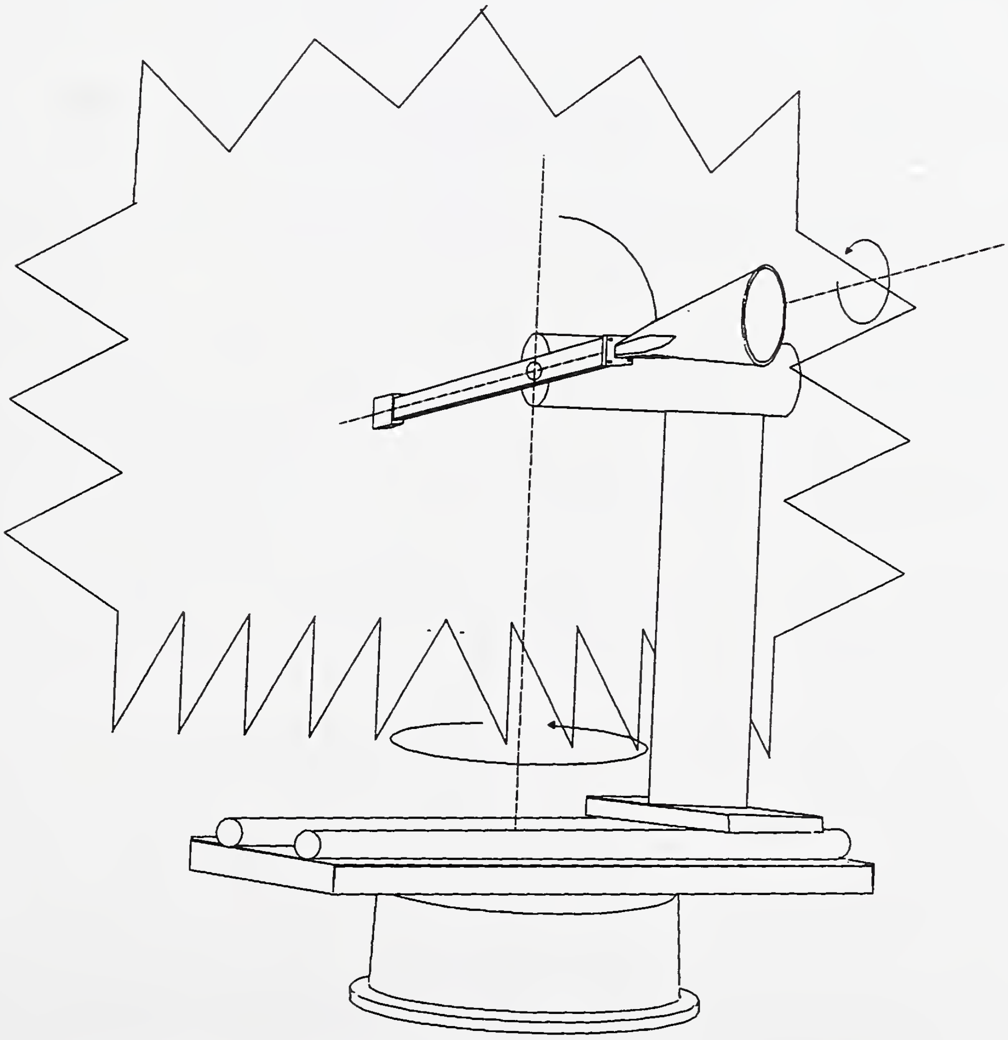

Figure 11.2 Roll-over-azimuth positioner

REFERENCES

[1] Jackson, J. D. (1975) Classical Electrodynamics, 2nd edition. New York: Wiley

[2] Yaghjian, A. D. (1982) Efficient computation of antenna coupling and fields within the near-field region, IEEE Trans. Antennas Propagat., **AP-30**:113-128

[3] Yaghjian, A. D., and Wittmann, R. C. (1985) The receiving antenna as a linear differential operator: Application to spherical near-field scanning, IEEE Trans. Antennas Propagat., **AP-33**:1175-1185

[4] Ma, M. T. (1974) Theory and Application of Antenna Arrays. New York: Wiley

[5] Wittmann, R. C. (1988) Spherical wave operators and the translation formulas, IEEE Trans. Antennas Propagat., **AP-36**:1078-1087

[6] Cruzan, O. R. (1962) Translational addition theorems for spherical vector wave functions, Quart. Appl. Math., **20**:33-40

[7] Bruning, J. H., and Lo, Y. T. (1971) Multiple scattering of EM waves by spheres, Part I--multipole expansion and ray-optical solutions, IEEE Trans. Antennas Propagat., **AP-19**:378-390

[8] James, R. W. (1976) New tensor spherical harmonics, for application to the partial differential equations of mathematical physics, Phil. Trans. R. Soc. Lond., **A281**:195-221

[9] Edmonds, A. R. (1974) Angular Momentum in Quantum Mechanics, 3rd edition. Princeton, NJ: Princeton University Press

[10] Tough, R. J. A. (1977) The transformation properties of vector multipole fields under a translation of coordinate origin, J. Phys. A: Math. Gen., **10**:1079-1087

[11] Danos, M., and Maximon, L. C. (1965) Multipole matrix elements of the translation operator, J. Math. Phys., **6**:766-778

[12] Gottfried, K. (1966) Quantum Mechanics, Vol. 1: Fundamentals. New York: Benjamin

[13] Merzbacher, E. (1970) Quantum Mechanics, 2nd edition. New York: Wiley

[14] Rose, M. E. (1957) Elementary Theory of Angular Momentum. New York: Wiley

[15] Tinkham, M. (1964) Group Theory and Quantum Mechanics, Chapter 5. New York: McGraw-Hill

[16] Condon, E. U., and Shortley, G. H. (1970) The Theory of Atomic Spectra. London: Cambridge

[17] Jensen, F. (1970) Electromagnetic near-field far-field correlations, Ph.D. dissertation, Technical University of Denmark, Lyngby

REFERENCES (continued)

[18] Kerns, D. M. (1981) Plane-wave scattering matrix theory of antennas and antenna-antenna interactions, Nat. Bur. Stand. (US) Monograph 162

[19] Yaghjian, A. D., RADC/EECT, Hanscom AFB, MA 01731 The field of a piston radiator in spherical harmonics. Private communication

[20] Abramowitz, M., and Stegun, I. A., editors (1968) Handbook of Mathematical Functions. New York: Dover

[21] Gradshteyn, I. S., and Ryzhik, I. M. (1980) Table of Integrals, Series, and Products. New York: Academic Press

[22] Hansen, J. E., editor (1988) Spherical Near-Field Antenna Measurements. London: Peregrinus

[23] Wacker, P. F. (1975) Non-planar near-field measurements: Spherical scanning, Nat. Bur. Stand. (US) NBSIR 75-809

[24] Hill, D. A. (1985) A numerical method for near-field array synthesis, IEEE Trans. Electromagn. Compat., **EMC-27**:201-211

[25] Yaghjian, A. D. (1984) Approximate formulas for the far field and gain of open-ended rectangular waveguide, IEEE Trans. Antennas Propagat., **AP-32**:378-390

☆U.S. GOVERNMENT PRINTING OFFICE: 1990-573-47

4A

U.S. DEPARTMENT OF COMMERCE
NATIONAL INSTITUTE OF STANDARDS AND TECHNOLOGY

BIBLIOGRAPHIC DATA SHEET

1. PUBLICATION OR REPORT NUMBER
NISTIR 3955

2. PERFORMING ORGANIZATION REPORT NUMBER

3. PUBLICATION DATE
July 1990

LE AND SUBTITLE

Spherical Near-Field Scanning: Experimental and Theoretical Studies

THOR(S)

. C. Wittmann, C. F. Stubenrauch

FORMING ORGANIZATION (IF JOINT OR OTHER THAN NIST, SEE INSTRUCTIONS)

. DEPARTMENT OF COMMERCE
TIONAL INSTITUTE OF STANDARDS AND TECHNOLOGY
ULDER, COLORADO 80303-3328

7. CONTRACT/GRANT NUMBER

8. TYPE OF REPORT AND PERIOD COVERED

NSORING ORGANIZATION NAME AND COMPLETE ADDRESS (STREET, CITY, STATE, ZIP)

ADC/EECT, Hanscom AFB, MA 01731

PLEMENTARY NOTES

TRACT (A 200-WORD OR LESS FACTUAL SUMMARY OF MOST SIGNIFICANT INFORMATION. IF DOCUMENT INCLUDES A SIGNIFICANT BIBLIOGRAPHY OR RATURE SURVEY, MENTION IT HERE.)

s report documents the evaluation of spherical near-field scanning altorithms and computer e developed at the National Institute of Standards and Technology. The experimental work rimarily a comparison of probe-compensated spherical and planar near-field measurement lts for a common test antenna. Theoretical work is largely supportive of the experimental ort, but some peripheral topics are developed: For example, (1) application of spherical -field measurements to the determination of incident fields in compact ranges; and, spherical-wave expansions for the fields of a uniformly excited circular aperture facilitate the creation of analytic test data).

ORDS (6 TO 12 ENTRIES; ALPHABETICAL ORDER; CAPITALIZE ONLY PROPER NAMES; AND SEPARATE KEY WORDS BY SEMICOLONS)

nna measurements; near-field measurements; probe correction; range evaluation; rical scanning; spherical waves

ABILITY

UNLIMITED
FOR OFFICIAL DISTRIBUTION. DO NOT RELEASE TO NATIONAL TECHNICAL INFORMATION SERVICE (NTIS).
ORDER FROM SUPERINTENDENT OF DOCUMENTS, U.S. GOVERNMENT PRINTING OFFICE, WASHINGTON, DC 20402.
ORDER FROM NATIONAL TECHNICAL INFORMATION SERVICE (NTIS), SPRINGFIELD, VA 22161.

14. NUMBER OF PRINTED PAGES
128

15. PRICE

NIC FORM